E-ISSN: 2148-6247

Turkish Journal of PHARMACEUTICAL SCIENCES

An Official Journal of the Turkish Pharmacists' Association, Academy of Pharmacy

Volume: 22 Issue: 3 June 2025

www.turkjps.org

Emerging Sources Citation Index · PubMed Central · PubMed · Scopus · TR Dizin

galenos Publishing House

Turkish Journal of
PHARMACEUTICAL SCIENCES

Turkish Journal of
PHARMACEUTICAL SCIENCES

Prof. Robert Rapoport, Ph.D.
ORCID: orcid.org/0000-0001-8554-1014
Cincinati University Faculty of Pharmacy, Department of Pharmacology and Cell Biophysics, Cincinati, USA
robertrapoport@gmail.com

Prof. Tayfun Uzbay, Ph.D.
ORCID: orcid.org/0000-0002-9784-5637
Üsküdar University Faculty of Medicine, Department of Medical Pharmacology, İstanbul, Türkiye
tayfun.uzbay@uskudar.edu.tr

Prof. Wolfgang Sadee, Ph.D.
ORCID: orcid.org/0000-0003-1894-6374
Ohio State University, Center for Pharmacogenomics, Ohio, USA
wolfgang.sadee@osumc.edu

Advisory Board

Turkish Journal of
PHARMACEUTICAL SCIENCES

Please refer to the journal's webpage (https://www.turkjps.org/) for "Editorial Policy" and "Instructions to Authors".

The editorial and publication process of the **Turkish Journal of Pharmaceutical Sciences** are shaped in accordance with the guidelines of ICMJE, WAME, CSE, COPE, EASE, and NISO. The Turkish Journal of Pharmaceutical Sciences is indexed in **PubMed, PubMed Central, Thomson Reuters / Emerging Sources Citation Index, Scopus, ULAKBİM, Türkiye Citation Index, Embase, EBSCO Host, Türk Medline, Cabi, CNK**I.

The journal is published online.

Owner: Turkish Pharmacists' Association, Academy of Pharmacy

Responsible Manager: Mesut Sancar

galenos yayınevi

Publisher Contact
Address: Molla Gürani Mah. Kaçamak Sk. No: 21/1
34093 İstanbul, Türkiye
Phone: +90 (530) 177 30 97
E-mail: info@galenos.com.tr/yayin@galenos.com.tr
Web: www.galenos.com.tr | **Publisher Certificate Number:** 14521

Publication Date: August 2025
E-ISSN: 2148-6247
International scientific journal published bimonthly.

Turkish Journal of
PHARMACEUTICAL SCIENCES

CONTENTS

Original Articles

Turk J Pharm Sci 2025;22(3):154-160
DOI: 10.4274/tjps.galenos.2025.25057

ORIGINAL ARTICLE

A Study on the Evaluation of the Effects of Talent Management Practices on Employee Performance in the Pharmaceutical Companies in Türkiye

Aslı YALDIZ*, Gülbin ÖZÇELİKAY

Ankara University Faculty of Pharmacy, Department of Pharmacy Management, Ankara, Türkiye

ABSTRACT

Objectives: It aimed to evaluate talent management practices in pharmaceutical companies according to different departments such as medical and marketing, and determine the effect of talent management on employee performance.

Materials and Methods: The impact of talent management practices on employee performance was evaluated by applying survey to medical directors/regional medical directors and product managers/brand managers/brand specialists working in pharmaceutical companies. The Talent Management Practices Scale and the Employee Performance Scale were used. The online survey was applied to volunteer participants between March 2021 and March 2023. The data obtained from the participants were analyzed using SPSS ver 22.0. The effect of the sub-dimensions of talent management on employee performance was determined. In this research, Pearson characteristic test, regression test, Independent Groups t-test, and analysis of variance test were used to determine the relationship between variables.

Results: A total of 112 people, 51 female (45.5%) and 61 men (54.5%), participated in the study. The impact of talent management practices on employee performance, it varies depending on age, gender, education level, position in the company, the company's national or multinational status, and working period. This study revealed statistically significant differences in talent management perceptions based on gender ($p<0.05$), education level ($p<0.05$), age categories ($p<0.05$), and job categories ($p<0.05$), with job categories also significantly impacting employee performance ($p<0.05$). Correlation analyses indicated a statistically significant positive relationship between talent management's commitment ($r=0.552$; $p<0.001$) and retention ($r=0.448$; $p<0.001$) sub-dimensions and overall employee performance. Furthermore, a statistically significant regression model ($F(7,104)=10.224$; $p<0.001$) demonstrated that commitment, retention, and training aspects of talent management collectively explain 40.8% of the variance in employee performance. As a result of the analyses, it was determined that commitment and employee retention, which are sub-dimensions of talent management practices, has a positive relationship with employee performance.

Conclusion: According to survey results talent management affects employee performance. Evaluations of participants in the pharmaceutical industry revealed that the Attraction, Selection-Placement, Training, and Talent pool sub-dimensions of talent management practices implemented by businesses had a positive but weak effect on employee performance. The commitment and retention sub-dimensions were found to have a positive, moderate effect on employee performance.

Keywords: Employee performance, pharmaceutical industry and performance, pharmaceutical industry and talent management

INTRODUCTION

Ability, in essence, encompasses an individual's physiological and cognitive capacity to perform tasks effectively. From a business standpoint, it refers to the knowledge, proficiency, and competencies that employees possess to carry out their roles successfully.[1,2]

Identifying competent individuals, placing them in appropriate key positions, ensuring their commitment to the organization,

***Correspondence:** asliculduz@gmail.com, **ORCID-ID:** orcid.org/0000-0002-9573-0377
Received: 14.03.2024 , **Accepted:** 29.04.2025 **Publication Date:** 01.08.2025

Cite this article as: YALDIZ A, ÖZÇELİKAY G. A study on the evaluation of the effects of talent management practices on employee performance in the pharmaceutical companies in Türkiye. Turk J Pharm Sci. 2025;22(3):154-160

keeping their motivation and performance high, and creating a development plan are within the scope of talent management.[3] Talent management for organizations can be defined in its most basic form as ensuring that the right individual is in the appropriate occupation at the correct time. Additionally, in 2004, Pascal defined talent as managing the supply, demand, and flow of human resources.[4]

When the topics covered by talent management are considered, it becomes evident that each of them has an impact on the employee. Talent management is examined under seven sub-dimensions. These sub-dimensions: attraction, selection-placement, commitment, retention, training, reward, and talent pool.[5] Effectively carried out talent management practices contribute to organizations in terms of financial, organizational and human resources.[6]

The concepts of talent management and human resources management can be confused with each other. Performance management serves as a model employed to assess employees' performance within an organization, aiming to enhance performance and offer appropriate guidance for improvement. This model includes measuring a person's individual and team performance, setting goals, providing feedback on performance and creating development plans. Performance management contributes to the business achieving its strategic goals.[7]

The correlation between talent management and performance management processes is that the data gathered through performance management serves as foundational information for talent management initiatives. For example, an employee's past performance, potential, and areas of development can be utilized during the talent management process to evaluate that employee's future role or promotion possibility.[8] Businesses that implement talent management practices contribute to an innovative culture and employee development. This increases employees' abilities and knowledge, thus helping them perform better.[9]

The concept of talent management has gained importance in the pharmaceutical industry, as it has all businesses. The Turkish pharmaceutical industry is a sector with a large scale and variety of exports, which has production opportunities and high economic value. Due to the obligation of businesses in this sector to employ qualified personnel, the sector is evaluated slightly differently than other businesses.[10]

Considering the drug development processes, many people are employed in this sector and they are assigned to different fields. There are numerous external factors affecting businesses in the pharmaceutical industry. Legislative updates, crisis environments, various competitive conditions, and environmental factors are some of these. Since it is a sector that is open to being affected by external factors, it is important to differentiate management styles within the business. Due to the emphasis on human health and the increasing awareness of this issue, these businesses readily embrace innovations to detect significant talents and ensure the continuity of their employment.[11,12]

Türkiye's total employment increased by 9.7% in 2021. On the other hand, the pharmaceutical industry workforce increased by 4.2% and reached 44,071 people.[13] Considering 2022, the data shows that the value was 47511 according to Turkish Statistical Institute data.[14]

Talent management practices in the pharmaceutical industry have a direct impact on organizational effectiveness.[15] Talent management is critical for improving operational excellence and achieving strategic goals in the pharmaceutical industry.[16] Retaining talent is crucial to the long-term success of the organization.[17] The pharmaceutical industry ought to constantly develop novel products, treatment methods, and technologies. This emphasizes the need for personnel with a high level of scientific and technical abilities.[18,19] All over the globe in our country, strict regulations are applied in the pharmaceutical industry due to health concerns. Government institutions have determined these regulation limits through various regulations and guidelines.[20] The safety and effectiveness of pharmaceuticals are strictly regulated. Therefore, expertise needs to comply with these regulations. Talent management in the pharmaceutical industry plays a critical role, considering the complexity and needs of the sector. A proper talent management strategy supports scientific progress, maintains competitive advantage and ensures compliance with regulations.[21]

In the contemporary era, possessing essential competencies, cognitive abilities, knowledge, and potential is crucial for workforce agility, ensuring that business strategies operate more effectively.[22] Organizations where the most productive employees can choose assignments according to their aspirations and competencies are seen as more beneficial and efficient for both the organizations and their employees. Multi-employee companies, such as those in the pharmaceutical industry, strive to properly use the talent management system, making it a way to optimize the performance of each employee.[23]

Effective performance management with suited talents plays a critical role in the pharmaceutical industry. It is thought that, in businesses where talent management practices are implemented effectively, the desire of individuals working there increases, enabling them to make a significant contribution to the businesses. Therefore, an effective talent management process in this sector is of great importance for both the success of the business and the quality of patient care.[24,25]

Considering the importance of talent management for all businesses, it is much more significant, especially for some departments in the pharmaceutical industry. The degree of importance of this issue may differ in separate companies within the same sector, and these behaviors affect employee performance and provide added value to companies. In this study, it aimed to evaluate talent management practices in pharmaceutical companies according to different departments, such as medical and marketing, and determine the effect of talent management on employee performance.

MATERIALS AND METHODS

This study was a descriptive study. An online survey was conducted to determine whether talent management practices are implemented by pharmaceutical companies and their impact on employee performance. The survey gathered responses from employees in separate departments, such as medical and marketing. These departments were chosen because their working strategies are different.

After receiving the ethics committee approval with the decision numbered: 28 and dated 12.02.2021 of the Ankara University Health Sciences Sub-Committee of Ethics, a survey form was requested to be sent to Medical Managers/Regional Medical Managers and Product Managers/Brand Managers/Brand Specialists working in the medical and marketing departments of pharmaceutical companies registered with the association and union through the Association of Research-Based Pharmaceutical Companies and the Pharmaceutical Industry Employers' Union, to volunteer participants between March 2021 and March 2023.

Employees working as Medical Manager/Regional Medical Manager or Product Manager/Brand Manager/Brand Specialist in a pharmaceutical company in Türkiye were included in the research. In this context, the population of the research consisted of medical managers, regional medical managers, product managers, brand managers, and brand experts working in the Turkish Pharmaceutical Industry.

The sample was calculated using Gpower 1.1.9 software and was determined to be 102. While using this software, a priori: Compute required sample size analysis was used and the effect size was selected as 0.5, the significance level was selected as 0.05, and the power as 0.80.

The data collection tool of the research was a survey form consisting of three parts. The first part included questions to determine the demographic information of the participants. The second part consisted of the talent management practices scale, and the third part consisted the performance scale. Talent Management Practices Scale was developed by Duran et al.[5]. Employee Performance Scale was developed by Uludağ.[26] The survey was conducted online, and survey was shared with companies which are included in IEIS and AIFD and peopleparticipate in the study voluntarily.

Statistical analysis

Study results were evaluated using SPSS v22.0 the program. Analysis was performed with a 95% confidence interval. Parametric tests were used in our analysis, and the Kurtosis and Skewness values of the scale scores were between +2 and -2. In the study, the Pearson correlation test, regression test, independent groups t-test, and analysis of variance (ANOVA) test were used to determine the relationship between variables and the direction of the relationship.

Two criteria were considered when examining the normality assumption for the scales and sub-dimensions used in this study. First, a small difference between the mean and median values was observed. Second, the values obtained by multiplying the skewness and kurtosis values by their respective standard errors were within the range of ±2.00. Both of these criteria led to the conclusion that the normal distribution assumption was met.[27] This examination revealed that the measurement tools generally exhibited a bell-shaped curve appearance. In light of all these evaluations, it was decided to use parametric tests.

Correlation analysis was used to interpret the relationship between two variables, and different levels of relationships were found. Therefore, regression analysis was subsequently performed. [29]

When evaluating the results of the correlation test, the *p*-value was examined to determine if there was a relationship between the two variables. If $p<0.05$, it was concluded that a relationship exists between these variables. After concluding that there was a relationship, the two variables were evaluated as weak or strong by looking at the correlation number, *i.e.*, the *r* value.

The sub-dimensions of the talent management practice scale were assigned to the regression analysis, and the "enter" method was preferred. This method, one of the frequently used methods in SPSS software, allows independent variables to be entered and evaluated as a block in a single step. As a result of this method, the regression model, in which the significant parameters were included, was estimated

RESULTS

All demographic information, the differences between the sub-dimensions of the talent management practices scale (attraction, selection-placement, commitment, retention, training, reward, and talent pool), and the average score of the employee performance scale were examined, and the results with significant differences ($p<0.05$) are listed in Table 1.

The correlation analysis in Table 2 examined the relationship between sub-dimensional total scores of the talent management practices scale and the overall total score averages of the employee performance scale. The *p* and *r* values are given in Table 2. The study concluded that a weak yet statistically significant positive association exists between the total scores of the talent management practices scale's various sub-dimensions (attraction, selection, placement, training, reward, and talent pool) and the overall total score of the employee performance scale ($p<0.05$). It was observed that a statistically significant positive and moderate-level relationship exists between the commitment and retention sub-dimensional total scores of the talent management practices scale and the overall total score of the employee performance scale ($p<0.05$).

The model, which was based on the significant parameters, was statistically significant [$F(7,104)=10.224$; $p<0.001$]. In the analysis, the total scores of the commitment, retention, and training sub-dimensions of the talent management practices scale were considered predictive parameters. The results, as displays in Table 3, indicated that this regression model accounts for 40.8% of the variability in the total score of the employee performance scale.

DISCUSSION

Talent management practices that are thought to affect employee performance. The study examined in detail the sub-dimensions of allocation, designation, placement, commitment, retention, training, reward, and talent pool, and it revealed the current situation. It is thought that employees are positively affected by Talent Management Practices because they provide added value for their business due to their increased loyalty. This study was conducted on people working in certain roles in the medical and marketing departments in the pharmaceutical industry. It shows some similarities with the results of various studies conducted on talent management practices and employee performance.

Talent management practices in pharmaceutical companies affect employee performance. In the analysis, the total scores of the Loyalty, Retention, and Training sub-dimensions of the Talent Management Practices Scale were considered independent variable parameters. Regression analysis shows that employee performance can be predicted by the development in the sub-dimensions of commitment, retention, and training.

Supporting this, Al-Qeed et al.[30] found that talent management significantly impacts organizational performance within

Table 1. Examining differences in terms of sociodemographic variables

Scale/sub-dimensions	Sociodemographic variables	n	$\bar{x}$	SD	p
Selection-Placement	Female (gender)	51	26.24	4.603	0.034*
	Male	61	26.87	5.242	
Commitment	25-34 (age)	68	32.65	3.133	0.043*
	35-44	34	30.79	4.443	
	45-54	10	31.70	3.561	
Attraction	Licence (educational backround)	60	27.57	4.735	0.023*
	Postgraduate	52	25.44	4.992	
Employee performance	Licence	60	21.58	2.733	0.044*
	Postgraduate	52	22.38	3.024	
Commitment	Multinational (company)	79	32.75	3.276	0.001*
	National	33	30.21	4.014	
Retention	Multinational	79	31.85	4.873	0.009*
	National	33	28.85	6.648	
Rewarding	Multinational	79	41.42	6.404	0.005*
	National	33	37.76	5.321	
Talent pool	Medical (department)	64	18.67	4.032	0.008*
	Commercial	48	16.71	3.458	
Commitment	Medical Manager (title)	41	32.29	3.084	0.007*
	Regional Medical Manager	28	32.07	4.610	
	Product Manager	23	33.52	0.994	
	Brand Manager	11	29.09	4.415	
	Brand Specialist	9	30.11	4.314	
Employee performance	Medical Manager	41	22.27	2.569	0.004*
	Regional Medical Manager	28	21.64	3.176	
	Product Manager	23	23.35	1.584	
	Brand Manager	11	19.64	3.722	
	Brand Specialist	9	20.78	2.991	

pharmaceutical companies in Jordan. Their study highlighted that skilled employees possessing high competence and knowledge perform better. A positive relationship exists between talent management and organizational performance.

Further, a study focusing on Jordanian pharmaceutical companies showed that effective talent management aligns with strategic goals, emphasizing its role in meeting future personnel needs.[31]

Almohtaseb is cited in their study to Nafei. Nafei (2016) investigated the impact of talent management on performance within Egyptian industrial firms and identified a correlation between talent management practices and organizational performance. Nafei recommended that Egyptian industrial companies enhance performance by improving their talent management strategies.[32]

Akar et al.[2] research underscored the necessity of skilled human resources for business sustainability. [2] He suggested that employee performance improves when businesses provide appropriate training, development opportunities, recognition, and a reward system for high performers.

Thilagham et al.[33] explored factors contributing to employee turnover in the Indian pharmaceutical industry, noting that effective management of talent assignment, retention, and engagement constitutes a significant competitive advantage. They emphasized that talent retention is crucial for organizational success and market sustainability, with management effectiveness reliant on aligning talent with strategic business goals.

Another study investigated the impact of talent management practices on employee motivation, finding a positive relationship between talent management dimensions and work motivation. This suggests that implementing talent management practices significantly influences performance by enhancing employee motivation.[34]

In Nigeria, research among pharmaceutical industry employees revealed that talent management, particularly in training and development, has a direct positive relationship with organizational performance. The study advocates for not only attracting but also retaining top talent to boost growth and sustainability.[35]

These findings collectively highlight the critical role of talent management practices in enhancing employee performance and organizational success, reinforcing the need for effective implementation and continuous improvement in these practices.

Table 2. Relationships between the sub-dimension total scores of the talent management practices scale and the overall score averages of the employee performance scale

Scal /Sub-dimensions	Employee performance	
Attraction	*r*=0.187	*p*=0.048*
Selection-placement	*r*=0.257	*p*=0.006**
Commitment	*r*=0.552	*p*=0.000***
Retention	*r*=0.448	*p*=0.000***
Training	*r*=0.221	*p*=0.019*
Rewarding	*r*=0.218	*p*=0.021*
Talent pool	*r*=0.240	*p*=0.011*

r : Correlation coefficient; *p*: Significance value, *$p<0.05$; **$p<0.01$; ***$p<0.001$

Table 3. Results of regression analysis to determine the predictions of the total score of the employee performance scale

Independent variables	B	se	Beta	t	F	R2
Constant (a)	7.723	2.134		3.620***	10.224***	0.408
Attraction	-0.057	0.075	-0.097	-0.756		
Selection-placement	0.008	0.114	0.009	0.071		
Commitment	0.360	0.072	0.458	5.013***		
Retention	0.258	0.069	0.501	3.729***		
Training	-0.182	0.081	-0.369	-2.251*		
Rewarding	-0.049	0.049	-0.106	-0.998		
Talent pool	0.156	0.088	0.211	1.775		

*$p<0.05$; **$p<0.01$; ***$p<0.001$. B: Regression vol, se: Standard error, Beta: Standardized Regression Coefficient, t: Independent significance test of regression, F: Total regression test, R2: Determination regression coefficient

Study limitations

Since pharmaceutical industry employees are also private sector employees, they have a busy work schedule and have difficulty in allocating time for the survey. It was not possible to access individual employee information due to the protection of personal data rights. Communication was attempted through companies, general information addresses, associations, and social media. Since one-on-one communication could not be established, it was difficult to reach the relevant group. [36] However, some companies responded that it was not possible for them to participate in the study or inform their employees. It is thought that it took a little longer to answer the survey questions online, which may have also created a limitation. However, it is known that online fatigue is high among private sector employees. [37]

CONCLUSION

This study evaluated the relationship between talent management and employee performance. A significant difference was observed in the selection and placement dimension based on gender, with male participants perceiving a more effective selection process. Younger employees placed greater emphasis on organizational loyalty in the commitment dimension. Participants with postgraduate education believed companies exert more effort in attracting the right talent. Employees in multinational companies scored higher in commitment, retention, and reward sub-dimensions compared to those in national companies.

Medical managers, regional medical managers, brand managers, and experts gave themselves lower performance ratings than product managers, potentially due to the frequency and rigor of evaluations within marketing departments.

Overall, the study concluded that talent management practices positively influence employee performance. There was a moderate positive relationship between the commitment and retention aspects of talent management and overall employee performance. However, the relationships with other dimensions were weaker.

To improve talent engagement and organizational effectiveness, especially in the pharmaceutical sector, it is recommended that talent management practices include initiatives such as better workplace management, emotional intelligence, and employee competencies.

Given the ongoing global challenges in talent management, further research is needed to examine how performance management systems impact the relationship between talent management and organizational outcomes across various sectors and economic contexts.

Ethics

Ethics Committee Approval: Ethics committee approval was obtained from the Ankara University Health Sciences Sub-Committee of Ethics (decision number: 28, dated 12.02.2021).

Informed Consent: There is no patient in this study.

Acknowledgments

Pharmaceutical industry employees who participated in the study: We would like to thank Cengiz DURAN, Dursun BOZ, Sema BEHDİOĞLU, and Songül KUTLU for developing the Talent Management Practices Scale used in the study, and Gökhan Uludağ for developing the Employee Performance Scale.

Footnotes

Authorship Contributions

Concept: A.Y., G.Ö., Design: A.Y., G.Ö., Data Collection or Processing: A.Y., Analysis or Interpretation: A.Y., G.Ö., Literature Search: A.Y., G.Ö., Writing: A.Y.

Conflict of Interest: The authors declare no conflicts of interest.

Financial Disclosure: The authors declared that this study received no financial support.

REFERENCES

1. Bos-Nehles A, Townsend K, Cafferkey K, Trullen J. Examining the ability, motivation and opportunity (AMO) framework in HRM research: conceptualization, measurement and interactions. Int J Manag Rev. 2023;25:725-739.
2. Akar H. İşletmelerde yetenek yönetimi uygulamalarının örgütsel bağlılık ve çalışan performansına etkisi. Yüksek Lisans Tezi. 2018.
3. Collings DG, Mellahi K. Strategic talent management: a review and research agenda. Hum Resour Manag Rev. 2009;19:304-313.
4. Lewis R, Heckman RJ. Talent management: a critical review. Hum Resour Manag Rev. 2006;16:139-154.
5. Duran C, Boz D, Behdioğlu S, Kutlu S. Talent management applications scale validity and reliability work. Eskisehir Osmangazi Univ Sos Bil Derg. 2019;20:158-189.
6. Bethke P, Mahler P, Staffelbach B. Effectiveness of talent management strategies. Eur J Int Manag. 2011;5:524-539.
7. Gruman JA, Saks AM. Performance management and employee engagement. Hum Resour Manag Rev. 2011;21:123-136.
8. Damarasri B, Ahman E. Talent management and work motivation to improve performance of employees. Dinasti Int J Educ Manag Soc Sci. 2020;1:490-498.
9. Nagi M, Mohammed Ali Y. The effect of talent management practices on employee performance. Int J Manag. 2020;11:1281-1287.
10. Türkiye İlaç Sektörü Strateji Belgesi ve Eylem Planı 2015-2018. 2015. Erişim tarihi: 11 Şubat 2024. https://www.titck.gov.tr/Dosyalar/Ilac/Saglikendustrilerikoordinasyon/EK-1%20T%C3%BCrkiye%20%C4%B0la%C3%A7%20Sekt%C3%B6r%C3%BC.Pdf
11. İlaç Sektörü Raporu. Erişim tarihi: 29 Ocak 2024. https://www.erdem-erdem.av.tr/bilgi-bankasi/ilac-sektoru-raporu
12. Lublóy Á. Factors affecting the uptake of new medicines: a systematic literature review. BMC Health Serv Res. 2014;14:469.
13. 2022 Türkiye İlaç Sektörü. 2022. Erişim tarihi: 11 Şubat 2024. https://www.ieis.org.tr/static/shared/publications/pdf/23623xaft_tr_ilac_sektoru_2022.pdf
14. Akbil Ş, Cebeci Z, Dinç Ş, Çakır OK. AİFD Türkiye ilaç sektörü raporu 2023. 2023. Erişim tarihi: 11 Şubat 2023. https://www.aifd.org.tr/wp-content/uploads/2023/12/ıqvıa_turkıye-ılac-sektoru_raporu_.pdf

15. Nana F. Measuring the impact of human resource management (HRM) practices on pharmaceutical industry's effectiveness: the mediating role of employee competencies. Employee Relat. 2020;42:1353-1380.
16. Barkhuizen EN, Welby-Cooke G, Schutte N, Stanz K. Talent management and leadership reciprocity: the case of the South African aviation industry. Mediterr J Soc Sci. 2014;5:11-17.
17. Tlaiss HA, Martin P, Hofaidhllaoui M. Talent retention: evidence from a multinational firm in France. Employee Relat. 2017;39:426-445.
18. Ashton C, Morton L. Managing talent for competitive advantage: taking a systemic approach to talent management. Strateg HR Rev. 2005;4:28-31.
19. Kular S, Gatenby M, Rees C, Soane E, Truss K. Employee engagement: a literature review. Kingston Business School Working Paper Series. 2008;C19.
20. Köse A. Türk ilaç politikalarına yönelik bir değerlendirme. Istanbul Gelisim Univ J Health Sci. 2022;18(18):1084-1099.
21. Thomas CC. Talent management and building high performance organisations. Ind Commer Train. 2012;44:429-436.
22. Aktan CC. Performance management: performance evaluation and measurement on organizations. 2009;1:25-49.
23. Kaleem M. The influence of talent management on performance of employee in public sector institutions of the UAE. Public Admin Res. 2019;8:8.
24. Mensah JK. A "Coalesced framework" of talent management and employee performance: for further research and practice. Int J Product Perform Manag. 2015;64:544-566.
25. Türkiye İlaç Sanayi Sektör Raporu. 2008. Erişim tarihi: 29 Ocak 2024. www.tobb.org.tr
26. Uludağ G. Lider-üye etkileşiminin, yetenek yönetimi ve işgören performansına etkileri üzerine bir araştırma: Ankara örneği. 2016.
27. Güriş S, Astar M. Bilimsel araştırmalarda SPSS ile istatistik (3. Basım). Der Yayınları; 2019.
28. Karadavut T. Hypothesis testing for independent correlation coefficients: SPSS and Microsoft Excel applications. Abant İzzet Baysal Univ Eğitim Fak Derg. 2020;21:375-389.
29. Kilic S. Linear regression analysis. J Mood Disord. 2013;3:90.
30. Al-Qeed MA, Abdul Halim Khaddam A, Al-Azzam ZF, Abd El Fattah Atieh K. The effect of talent management and emotional intelligence on organizational performance: applied study on pharmaceutical industry in Jordan. J Bus Retail Manag Res. 2018;13:1-14.
31. Al-Awamleh TAHAA, Hamdan REAR, Khlaifat SAAS. The impact of talent management on achieving strategic objectives: a study on the Jordanian pharmaceutical industries. Int J Ebusiness Egovernment Stud. 2022;14:1-25.
32. Ali Almohtaseb A, Kareem Shaheen HA, Mohummed Alomari K, Yousef Almahameed MA. Impact of talent management on organizational performance: the moderating role of an effective performance management system. Int J Bus Manag. 2020;15:11.
33. Thilagham KT, Malini TN, Tirumala P, Auadhati D, Gauri Singh Bhadauria, Priyanka Agarwal. Study on talent management practices in pharma sector with focus on "employee retention". J Pharm Negative Results. 2022;1366-1376.
34. Güner MB. Çalışanların yetenek yönetimi algısının iş motivasyonuna etkisi. Yüksek Lisans Tezi. Doğuş Üniversitesi Sosyal Bilimler Enstitüsü; 2016.
35. Mgbemena GC, Enetanya ID, Nsofor MN, Ogbogu FO. Talent management and organization performance in pharmaceutical companies in Anambra State, Nigeria. Int J Bus Law Res. 2022;10:1-16.
36. Brown A, Davis B. Challenges in organizational research: Gaining access and cooperation. Journal of Applied Psychology. 2018;103(5):550-562.
37. Johnson C, Lee D, Chen E. The pervasive impact of online fatigue on employee engagement and well-being in the private sector. Journal of Digital Workplace Studies. 2021;15(2):112-128.

Turk J Pharm Sci 2025;22(3):161-169
DOI: 10.4274/tjps.galenos.2025.25668

ORIGINAL ARTICLE

Ethnopharmacological Survey of Plants Used as Folk Remedy in Gerze (Sinop, Türkiye)

Tuğba GÜNBATAN[1]*, Onur KABAŞ[2], Ekrem SEZİK[3], İlhan GÜRBÜZ[1]

[1]Gazi University Faculty of Pharmacy, Department of Pharmacognosy, Ankara, Türkiye
[2]Yumuk Pharmacy, Sinop, Türkiye
[3]Yeditepe University Faculty of Pharmacy, Department of Pharmacognosy, İstanbul, Türkiye

ABSTRACT

Objectives: Folk medicines used in the Gerze district of Sinop have not been previously studied in detail. This study aimed to record and compily the folk medicines used in Gerze (Sinop, Türkiye).

Materials and Methods: In this ethnobotanical inventory study, scientific trips were organized to 18 villages in the Gerze district between May and August in 2009, and folk medicine information was obtained using open and semi-structured questionnaires. The obtained data were analysed by calculating use value", informant consensus factor, and relative frequency of citation.

Results: As a result, 63 plant species from 41 families were determined to be used as folk medicine. Plants from the *Rosaceae* and *Asteraceae* families are preferred in preparing folk medicines. *Sempervivum brevipilum* Muirhead and *Serapias vomeracea* (Burm.f.) Briq. were recorded for the first time as folk medicine in this research. In Gerze, folk medicines were mostly used in the respiratory tract (86 citations), and dermatological system diseases (86 citations). However, when informant consensus factor values are considered, dermatological system disorders are ranked first (0.7529) and, followed by musculoskeletal (0.7049), respiratory (0.6941), and cardiovascular system disorders (0.5882). The most cited plants were *Olea europaea* L. (27 citations) and *Sambucus ebulus* L. (23 citations). The highest use value was calculated for *O. europaea* subsp. *europaea* (0.293), and *S. ebulus* (0.260). At the same time, *S. ebulus* took first place with an relative frequency of citation value of 0.239, *O. europaea* subsp. *europaea* (0.184) fell in second place.

Conclusion: The use of 63 different plant species in folk medicine in Gerze has been recorded to eliminate a deficiency in the Turkish folk medicine inventory and be a source for future scientific studies. However, as in other regions of Türkiye, it has emerged that the folk medicine knowledge was being lost in Gerze District, and that ethnobotanical inventory studies should be carried out rapidly throughout the country.

Keywords: Ethnobotany, folk medicine, Gerze, medicinal plant, Sinop

INTRODUCTION

Archaeological findings show that plants have been used for different purposes besides nutrition (e.g., tool making, religious ceremonies) since Neanderthals.[1] Although this situation is not different today, the tendency to use plants, under the influence of ideas such as adopting a natural lifestyle and avoiding the side effects of synthetic drugs, is increasing, especially in the field of medicine. In this context, ethnobotanical knowledge/folk medicines, considered effective and reliable since they have been used for many years, are very valuable resources for new drug discovery. Compounds artemisinin, digoxin, and aspirin are some examples of drugs developed from ethnobotanical records and available on the market today.[2] It is thought that the number of such examples will gradually increase as a

***Correspondence:** tugbagunbatan@gazi.edu.tr, **ORCID-ID:** orcid.org/0000-0002-1138-3145
Received: 24.01.2025, **Accepted:** 01.05.2025 **Publication Date:** 01.08.2025

Citethisarticleas: GÜNBATANT,KABAŞO,SEZİKE,GÜRBÜZİ.Ethnopharmacologicalsurveyofplantsusedasfolkremedyin Gerze(Sinop,Türkiye).TurkJPharmSci.2025;22(3):161-169

result of phytochemical and bioactivity studies on plants with ethnobotanical uses.

Anatolia is a center of attraction for ethnobotanical studies due to its cultural richness provided by being one of the important settlement centers since ancient times, rich flora due to geographical diversity, and being under the influence of three phytogeographical regions.[3] Ethnobotanical studies started in Türkiye in the mid-1980s and continue with acceleration today. One thousand two hundred eighty plants, about 11% of Turkish flora, were identified as being used in folk medicine, but it is estimated that this number has increased more with new studies.[4] In addition, considering that about 7% of plants are used as traditional medicine worldwide, the rate in Türkiye is quite high.[5] However, this valuable cultural heritage is being lost day by daydue to modernization, migration to big cities, easier access to health institutions and medicines, loss of knowledgeable people about folk medicine, difficulty in accessing plants used as folk medicine with urbanization, and young people's indifference to the subject.[6] Therefore, quickly recording this valuable heritage before it is completely lost is extremely important.[7]

When the folk medicinal studies conducted in Türkiye were examined, it was seen that no studies had yet been carried out on some regions. To the best of our knowledge, no comprehensive folk medicinal research has been conducted in the Gerze district of Sinop. In a study investigating the ethnobotanical characteristics of the central and western Black Sea regions of Türkiye using a sampling method, five localities from the city center, Dikmen, Boyabat, and Durağan districts of Sinop were visited. In this research, 25 plant species belonging to 24 genera from 21 families and two animal species were determined to be used as folk medicine.[8] However, Gerze was not visited in this study. Indeed, the data obtained from 5 localities only are sufficient to understand the folk medicinal richness of the region. Therefore, this study aimed to record the folk medicines used in the region by conducting comprehensive research in the Gerze district of Sinop. In addition, the study aimed to find new folk medicines or different usages of previously identified folk medicines by comparing the results with the data obtained from previous studies in different regions of Türkiye. In addition, to increase the reliability of the results, and the data obtained was analysed using various statistical methods.

MATERIALS AND METHODS

Study area

Gerze, the district of Sinop, has been chosen as a settlement and shelter by societies since ancient times. It was founded as a small village by the Kaskians in 1400 B.C.. It came under the domination of the Hittites, Phrygians, Persians, Alexander the Great, Romans, Byzantines, Seljuks, and Ottoman Empire. Gerze, which was made a township of Sinop City in 1896, became a district in 1920 in the Republic of Türkiye.[9]

The Gerze district is located in A5 square (41° 48′ 6″ N, 35° 11′ 48″ E) according to Davis' grid system[10] and is surrounded by the Black Sea in the north; Boyabat district in the south; Dikmen district in the east and Sinop center in the west (Figure 1). The district is 39 km from the city centre, encompassing a total area of 594 km^2, and its altitude is 50 m.

Elma, Köse, Dede, and Hasan Mountains are significant elevations of the region. The main streams of the district are Sarımsak, Çakıroğlu, and Sarıyer Streams.[11] Ithough it is not possible to define the climate of the region with precise boundaries, it can be said that in addition to the oceanic climate, which constitutes the main climate type of the Black Sea region, the region is also under the influence of the Mediterranean climate, which has become more dominant occasionally in some areas.[12]

The district has a rich forest structure due to the abundant precipitation characteristic of the Black Sea climate. Trees such as pine, beech, oak, fir, hornbeam, and ash that extend from the coast to the mountains form this rich forest texture. Various orchards and olive groves in the valleys constitute a separate aspect of the vegetation.[9] In the few floristic studies conducted in the region, plants from three phytogeographic regions (Euro-Siberian, Mediterranean, and Irano-Turanian) were recorded, and Asteraceae, Fabaceae, and Poaceae were found to be the most common families.[12]

Agriculture, textiles, aquaculture, and tourism are the important sources of income in the district. It supplies approximately 11.8% of Sinop's agricultural area with 109,370 decare. In the district, legumes, grains, tobacco, vegetables such as tomato, cucumber, zucchini, leek, and fruits such as figs, mulberries, and cherries are widely cultivated in the region.[11]

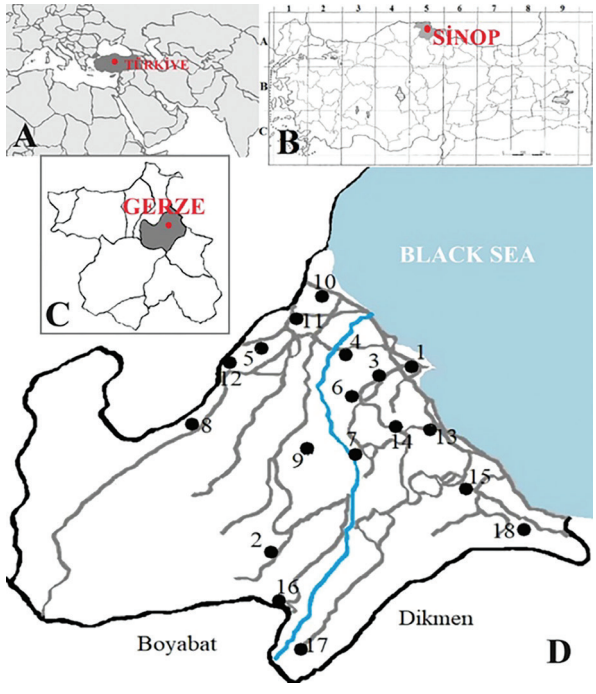

Figure 1. A) Türkiye's position in the world; B) the position of Sinop in Davis's grid system;[10] C) position of Gerze in Sinop; D) map of Gerze and visited locations (1) Gerze Centre; (2) Kiren Çukuru; (3) Abdaloğlu; (4) Belören; (5) Karlı; (6) Acısu, (7) Sazak; (8) Kuzsökü; (9) Dere (Gürsökü); (10) Yaykıl; (11) Çırnık; (12) Kabanlar; (13) Hızarçayı; (14) Çakallı; (15) Çeçe (Yenikent); (16) Tatlıcak; (17) Tilkilik (Çağlayan); (18) Hacıselli

Selection of visited locations

Instead of visiting all the villages in the region, it was preferred to collect information from 18 villages situated in various locales to reveal the general situation. Criteria such as distance to city centers, accessibility to health services, population, altitude, and transportation facilities were taken into account in the selection of fieldwork regions. The visits to the selected villages were organized between May and August in 2009. The locations visited and folk medicine information obtained are given in Figure 1.

Interviews, botanical investigations,

Folk medicinal information was collected through face-to-face interviews using the methodology described by Sezik et al.[6] and the modified open and semi-structured questionnaire of Thring and Weitz.[13,14] During these face-to-face interviews, direct questions were avoided as much as possible to prevent influencing the participants. Since folk remedies are based on ancestral knowledge, only well-established information was taken into account, and information suspected to be contaminated from sources such as television, the internet, and books was excluded.[15,16]

Information about the local name, used parts, usage, and detailed preparation methods of folk remedies was recorded using the questionnaire during the interviews. After the interviews, the plants used as folk medicine were recognized and collected in situ under the guidance of informants.[16] Collected plant specimens were identified by Prof. Dr. Ekrem SEZİK consulting Flora of Türkiye and the East Aegean Islands[10,17-19] and by comparison with previously registered herbarium specimens. After identification, prepared herbarium specimens were deposited in GUE (Gazi University Faculty of Pharmacy Herbarium). The taxonomical hierarchy of identified plants was updated according to World Flora Online.[20]

Statistical analysis

To assess the reliability of results, folk medicinal data were analyzed through three quantitative indices: informant consensus factor (FIC), use value (UV), and relative frequency of citation (RFC). FIC indicated the consistency of knowledge on the usage of folk medicines among the informants for a specific illness. Folk medicines were evaluated under 12 illness categories based on their usage (Table 1), and FIC was calculated for each category by using the following formula:

$FIC = (\Pi ur - \Pi t) / (\Pi ur - 1)$.

Πur is the number of citations used in each illness category, and Πt stands for the number of taxa used to treat disorders in this illness category. The FIC value will be close to 1 if there is agreement among informants about the use of folk medicine in specific situations, while low values (close to 0) indicate disagreement about taxa, or the selection was random.[21-24]

The other quantitative parameter for data evaluation was UV, which revealed the relative cultural importance of the uses of each folk medicine. This index, suggested by Prance et al.[25] was calculated as follows:

$UV = \Sigma U/n$

U refers to the number of citations recorded for a specific plant species, while n is the total number of informants involved in the study. If folk medicine is important for a community, it will be highly cited; therefore, its UV index will be high (close to 1). Contrarily, UV will be near 0 when there are few citations.[24,26]

Similarly, the RFC was calculated using the following formula to assess the local importance of folk medicines:

$RFC = FC/N$

FC is the number of informants who reported a specific folk medicine, and N is the total number of informants who took part in the survey.[27] Similar to the UV index, obtaining result values close to 1 indicates the importance of folk medicine in the studied area.

Table 1. Distribution of herbal folk medicines with respect to pharmacological categories and FIC values

Pharmacological categories	Species	All species (%)	Use citation	All use citation (%)	FIC value
Dermatological system disorders	22	34.92	86	20.77	0.7529
Musculoskeletal system disorders	19	30.15	62	14.97	0.7049
Respiratory system disorders	27	42.85	86	20.77	0.6941
Cardiovascular disorders	8	12.69	18	4.34	0.5882
Metabolic disorders	14	22.22	31	7.48	0.5666
Gastrointestinal system disorders	29	46.03	59	14.25	0.5172
Central nervous system disorders	9	14.28	17	4.10	0.5000
Genitourinary system disorders	16	25.39	28	6.76	0.4444
Eye-ear disorders	5	7.93	7	1.69	0.3333
Immunity disorders	8	12.69	11	2.65	0.3000
Mouth and tooth disorders	1	1.58	1	0.24	0
Others	4	6.34	4	0.97	0

FIC: Informant Consensus Factor

RESULTS

During the field survey carried out in 18 different villages, 92 people [31 women (33.7%); 61 men (66.3%)] who have knowledge about folk medicine were interviewed, and an inventory of folk medicine of the region was attempted to be prepared. Demographic statistics of the informants are given in Table 2. As can be seen in Table 2, the average age of informants is 59.4, and about 80% of them are older than 46 years. Younger than 25-year-olds made up a relatively small portion of informants (3.3%). Nearly half of the informants (48.9%) were primary school graduates, 3% were unschooled, and 13% were only literate. More than half of the informants were farmers, and almost half of the female informants were housewives. Most informants were native-born (93.5%) and had lived in Gerze since birth (81.5%). When asked about their ethnic origins during the interviews, all informants except for two (one was Georgian, and one of them was Circassian) declared that they were of Turkish origin.

As a result of these interviews, 63 plant species from 41 families have been determined to be used as folk medicine in the Gerze district. All the plants used as folk medicine in the region are presented in Supplementary Table 1 in alphabetical order. In this table, their local names, phytogeographical regions to which the plants belong, threat categories, parts used as folk medicine, purposes of use, preparation methods, locations where they were detected, citations, statistical results (UV, RFC), and previously identified uses are included.

The distribution of plants according to phytogeographical regions is as follows: 13 Euro-Siberian (21%) species, 9 Mediterranean (14%) species, and 3 Irano-Turanian (5%) species. Of the recorded folk medicines, 14 (22%) plants were cultivated, and two plants are exotic. The remaining 26 species (41%) were cosmopolitan and multi-regional. In Figure 2, the distribution according to families of plants used as folk medicine in the region is shown. As can be seen in this graphic, the Rosaceae family is the most preferred family in the preparation of folk remedies, with 7 species. Asteraceae (4 species), Malvaceae (3 species), and Solanaceae (3 species) are the other widely cited families in Gerze. As mentioned before, in floristic studies, Asteraceae has been determined as the family that represents the highest number of species in the region, as in all of Türkiye.[12,28,29] Therefore, it is not surprising that Asteraceae and Rosaceae, which are widespread and large families, appear as two of the most used families in the preparation of folk medicine. Similarly, in the previous folk medicine research in the Black Sea region, where Gerze (Sinop) is also located, Asteraceae and Rosaceae were the most frequently referred families.[15,30-32]

Table 2. Demographic data of the informants

Characteristic (n=92)	Count	%	Characteristic (n=92)	Count	%
Gender			**Marital status**		
Female	31	33.7	Single	5	5.4
Male	61	66.3	Married	87	94.6
Age			**Employment**		
≤25	3	3.3	Self-employed	5	5.4
26-35	9	9.8	Worker/public servant	20	21.8
36-45	7	7.6	Housewife	15	16.3
46-55	14	15.2	Farmer	47	51.1
56-65	29	31.5	Retired	5	5.4
66-75	15	16.3	**Ethnicity**		
76-85	11	12.0	Turkish	90	97.8
>85	4	4.3	Circassian	1	1.1
Education			Georgian	1	1.1
Illiterate	3	3.3	**Duration of residence**		
Literate	12	13.1	Less than 10 years	4	4.4
Primary school	45	48.9	More than 10 years	13	14.1
Middle school	13	14.1	Since birth	75	81.5
High school	11	11.9	**Birthplace**		
College	8	8.7	Native-born	86	93.5
			Incomer	6	6.5

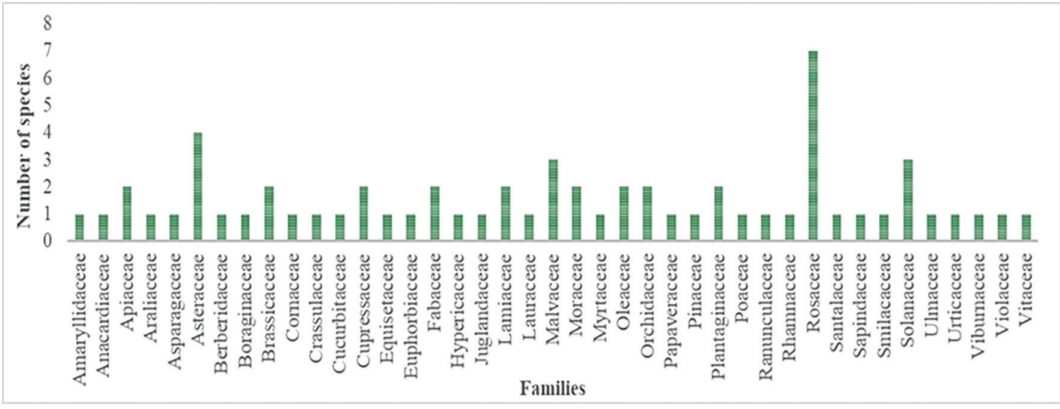

Figure 2. Distribution of folk medicines according to families

In Gerze, the most cited plant species was *Olea europaea* L. subsp. *europaea* (27 citations), followed by *Sambucus ebulus* L. (23 citations), *Brassica oleracea* L. (21 citations), *Urtica dioica* L. (20 citations), *Pinus nigra* J.F. Arnold subsp. *nigra* (18 citations) and *Nicotiana tabacum* L. (18 citations). The same order is observed when considering the UV values: the highest UV value was calculated for *O. europaea* subsp. *europaea* (0.293), while *S. ebulus*, *B. oleracea*, *U. dioica*, *P. nigra* subsp. *nigra*, and *N. tabacum* had subsequent UV values of 0.260, 0.228, 0.217, 0.195, and 0.195, respectively. Although not very common, there are olive groves in Sinop. Olive is an important product currently produced in large quantities in Türkiye, and its oil and fruit are widely consumed. The olive tree and the products obtained from it also have historical and mythological importance. Therefore, coming across olives as the most cited folk medicine is not surprising. *B. oleracea* and *N. tabacum* are widely cultivated in the Black Sea region. *P. nigra* and *U. dioica* are the plants that grow in forest areas and almost every garden in the study area, as well as in many regions of Türkiye. It is expected that these easily accessible plants are frequently used as folk remedies. However, this order slightly varies when considering the RFC values. At the same time, *S. ebulus* took first place with an RFC value of 0.239, *O. europaea* subsp. *europaea* (0.184) fell in second place. *N. tabacum* and *U. dioica*, with RFC values of 0.173 and 0.163, respectively, ranked third and fourth.

In Gerze, folk medicines are generally used after being subjected to processes like boiling, infusion preparation, decoction, and poultice; only 26% are used directly. Those for internal use are primarily used in tea formulations, primarily in the form of decoction and infusion (40%). For external usages, different preparation techniques, such as withering and making poultices, are used. The rate of internally used folk medicines is slightly higher (55%) than that of externally used folk medicines (Figure 3). Leaves (44%) and fruits (21%) were the most preferred plant parts in the preparation of folk remedies; they are followed by aerial parts (11%) and flowers (7%). Plant parts such as essential oil and tubers were also used, albeit in small amounts (Figure 4).

As mentioned before, folk medicines are evaluated under 12 illness categories according to the diseases for which they are used, as shown in Table 1. As this table shows, in our study area, folk medicines are mostly used in for respiratory diseases, with 27 species cited 86 times, and dermatological diseases, with 22 species cited 86 times. Musculoskeletal (19 species, 62 citations) and gastrointestinal system diseases (29 species, 59 citations) are the other categories in which folk remedies are most frequently used. However, when FIC values are considered, dermatological system disorders are ranked first (FIC: 0.7529) and, followed by musculoskeletal (FIC: 0.7049), respiratory (FIC: 0.6941), and cardiovascular system disorders (FIC: 0.5882). The difference between sorting by FIC and citation was thought to be due to disagreements and the utilization of the same plant for diverse purposes.

Threat categories of plants were determined according to the Red Data Book of Turkish Plants and the International Union for Conservation of Nature. One of the plants used as folk medicine in the region, *Sempervivum brevipilum* Muirhead (Figure 5), is endemic, and its IUCN category is Least Concern (LC). *Platycladus orientalis* (L.) Franco is categorized as near threatened, while the 28 folk medicines identified in the research area are categorized as LC.[33]

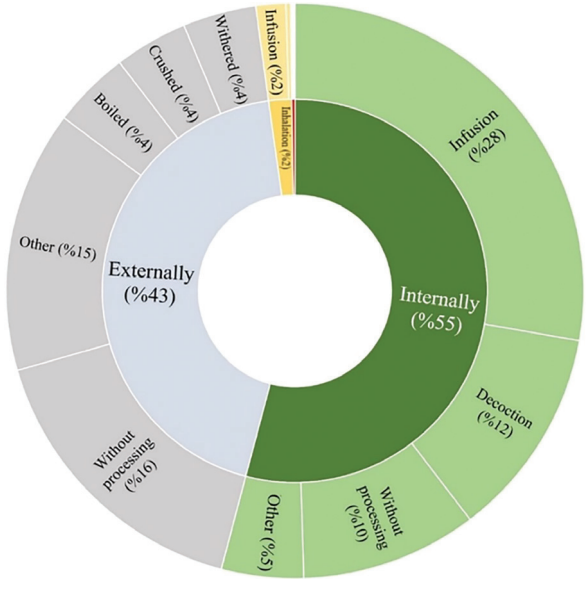

Figure 3. Application and preparation methods of folk medicines

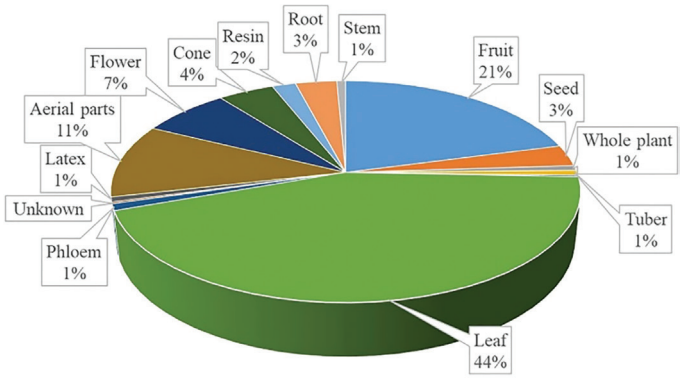

Figure 4. Distribution of plants according to the parts used as folk medicine

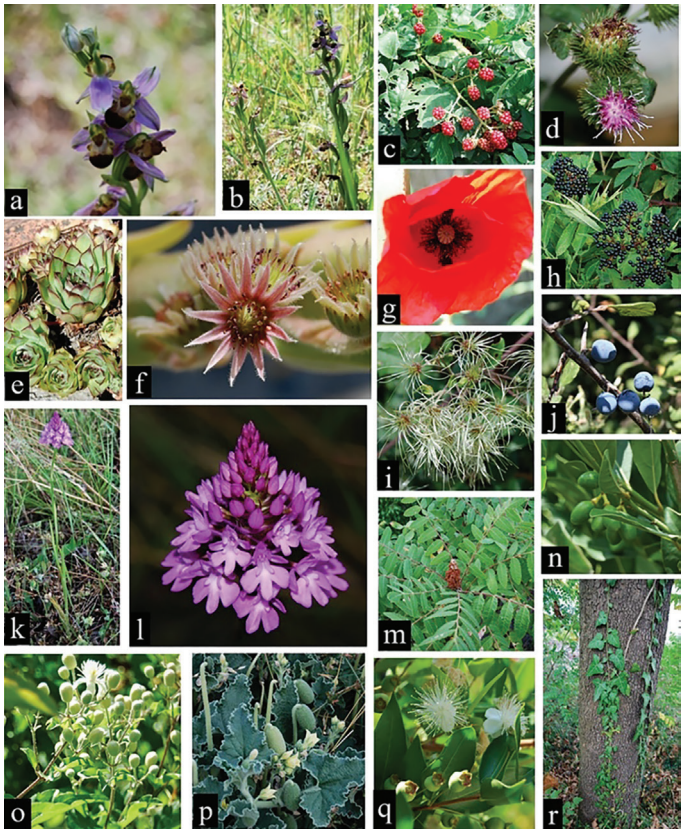

Figure 5. Examples of some interesting folk medicines

a, b: Serapias vomeracea; c: Rubus sanctus; d: Arctium minus; e, f: Sempervivum brevipilum; g: Papaver rhoeas; h: Sambucus ebulus; i: Clematis vitalba; j: Berberis crataegina, k, l: Anacamptis pyramidalis; m: Rhus coriaria; n: Laurus nobilis; o: Smilax excelsa; p: Ecballium elaterium; q: Myrtus communis subsp. communis; r: Hedera helix

DISCUSSION

The results of this investigation are expected to essentially contribute to the ethnobotanical inventory of Türkiye. To the best of our knowledge, *S. brevipilum* and *Serapias vomeracea* (Burm.f.) Briq. were recorded as folk medicine for the first time with this research. In addition, 33 new usages for 25 species previously reported as folk medicine have been identified. In the Supplementary Table 1, the new usage records identified in this study regarding the previously identified folk remedies are underlined. For instance, this study is the first to document the traditional use of *Anacamptis pyramidalis* (L.) Rich as an antitussive remedy in folk medicine. Similarly, *Datura stramonium* L. and *F. carica* have been documented here for their ethnobotanical use in the treatment of jaundice. Notably, the use of *Xanthium spinosum* L. for managing malaria is also recorded for the first time in this research. These findings suggest that future investigations could focus on evaluating the antimalarial activity of *X. spinosum* and isolating the bioactive compounds responsible for its effects. Additionally, the traditional use of *Rubus sanctus* Schreb. in the treatment of gonorrhea represents a novel finding. Microbiological and clinical studies may facilitate the identification of potential therapeutic compounds from this species, contributing to the development of alternative treatments for gonorrhea, a disease that continues to impact a significant global population.

No previous ethnobotanical study has been conducted in the Gerze district. However, it appears that a study covering the central and western Black Sea regions of Türkiye, including 5 localities from Sinop's districts other than Gerze, was conducted. In this research, 25 plant species belonging to 24 genera from 21 families were identified as being used as folk medicine in Sinop historically. When the findings of this study were compared with our results, it was observed that there are many similarities to folk remedies in the neighboring districts of Gerze, such as Boyabat and Dikmen. For instance, *Cornus mas* L.; used against diarrhoea, *Juniperus oxycedrus* L.; is used against haemorrhoid, *Cydonia oblonga* Mill.; used against cough, *Tilia rubra* (Weston) DC.; is used against common cold and cough, and *U. dioica*; used to reduce blood sugar levels, are used for the same conditions in both districts.[8] The similarities in the local names given to the same species were also noted: *S. ebulus* (yüyün, yetün, yiğtün), *Arctium minus* (Hill) Bernh. (kabalak, kabalayık), *Euphorbia stricta* L. (sütliğen), and *Plantago major* L. (siğil yaprağı, siyil yaprağı) were found to have the same or very similar local names in the present study, and Fujita et al.[8] research conducted in different districts of Sinop. In addition, similarities were observed with folk medicines in different cities of Türkiye as well as in neighboring, nearby districts. For example, *C. mas* is utilized for diarrhea in different parts of Türkiye (e.g., Düzce, Manisa, Erzurum), including Gerze.[16,34-36] *Ecballium elaterium* (L.) A. Rich. is used in the treatment of sinusitis in Gerze, as in many regions of Türkiye.[16,34-41] Latex of *F. carica* is used to remove warts in Düzce, Gaziantep, and Denizli, just as it is in Gerze.[16,40]

Likewise, *S. ebulus* leaf is used against pain in Düzce, Kocaeli, Sakarya, Zonguldak, Hatay, Kahraman Maraş, as in Gerze.[16,42,43] As in many regions of Türkiye, the use of *Plantago* species for wound healing and maturation of abscess and the use of *Urtica* species in joint diseases, such as rheumatism, is common in Gerze as well.[16,31,34-36,40] Furthermore, *C. oblonga*, *Laurus nobilis* L., *Mespilus germanica* L., *Morus alba* L., *N. tabacum*, *P. nigra* subsp. *nigra*, *Smilax excelsa* L., and *Sorbus domestica* L. were used in different provinces in a similar manner to determine in

our study area.[16,31,34-36,38] Because of the similar flora and ease of information exchange, encountering similarities in neighboring or close regions is expected. The reasons for identifying the same folk remedies in remote areas are considered to include internal migration and information reaching remote areas due to improvements in communication facilities. In addition, obtaining similar folk medicinal usages for a plant in different regions supports the accuracy of the information obtained.

Different species of one genus have also been observed to be used for similar purposes in Gerze and other parts of Türkiye. One example of this situation is the *Malva* species. In Düzce and Erzurum, *Malva neglecta* Wallr. and *Malva nicaeensis* All. are used against stomach ailments like stomach ache, gastric ulcers,[16,34] similarly, *Malva sylvestris* L. is also used for stomach ache in Gerze. Another example is *Equisetum* species; *Equisetum hyemale* L. is used against stomach disorders in Gerze, another *Equisetum* species, *Equisetum ramosissimum* Desf. is also determined to be used for stomach aches in Manisa.[35] *Euphorbia coniosperma* Boiss. & Buhse is used in the treatment of warts, similar to the documented uses of *E. stricta* in Gerze.[37] The reason for this may be that local people consider different species of the same genus as the same plant, which are morphologically similar and can only be differentiated by expert botanists, leading to their use for the same purposes. In other words, local people may have learned the folk remedies used in different regions, prepared them with similar plants grown in their own region and tried them. Consequently, they may have continued to use that folk medicine after seeing a beneficial effect. It can be argued that immigrants use other plants similar to those grown in the places they come from, and these new folk medicines may have been included in the folk medicine knowledge of that region over time.

In contrast to these similarities, the same plant species is used for quite different purposes when compared to nearby regions. For example, *Vicia faba* L. is used for memory impairment and for reducing symptoms of dementia in Gerze, but in Fujita et al.[8] research, it is used for the maturation of abscesses in Dikmen (Sinop), one of the neighboring districts. *Berberis crataegina* DC., used against anal fistula in Boyabat (Sinop), is also used in eye diseases in Gerze. Another example of this situation is *A. minus*. It is used for sunstroke in the Durağan and Boyabat districts of Sinop, while in Gerze, it is used for knee and abdominal pain.[8] During the search for treatments for diseases observed in themselves or their relatives, people may have tried medicines prepared from easily accessible plants, and thus, quite different uses for the same plant may have been derived.

In accordance with the definition of folk medicine, the folk remedies used in Gerze are usually mono-component and prepared by simple methods such as infusion and decoction. However, there are also folk medicines in which multi-component, more complex preparation techniques are applied. For example, in the treatment of hernia, *Ficus carica* L. fruits are mixed with fava beans and lemon juice, and this mixture is cooked to obtain a poultice, which is then applied. Another example of this situation is the use of *P. nigra* subsp. *nigra* resin for treating wounds and abscesses. An ointment used for wound healing is obtained by mixing its resin with soap and heating. Likewise, its resin and soap are placed in hollowed onion, heated and used against abscesses.

In many regions of Türkiye, plants that are considered useful for many diseases have been evaluated as a "panacea" among the people. *Anthemis cotula* L., *Hypericum perforatum* L., *Matricaria chamomilla* L. var. *recutita* (L.) Grierson, and *Papaver rhoeas* L. are reported to be used as a panacea in Gerze as well.

The use of *B. crataegina* in the region provides an example of issues that highlight the importance of folk medicinal studies from another perspective. *B. crataegina* fruit is used to reduce blood sugar levels in Gerze. The α-amylase and α-glucosidase inhibitory effect of three different extracts [ethanol (0.1% trifluoroacetic acid), ethanol:water (70:30, 0.1% trifluoroacetic acid) and water (0.1% trifluoroacetic acid)] prepared from *B. crataegina* fruit has been studied *in vitro*. In this study, the aforementioned *B. crataegina* extracts were determined to inhibit the α-glucosidase and α-amylase by 23% and 76%.[44] These data suggest that *B. crataegina* may also exhibit antidiabetic activity in a bioactivity study to be carried out.

Interestingly, the use of an intoxicating plant was also determined while researching folk medicines in the region. The seeds of *D. stramonium* are placed in cigarettes and smoked as a hallucinogen.

As can be seen in the Supplementary Table 1, macerate of *P. rhoeas* flowers is used against cough. Although phytochemical studies have shown no or very low levels of codeine in *P. rhoeas*, different alkaloids with a structure similar to codeine in the plant are thought to be responsible for this effect.

As in different parts of Türkiye, *S. ebulus* is used against pains or for musculoskeletal system diseases such as sprains and bruises in most of the visited locations.[16,42,45-48] Different extracts prepared from *S. ebulus* and the isolated compounds have been shown to have antinociceptive activity in bioactivity studies.[49-50] The consistency of the folk medicine records obtained in the region with bioactivity studies supports the reliability and value of our findings.

Study limitations

This study was geographically limited to the Gerze district. A significant limitation was the declining population in rural villages, primarily due to migration to urban centers or larger cities such as Ankara and İstanbul. Additionally, the younger generation's diminishing interest in folk medicine further restricted the availability of ethnobotanical knowledge. The inability to access some knowledgeable elderly individuals during the study period posed another challenge, further limiting the scope of the investigation.

CONCLUSION

As far as we know, this is the first study recording folk medicines in the Gerze District. It is thought that this research has made an essential contribution to the ethnobotanical inventory of Türkiye. In addition, 33 new usages for 25 previously reported

folk medicines, *S. brevipilum*, and *S. vomeracea* were recorded as folk medicines for the first time with this research. Besides their cultural importance, folk remedies are important sources for new drug discovery. However, this study has shown once again that folk medicine knowledge is rapidly disappearing due to decreasing village populations, increased educational status, and ease of reaching orthodox medicine and drugs. The loss of knowledgeable elders and the lack of interest among younger generations further contribute to the erosion of traditional knowledge. Although awareness of this issue has been increasing in recent years, and ethnobotanical inventory studies have gained momentum across Türkiye, many regions remain unexplored in an ethnobotanical context. It is therefore essential to document this valuable cultural heritage before it disappears entirely.

Ethics

Ethics Committee Approval: Not required.

Informed Consent: Not required.

Footnotes

Authorship Contributions

Concept: E.S., İ.G., Design: E.S., İ.G., Data Collection or Processing: T.G., O.K., Analysis or Interpretation: T.G., O.K., E.S., İ.G., Literature Search: T.G., O.K., Writing: T.G., O.K., E.S., İ.G.

Conflict of Interest: The authors declare no conflicts of interest.

Financial Disclosure: The authors declared that this study received no financial support.

REFERENCES

1. Yesilada E. Past and future contributions to traditional medicine in the health care system of the Middle-east. J Ethnopharmacol. 2005;100:135-137.
2. Gertsch J. How scientific is the science in ethnopharmacology? Historical perspectives and epistemological problems. J Ethnopharmacol. 2009;122:177-183.
3. Yesilada E, Sezik E. A survey on the traditional medicine in Turkey: Semi-quantitative evaluation of the results. In: Singh V, Govil J, Hashmi S, Singh G, eds. Ethnomedicine and Pharmacognosy-II. Texas; Studium Press; 2003.
4. Yesilada E. An overview of Turkish folk medicine; past and present. Curr Drug Deliv. 2013;10:92-95.
5. Dalar A, Mukemre M, Unal M, Ozgokce F. Traditional medicinal plants of Agri Province, Turkey. J Ethnopharmacol. 2018;226:56-72.
6. Sezik E. Türkiye'de Halk İlaçları Araştırmaları ve Önemi. In: Başer KHC, eds. 9. Bitkisel İlaç Hammaddeleri Toplantısı. Eskişehir; Anadolu Üniversitesi Yayınları; 1991. p.1-7.
7. Gurbuz I, Ozatkan G, Akaydin G, Gunbatan T. Ethnopharmacobotanical findings of medicinal plants in the Kızılcahamam district of Ankara, Turkey. Turkish J Pharm Sci. 2021;18:667-682.
8. Fujita T, Sezik E, Tabata M, Yesilada E, Honda G, Takeda Y, Tanaka T, Takaishi Y. Traditional medicine in Turkey VII. Folk medicine in middle and west Black Sea regions. Econ Bot. 1995;49:406-422.
9. T.C. Gerze Kaymakamlığı. http://www.gerze.gov.tr/ilcemiz
10. Davis PH. Flora of Turkey and the East Aegean Islands. Edinburgh: Edinburgh University Press; 1965-1985.
11. T.C. Kuzey Anadolu Kalkinma Ajansi, Gerze İlçe Analizi. https://www.kuzka.gov.tr/Icerik/Dosya/www.kuzka.gov.tr_18_IO6E24UD_gerze_ilce_analizi.pdf).
12. Ozen F. Alaçam-Gerze ve Boyabat-Durağan arasında kalan bölgenin vejetasyonu üzerinde floristik fitososyolojik ve ekolojik bir araştırma. Fac Arts Sci Ondokuz Mayıs Univ. 1993.
13. Sezik E, Tabata M, Yesilada E, Honda G, Goto K, Ikeshiro Y. Traditional medicine in Turkey I. Folk medicine in northeast Anatolia. J Ethnopharmacol. 1991;35:191-196.
14. Thring TSA, Weitz FM. Medicinal plant use in the Breadasdorp/Elim region of the Southern Overberg in the Western Cape Province of South Africa. J Ethnopharmacol. 2006;103:261-275.
15. Karci E, Gurbuz İ, Akaydin G, Günbatan T. Folk medicines of Bafra (Samsun-Turkey). Turkish J Biochem. 2017;42:381-399.
16. Gürbüz İ, Gençler Özkan AM, Akaydın G, Salihoğlu E, Günbatan T, Demirci F, Yeşilada E. Folk medicine in Düzce province (Turkey). Turkish J Bot. 2019;43:769-784.
17. Davis PH, Mill R, Tan K. Flora of Turkey and the East Eagean Islands. Edinburgh: Edinburgh University Press; 1988.
18. Guner A, Ozhatay N, Ekim T, Baser KHC. Flora of Turkey and the East Aegean Islands. Vol. 11. Edinburgh: Edinburgh University Press; 2000.
19. Güner A, Kandemir A, Menemen Y, Yıldırım H, Aslan S, Çimen AÖ, Ekşi Bona G, Güner I, Şen Gökmen F. Resimli Türkiye Florası (Illustrated Flora of Turkey). Vol. 2. İstanbul: ANG Vakfı Nezahat Gökyiğit Botanik Bahçesi Yayınları; 2018.
20. World Flora Online. https://wfoplantlist.org/plant-list/
21. Trotter RT, Logan MH. Informant Concensus, a New Approach for Identifying Potentially Effective Medicinal Plants. In: Etkin NL, eds. Plants in Indigenous Medicine and Diet, Biobehavioural Approaches. New York: Redgrave Publishing Company; 1986.
22. Heinrich M. Ethnobotany and its role in drug development. Phytother Res. 2000;14:479-488.
23. Byg A, Balslev H. Diversity and use of palms in Zahamena, Eastern Madagascar. Biodiv Conserv. 2001;10:951-970.
24. Albuquerque UP, Lucena RFP, Montero J, Florentino ATN, Almeida CFCBR. Evaluating two quantitative ethnobotanical techniques. Ethnobot Res Appl. 2006;4:51-60.
25. Prance GT, Balee W, Boom BM, Carneiro RL. Quantitative ethnobotany and the case for conservation in Amazonia. Conserv Biol. 1987;1:296-310.
26. Abe R, Ohtani K. An ethnobotanical study of medicinal plants and traditional therapies on Batan Island, the Philippines. J Ethnopharmacol. 2013;145:554-565.
27. Tardío J, Pardo-De-Santayana M. Cultural importance indices: a comparative analysis based on the useful wild plants of Southern Cantabria (Northern Spain). Econ Bot. 2008;62:24-39.
28. Karaer F. Sinop yarımadasının florası üzerinde bir araştırma. Fac Arts Sci Ondokuz Mayıs Univ. 1989.
29. Guner A. Resimli Türkiye Florası. Vol. 1. İstanbul: Flora Araştırmaları Derneği, Türkiye İşbankası Kültür Yayınları; 2014.
30. Ezer N, Arisan OM. Folk medicines in Merzifon (Amasya, Turkey). Turkish J Bot. 2006;30:223-230.

31. Akbulut S, Bayramoğlu MM. Reflections of socio-economic and demographic structure of urban and rural on the use of medicinal and aromatic plants: The sample of Trabzon province. Stud Ethno-Med. 2014;8:89-100.

32. Polat R, Cakilcioglu U, Kaltalioglu K, Ulusan MD, Turkmen Z. An ethnobotanical study on medicinal plants in Espiye and its surrounding (Giresun-Turkey). J Ethnopharmacol. 2015;163:1-11.

33. Ekim T, Koyuncu M, Vural M, Duman H, Aytac Z, Adıgüzel N. Türkiye Bitkileri Kırmızı Kitabı (Eğrelti ve Tohumlu Bitkiler). 1st ed. Ankara: Barışcan Ofset; 2000.

34. Sezik E, Yeşilada E, Tabata M, Honda G, Takaishi Y, Fujita T, Tanaka T, Takeda Y. Traditional medicine in Turkey VIII. Folk medicine in east Anatolia; Erzurum, Erzincan, Ağrı, Kars, Iğdır provinces. Econ Bot. 1997;51:195-211.

35. Bulut G, Tuzlaci E. An ethnobotanical study of medicinal plants in Turgutlu (Manisa-Turkey). J Ethnopharmacol. 2013;149:633-647.

36. Altundag E, Ozturk M. Ethnomedicinal studies on the plant resources of east Anatolia, Turkey. Procedia Soc Behav Sci. 2011;19:756-777.

37. Sezik E, Yesilada E, Honda G, Takaishi Y, Takeda Y, Tanaka T. Traditional medicine in Turkey X. Folk medicine in central Anatolia. J Ethnopharmacol. 2001;75:95-115.

38. Akaydın G, Simsek I, Arıtuluk ZC, Yesilada E. An ethnobotanical survey in selected towns of the Mediterranean subregion (Turkey). Turkish J Biol. 2013;37:230-247.

39. Akyol Y. Ethnobotanical studies in the Maldan Village (Province Manisa, Turkey). Marmara Pharm J. 2013;1:21-25.

40. Bulut G, Haznedaroglu MZ, Dogan A, Koyu H, Tuzlacı E. An ethnobotanical study of medicinal plants in Acıpayam (Denizli-Turkey). J Herb Med. 2017;10:64-81.

41. Akgul A, Akgul A, Senol SG, Yildirim H, Secmen O, Dogan Y. An ethnobotanical study in Midyat (Turkey), a city on the silk road where cultures meet. J Ethnobiol Ethnomed. 2018;14:1-18.

42. Yeşilada E, Honda G, Sezik E, Tabata M, Fujita T, Tanaka T, Takeda Y, Takaishi Y. Traditional medicine in Turkey V. Folk medicine in the inner Taurus Mountains. J Ethnopharmacol. 1995;46:133-52.

43. Yesilada E, Sezik E, Honda G, Takaishi Y, Takeda Y, Tanaka T. Traditional medicine in Turkey IX: Folk medicine in north-west Anatolia. J Ethnopharmacol. 1999;64:195-210.

44. Varol C. Researches on *in vitro* α-Amylase ve α-Glucosidase enzyme inhibitor activities of some plants which are used for diabetes in Anatolian ethnobotany. Ege Üniv. 2020.

45. Genc GE, Ozhatay N. An ethnobotanical study in Catalca (European part of Istanbul) II. Turkish J Pharm Sci. 2006;3:73-89.

46. Demirci S, Ozhatay N. An ethnobotanical study in Kahramanmaraş (Turkey); Wild plants used for medicinal purpose in Andırın, Kahramanmaraş. Turkish J Pharm Sci. 2012;9:75-92.

47. Bulut G, Tuzlaci E. An ethnobotanical study of medicinal plants in Bayramiç. Marmara Pharm J. 2015;19:268-282.

48. Badem M, Korkmaz N, Sener S, Kanpolat S, Ozge U, Sevgi S, Aliyazıcıoğlu R, Coşkun M. Biological screening of traditional medicinal plants from villages of Akkus (Ordu) in Turkey on the effects of tyrosinase. J Pharm Res Int. 2018;25:1-10.

49. Schwaiger S, Zeller I, Pölzelbauer P, Frotschnig S, Laufer G, Messner B, Pieri V, Stuppner H, Bernhard D. Identification and pharmacological characterization of the anti-inflammatory principal of the leaves of dwarf elder (*Sambucus ebulus* L.). J Ethnopharmacol. 2011;133:704-709.

50. Tasinov O, Dincheva I, Badjakov I, Kiselova-Kaneva Y, Galunska B, Nogueiras R, Ivanova D. Phytochemical composition, anti-inflammatory and ER stress-reducing potential of Sambucus ebulus L. fruit extract. Plants. 2021;10:2446.

Click the link to access Supplementary Table 1: https://d2v96fxpocvxx.cloudfront.net/a426c3a3-a110-40af-a6dd-1b2b563ce9ac/content-images/31d38b12-a104-41e4-8e75-088b1515b253.pdf

Turk J Pharm Sci 2025;22(3):170-177
DOI: 10.4274/tjps.galenos.2025.46837

ORIGINAL ARTICLE

Effect of PGV-1 on Apoptosis *via* Mitotic Arrest and Senescence in Polyploid Giant Cancer Cells of Hepatocellular Carcinoma JHH4

Nadzifa NUGRAHENI[1], Beni LESTARI[2], Edy MEIYANTO[3], Rohmad Yudi UTOMO[4]*

[1]Universitas Gadjah Mada, Graduate School of Biotechnology, Yogyakarta, Indonesia
[2]Universitas Gadjah Mada, Faculty of Medicine, Department of Pharmacology and Therapy, Division of Public Health and Nursing, Yogyakarta, Indonesia
[3]Universitas Gadjah Mada, Faculty of Pharmacy, Department of Pharmaceutical Chemistry, Laboratory of Macromolecular Engineering, Yogyakarta, Indonesia
[4]Universitas Gadjah Mada, Faculty of Pharmacy, Department of Pharmaceutical Chemistry, Laboratory of Medicinal Chemistry, Yogyakarta, Indonesia

ABSTRACT

Objectives: Senescent cells release a senescence-associated secretory phenotype, promoting polyploid giant cancer cells (PGCCs) to emerge, fostering tumor heterogeneity and resistance. Pentagamavunone-1 (PGV-1) emerges as a promising agent inducing senescence and prometaphase arrest, resulting in permanent cytotoxicity. This study was aimed to investigate the effect of PGV-1 in dysregulating mitosis through the modulation of PGCCs and senescence in low MYCN-expressing hepatocellular carcinoma (HCC) cells JHH4.

Materials and Methods: To assess the physiological effects of PGV-1, several *in vitro* tests were done including the MTT assay, cell cycle assay, May-Grünwald-Giemsa staining, senescence associated-β-galactosidase (SA-β-Gal) assay, and apoptosis assay. The protein levels of the apoptosis regulatory protein were evaluated using western blot analysis. The interaction of PGV-1 toward the protein that plays a role in PGCCs formation was simulated by molecular docking and molecular dynamics (MD).

Results: The cytotoxic assay revealed that PGV-1 inhibited the proliferation of JHH4 liver cancer cells permanently. Inhibition of cell proliferation by PGV-1 was associated with the modulation of G2/M phase, particularly mitotic arrest and formation of PGCCs. The SA-β-Gal verified that PGV-1 induced senescence in cells (p<0.01), inducing PGCCs formation. Apoptotic mechanisms were validated *via* Annexin V staining, which showed the level of cleaved poly (ADP-ribose) polymerase (p<0.001). Molecular docking and MD simulations suggested that PGV-1 could interfere with the conformation of the chromosomal passenger complex (CPC) protein, particularly disrupting essential interactions within the inner centromere protein, Survivin, and Borealin.

Conclusion: PGV-1 induced strong cytotoxicity in HCC cells by disrupting mitosis leading to PGCC formation, senescence, and subsequent apoptotic cell death.

Keywords: PGV-1, polypoid giant cancer cells, senescence, apoptosis, hepatocellular carcinoma

INTRODUCTION

Polyploid giant cancer cells (PGCCs) and cellular senescence play multifaceted roles in the cell cycle machinery of hepatocellular carcinoma (HCC). PGCCs are characterized by abnormal polyploidization, leading to errors in mitotic spindle assembly and chromosomal segregation during mitosis.[1] Aberrant centrosome function in PGCCs contributes to the enlarged cell size and genomic instability, defining the characteristic morphology of PGCCs.[2,3] PGCCs exhibit a senescence-like phenotype, contributing to chemoresistance by evading the cytotoxic effects of chemotherapy drugs.[4] Simultaneously, the irreversible growth arrest characteristic of cellular senescence can create a microenvironment rich in senescence-associated secretory phenotype (SASP) factors,

***Correspondence:** rohmad.yudi.utomo@ugm.ac.id, **ORCID-ID:** orcid.org/0000-0003-4803-9417
Received: 20.05.2024 , **Accepted:** 02.06.2025 **Publication Date:** 01.08.2025

Cite this article as: NUGRAHENI N, LESTARI B, MEIYANTO E, UTOMO R. GV-1 promotes apoptosis *via* mitotic arrest and senescence in polyploid giant cancer cells of hepatocellular carcinoma JHH4 Turk J Pharm Sci. 2025;22(3):170-177

influencing the behavior of neighboring cancer cells, including the emergence of PGCCs.[5,6] The dynamic interaction between PGCCs and cellular senescence promotes heterogeneity within the tumor, fostering adaptability and resistance mechanisms.[7] Understanding the crosstalk between PGCCs and senescence is crucial for developing chemotherapeutic agents targeting cell cycle machinery in HCC.

The induction of senescence and dysregulation of mitosis represent two primary physiological effects of pentagamavunone-1 (PGV-1) (Figure 1a) in various cancer cells. PGV-1 triggers senescence through transient elevation in reactive oxygen species (ROS) by interacting with several ROS-metabolizing enzymes.[8] PGV-1 promotes prometaphase arrest, leading to permanent cytotoxic effects on leukemia.[8] In both triple-negative breast cancer (TNBC) and non-TNBC cells, PGV-1 increased polyploid cells as an indication of mitotic catastrophe.[9-11] Functional network analysis with molecular docking studies revealed that PGV-1 could target several mitotic checkpoints such as aurora kinase A (AURKA), aurora kinase B (AURKB), polo-like kinase 1 (PLK1), and cyclin-dependent kinase 1 (CDK1).[12] AURKB is a member of the chromosomal passenger complex (CPC) localized at the centromere from prophase to the metaphase-anaphase transition. The CPC consists of four proteins: the AURKB, the scaffold protein inner centromere protein (INCENP) and two targeting proteins, Survivin and Borealin. Reducing or disrupting the activity of any component within CPC results in cytokinesis defects, leading to subsequent multinucleation, resembling the phenotype of PGCCs.[13-15] The effect of PGV-1 on the CPC complex remains unexplored.

Dysregulation of mitosis and induction of senescence by PGV-1 also persist in MYCN-expressing HCC, including HepG2 and JHH7 cells.[15,16] During mitosis, aberrant MYCN expression contributes to centrosome duplication, spindle formation, and chromosome segregation in HCC.[17] MYCN also activates CDK1 to promote mitosis through Aurora A-PLK1 cascades.[18] However, PGV-1 does not affect the mRNA level of MYCN, suggesting that PGV-1 targets different proteins in the dysregulation of centrosomes during mitosis in HepG2 and JHH7.[16] These distinctive phenotypic changes induced by PGV-1, especially in the cell cycle machinery of HCC, provide attractive attributes for targeting PGCCs.

In this study, we aimed to investigate the effect of PGV-1 in dysregulating mitosis through the modulation of PGCCs and senescence in low MYCN-expressing HCC, JHH4 cells. Similar to other cancer types, PGV-1 is expected to exhibit potent cytotoxic effect in JHH4 cells. We identified changes in the phenotype of JHH4 cells based on the cell cycle profile, mitotic phase profile, the presence of senescent cells, and predicted CPC-related targets through computational analysis.

MATERIALS AND METHODS

Compound

PGV-1 was obtained from our compound collection and synthesized as previously reported.[19] For each biological assay, PGV-1 is dissolved in dimethyl sulfoxide to prepare a stock solution. These stock solutions are then diluted for various concentrations for specific experiments.

Cell culture and reagents

JHH4 cells were kindly provided by Professor Yoshitaka Hippo and Dr. Yusuke Suenaga (JRBC® CRL-2359) from Chiba Cancer Center Research Institute, Japan. The cells were maintained under standard conditions (37 °C, 5% CO^2) in high glucose Dulbecco's Modified Eagle Medium (Gibco USA) enriched with HEPES (Sigma), 10% fetal bovine serum (Gibco USA), and 1% penicillin-streptomycin (Gibco USA).

MTT assay

A 96-well plate was seeded with 1×10^4 cells per well, and the cells were cultured until reaching 80% confluency. PGV-1 (0.1-10 μM) was then administered to the cells in repeated doses, followed by incubation for 24 and 48 hours. After the incubation period, MTT (Sigma) reagent was added, and absorbance was measured at 595 nm using a multi-plate reader (BioRad). The absorbance values were converted into percentages of cell viability using Hill's equation to determine the half-maximal inhibitory concentration (IC_{50}) value.[20]

Cell cycle analysis

In brief, JHH4 cells were cultured and treated with PGV-1 for 24 hours. The cells were trypsinized and washed with cold 1X phosphate-buffered saline (PBS). Fixation was performed by adding 70% ethanol for 30 minutes, followed by replacement with 1X PBS. The cells were incubated with a staining solution containing 200 μL 1X propidium Iodide and RNase, prepared according to the kit protocols (Abcam, ab139418), for 20-30 min. The distribution of the cell cycle BD fluorescence-activated cell sorting Calibur flow cytometer.

May-Grünwald Giemsa staining

JHH4 cells were seeded in a 6-well plate at a density of 2.5×10^4 cells per well and incubated with PGV-1 for 24 hours. After removing the medium and washing with 1X PBS, the cells were stained with May-Grünwald stain solution for 5 min, followed by two washes with 1X PBS. Additional staining was performed using 1:20 *v/v* Giemsa solution, followed by air drying. The mitotic phase was evaluated based on the chromosomal formation observed under a phase-contrast microscope.[10]

Senescence associated-β-galactosidase (SA-β-gal) assay

PGV-1 was applied to JHH4 cells that had been seeded at a density of 3×10^6 cells per well on a 6-well plate and incubated for 24 hours. After two washes with 1X PBS, the cells were fixed for 10 to 20 minutes and then washed again with 1X PBS. Cells were stained using an X-gal solution for 72 hours at 37 °C. The presence of senescence was indicated by the green color under the microscope.[21]

Apoptosis assay

Apoptosis assays were performed according to the manufacturer's instructions (Apoptosis Detection Kit I, Cat. 556547). JHH4 cells were treated with PGV-1 for 24 hours. After treatment, cells were harvested using trypsin and washed

with cold 1x PBS. The cells were then resuspended in 1x binding buffer, and equal amounts of fluorescein isothiocyanate Annexin V and propidium iodide were added. The cells were gently vortexed and incubated at 25 ˚C in the dark for 15 minutes. Apoptotic cells were detected using the FACSCalibur flow cytometer.

Western blotting

Briefly, JHH4 cells were seeded at a density of 1 × 10^6 cells per well in a 6-well plate and treated with or without PGV-1 for 24 hours. After treatment, cell lysates were collected using a radioimmunoprecipitation assay buffer. The samples were separated by Sodium dodecyl sulfate – polyacrylamide gel electrophoresis and transferred to a polyvinylidene fluoride membrane. After blocking with 5% bovine serum albumin for 2 hours, the membranes were incubated with primary antibodies: anti-poly(ADP-ribose) polymerase (PARP) antibody (Cell Signaling Technology, PARP (46D11) Antibody #9532) at a 1:1000 dilution, and anti-β-actin antibody (Cell Signaling Technology, #3700) at a 1:5000 dilution, which served as the housekeeping protein. The membranes were probed overnight with primary antibodies at 4 ˚C with gentle agitation. After washing with PBST, the membranes were incubated with an anti-rabbit immunoglobulin G (IgG) secondary antibody (anti-rabbit IgG, horseradish peroxidase-linked Antibody #7074) for 1 hour at room temperature. Chemiluminescent signals were detected using the ImageQuantTM TL with enhanced chemiluminescence Western Blotting Substrate (Bio-Rad). ImageJ software was then used to semi-quantify and normalize the intensity of each band relative to the housekeeping protein (anti-β-actin antibody).[16]

Molecular docking

Molecular docking was performed to predict the binding interaction between PGV-1 and CPC protein, which is among the proteins involved in PGCC generation. The crystal structure of CPC was obtained from the PDB (ID: 2QFA). The binding site for the molecular docking simulation was identified based on the core of CPC, which consists of the interacting amino acids among INCENP, Borealin, and Survivin.[22] The molecular docking simulation was carried out using the default protocol in molecular operating environment, with slight modifications.[23] The conformation of PGV-1 with the lowest docking score was selected for binding interaction analysis.

Molecular dynamics

The stability and conformational changes of PGV-1 in complex with CPC were evaluated by molecular dynamics (MD) simulation. Nanoscale molecular dynamics 2.14 was used for the MD simulation, and the resultant trajectories were visualized with visual molecular dynamics 1.9.4.[24,25] The ligands and protein were parameterized using CGenFF and CHARMM36, accessed through the CHARMM-GUI web server.[26] The preparation included adding water molecules in a cubic box with 20-Å padding for solvation and neutralization, followed by the introduction of K^+ and Cl^- ions. The complex then underwent 70 ps of minimization and a 1000 ps equilibration simulation. To further refine the MD simulation, a 1000 ps production run was performed under the NPT ensemble, maintaining a temperature of 303 K and pressure of 1 atm. The MD results were analyzed based on conformational changes and root mean square deviation (RMSD).

Statistical analysis

The data are expressed as the mean ± standard deviation or standard error (SE) from three independent experiments. Statistical analysis was performed using analysis of variance, followed by the Student's t-test with a 95% and 99% confidence level ($p<0.01$; $p<0.001$). All analyses were conducted using GraphPad Prism software, version 9.0 (GraphPad, San Diego, CA, USA).

RESULTS

PGV-1 permanently inhibits proliferation by inducing G2/M arrest

The establishment of a permanent cytotoxic effect has proven to be a crucial factor in the advancement of chemotherapeutic agents, addressing the challenge of relapse incidence upon the discontinuation of treatment.[27] Based on wash-out experiments, PGV-1 (Figure 1a) exerted strong cytotoxic effects, particularly after withdrawal, in chronic myeloid leukemia, breast cancer, colon cancer, and hepatocellular carcinoma (HCC), with an IC_{50} range of 1-7 μM for 72 h treatment.[8,15,28] However, in high MYCN HCC JHH7, PGV-1 exhibited strong cytotoxicity only after 96 h without affecting MYCN mRNA levels.[16] We are then interested in evaluating the cytotoxicity of PGV-1 toward HCC with low expression of MYCN, the JHH4 cell line. The MTT assay revealed the dose-dependent cytotoxic effect of PGV-1, with IC_{50} values of 10 μM and 1.5 μM for 24 and 48 hours, respectively (Figure 1b). Upon the withdrawal of PGV-1 after three days, the potent cytotoxic effect of PGV-1 remained until six days of observation, indicating the permanent inhibition of proliferation (Figure 1c). The potent cytotoxicity of PGV-1 in JHH4, as reported in other types of cancer cells, confirmed its potential novel phenotypic cytotoxic effect. The induction of a persistent cytotoxic effect has the potential to disrupt the cell cycle. Cell cycle modulation of PGV-1 is associated with G2/M arrest in various cancer cells.[8,15,28,29] We found that PGV-1 consistently induced G2/M arrest in JHH4 and increased the sub-G1 population (Figure 1d). In addition, PGV-1 increased the number of hyperdiploid cells in a dose-dependent manner (Figure 1e). The presence of hyperdiploid cells could indicate an abnormality of genetic material, which could lead to cancer survival or death.[2]

PGV-1 triggers multiple arrests in mitosis and increases senescence cells

The precise regulation of mitosis plays a pivotal role in the action of chemotherapeutic drugs, as aberrations in cell division are a hallmark of cancer.[30] In MYCN-expressing HCC, PGV-1 specifically demonstrated prometaphase and metaphase arrest.[15,16] The May-Grünwald Giemsa staining was used to analyze the mitosis phase affected by PGV-1. At low concentrations, PGV-1 induced chromatin condensation resulting

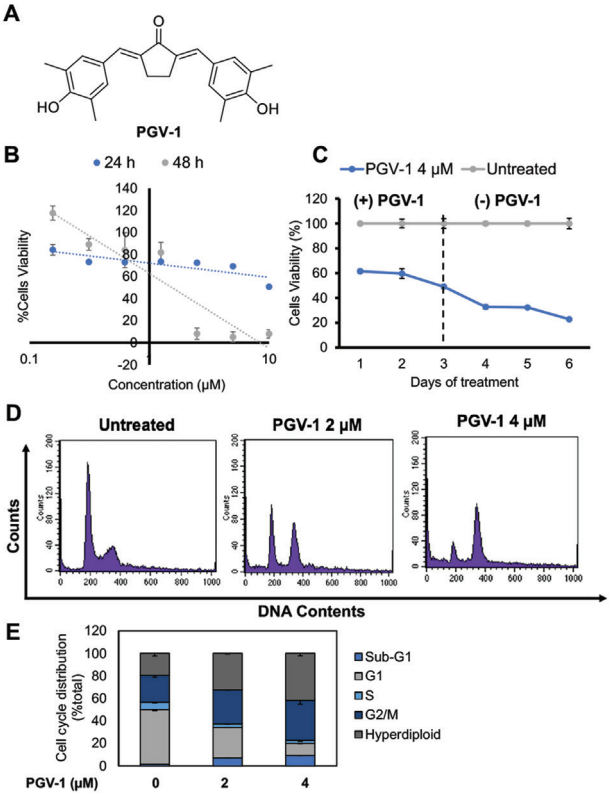

Figure 1. Cytotoxicity of PGV-1 toward JHH4 cells. (A) Chemical structure of PGV-1. (B) Dose-dependent cytotoxic effect in JHH4 cells after PGV-1 is incubated for 24 h and 48 h. (C) JHH4 cells were treated with PGV-1 (4 μM) for 3 days; then the compounds were removed from the medium. Cells viabilitiy was determined at indicated days. (D) JHH4 cells ($2.5x10^5$ cells/mL) were treated with PGV-1 for 24 h, then subjected to propidium iodide-staining flow cytometry for cell cycle analysis. (E) The percentage of cells in each phase as in panel A. Data were expressed on average with SEM (n=3)

SEM: Scanning electron microscope, PGV-1: Pentagamavunone-1

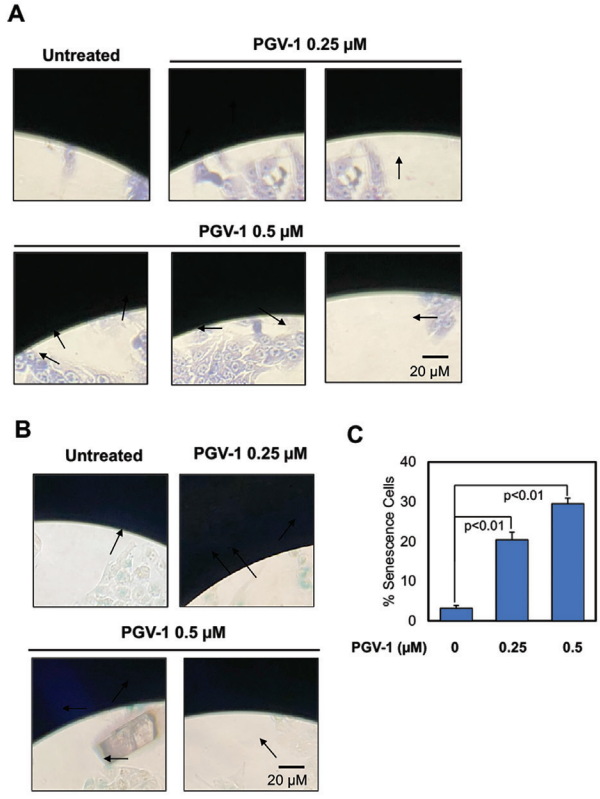

Figure 2. PGV-1 induced metaphase arrest and senescence. (A) JHH4 (3×10^5 cells/well) cells were treated with PGV-1 for 24 h, then stained with a May-Grünwald Giemsa solution. PGV-1 at a concentration of 0.25 μM induced chromatin condensation (left) and mitotic catastrophe (right). At a concentration of 0.5 μM, PGV-1 induced metaphase arrest (left), abnormal anaphase (middle), and PGCCs (right). (B) The percentage of metaphase cells. (C) JHH4 cells (3×10^5 cells/well) were treated with PGV-1 for 24 hours, then stained with an X-gal solution. Senescent cells were marked with arrows. (D) The percentage of senescence cells. Data was expressed on average with SEM (n=3)

SEM: Scanning electron microscope, PGV-1: Pentagamavunone-1

in mitotic catastrophe (Figure 2a). Higher concentrations of PGV-1 triggered metaphase arrest, anaphase abnormality, and PGCCs (Figure 2a). The emergence of PGCCs, characterized by an abnormal number of chromosomes, suggested a unique phenotypical change in PGV-1 in JHH4 cells.

Uncontrolled mitotic activity, which triggers genomic instability, could lead to senescence as a protective mechanism to curb the unbridled proliferation of cancer cells.[31] A reduced prevalence of senescent cells has been implicated in the progression of hepatocarcinogenesis within HCC. Conversely, an elevated abundance of senescent cells is associated with the activation of anti-tumoral mechanisms.[6] The involvement of PGV-1 in eliciting metaphase arrest associated with the senescence arrest in HCC is reported.[16] We found, by SA-β-gal assay, that a low level of cellular senescence was observed in untreated cells and significantly increased in PGV-1-treated cells in a dose-dependent manner (Figure 2b, c). Notably, senescent cells were also identified within the PGCCs, suggesting a connection between genomic rearrangements and the effects of PGV-1 treatment.

The apoptosis mechanism as the final step of the permanent cytotoxic effect by PGV-1

Evidence of senescence in PGCCs facilitated genetic rearrangement in cancer, which led to cancer chemoresistance.[3] The failure of PGCCs regulation could lead to abnormality in cell division, resulting in cell death.[32] We conducted an annexin-V staining to confirm the apoptosis induction of PGV-1, which triggers the PGCCs and senescence in JHH4. PGV-1 increases the incidence of early and late apoptosis (Figure 3a, b). Apoptosis induction by PGV-1 was also identified by the increased protein level of cleaved PARP (Figure 3c, d). Our results confirmed that the induction of senescence and apoptosis by PGV-1 acted as mechanisms to restrict the proliferation of PGCCs, preventing further genomic instability and tumor progression.

Binding interaction of PGV-1 in the chromosomal passenger complex

AURK-PLK1 cascades involving CEP192 and TPX2 tightly regulate the transition of prometaphase to metaphase in mitosis. During preparation to enter anaphase, PLK1 and AURKB

form a complex with CPC, consisting of INCENP, Survivin, and Borealin, to regulate chromosome attachment to the mitotic spindle and ensure proper chromosome segregation (Figure 4a).[18] We hypothesize that the persistent metaphase arrest caused by PGV-1, leading to mitotic catastrophe and PGCCs, was associated with the disruption of the CPC complex. Our molecular docking simulation, focusing on the core of CPC complex, showed PGV-1 interacting with INCENP by forming hydrogen bonding with Gln38 and hydrophobic bonding with Asp27. In addition, PGV-1 formed hydrophobic bonding with Thr127 on survivin (Figure 4b). The multiple interactions of PGV-1 on the core structure might affect the conformational stability of the CPC.

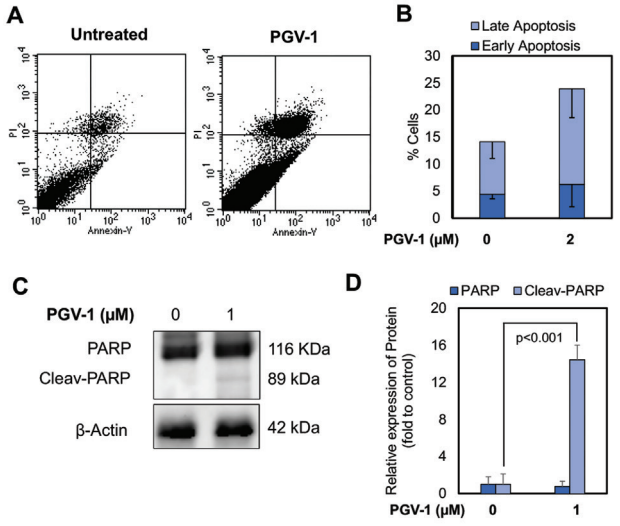

Figure 3. (A) PGV-1 induced apoptosis. JHH4 cells (2.5 x 10^5 cells/mL) were treated with PGV-1 (4 μM) for 24 h, then subjected to Annexin V-staining for apoptosis assay. (B) The percentage of cells undergoing apoptosis as in panel A. Data was expressed on average with SEM (n=3). (C) Protein expression level of PARP in JHH4 after treatment with PGV-1 determined by western blotting. (D) Quantitative analysis of C, PARP, and Cleav-PARP normalized against β-actin. Data was expressed on average with SEM (n=3)

SEM: Scanning electron microscope, PGV-1: Pentagamavunone-1, PARP: Poly (ADP-ribose) polymerase

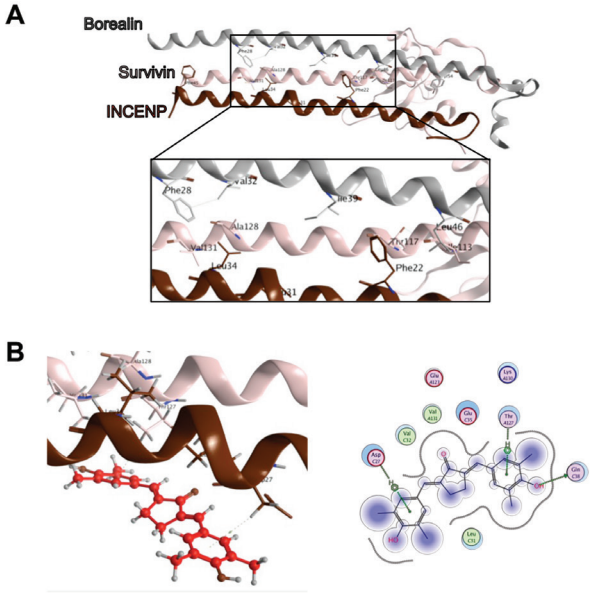

Figure 4. Visualization of binding interaction of PGV-1 in the core of CPC. (A) The core of CPC consisted of the essential interaction between the complex of INCENP, Survivin, and Borealin. (B) PGV-1 interacted with the complex between Survivin and INCENP through hydrogen bonding with Gln38 and hydrophobic bonding with Asp27 and Thr127

CPC: Chromosomal passenger complex, PGV-1: Pentagamavunone-1

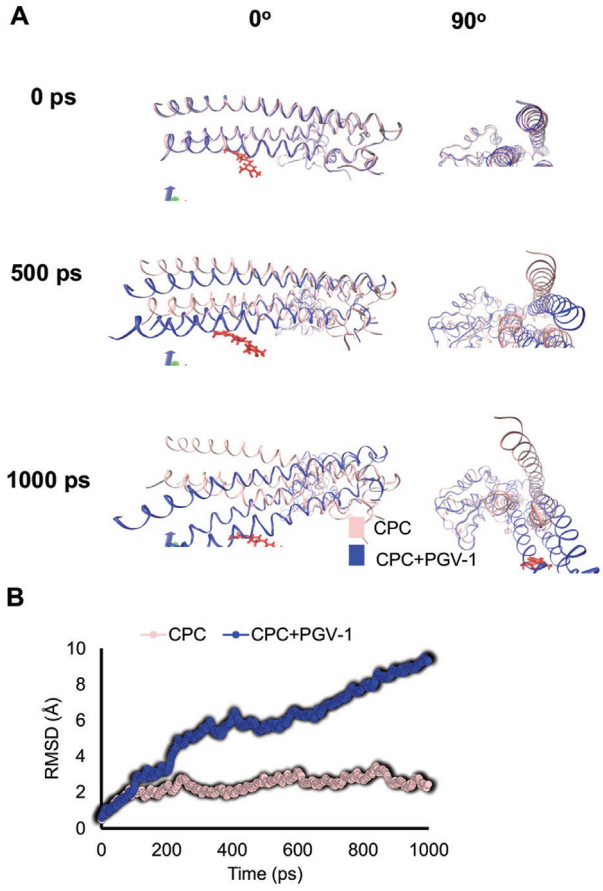

Figure 5. PGV-1 induced conformational change identified by molecular dynamic simulation. (A) Superimposed visualization of the CPC with or without PGV-1 after 1000 ps simulation (B) Comparison of RMSD profile of CPC with or without PGV-1 shown in 1000 frames

CPC: Chromosomal passenger complex, PGV-1: Pentagamavunone-1, RMSD: Root mean square deviation

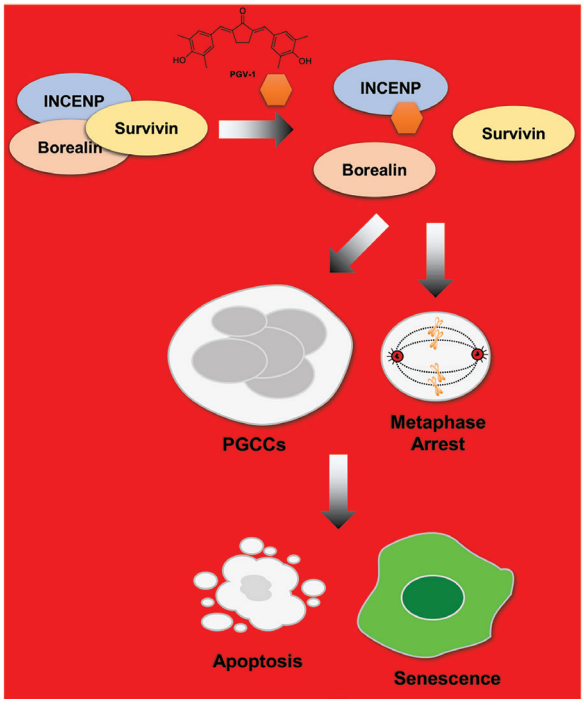

Figure 6. Plausible anticancer mechanism of PGV-1 in JHH4 cells
PGV-1: Pentagamavunone-1

MD simulations were conducted to investigate the stability and potential conformational changes of the CPC complex further. At 500 ps, PGV-1 slightly modified the conformation of the CPC complex (Figure 5a). CPC showed a significant conformational change in the presence of PGV-1 after 1000 ps (Figure 5a). The conformational change was located mainly in the helical structure of INCENP, Survivin, and Borealin, suggesting the binding interaction promoted destabilization of the CPC complex (Figure 5a). The destabilization of CPC in the presence of PGV-1 was also indicated by an increase in RMSD value up to 9.2 Å (Figure 5b). Our MD simulations suggest that PGV-1 promotes a conformational change in the CPC complex, potentially contributing to the dysregulation of chromosome localization during the transition from metaphase to anaphase.

DISCUSSION

PGV-1 has previously exhibited potent cytotoxicity in HepG2 and JHH7 cells without affecting the mRNA level of MYCN.[15,16] This study explored the distinctive phenotypic changes induced by PGV-1 in JHH4 cells with low MYCN expression, contributing valuable foundational knowledge for the development of chemotherapeutic agents for HCC. Examining these phenotypic changes is crucial for elucidating potential signaling pathways activated by PGV-1 in HCC. The utilization of cells with low MYCN expression enables us to distinguish the correlation between MYCN/NCYM signaling regulation and the mechanism of action of PGV-1. While the specific target of PGV-1 remains elusive, our study highlights a cluster of essential targets regulated by PGV-1 in HCC.

HCC is classified as a malignant cancer with only a 10% survival rate for patients within five years of diagnosis.[33] The high rate of recurrence is a major factor contributing to the poor prognosis of HCC compared to other liver cancers.[34] Given the limited treatment options for HCC, there is a critical need for potent and effective cytotoxic chemotherapeutic agents. PGV-1 exhibited potent cytotoxicity in JHH4, greater than in HepG2 and JHH7 after a 48-hour treatment, suggesting that MYCN signaling may not be the primary target of PGV-1. Our results also confirm the persistent cytotoxicity of PGV-1 even after removal from the culture medium, aligning with previous reports.[8,15,16] This observation could indicate the ability of PGV-1 to overcome the recurrence phenomenon in HCC. Revealing the molecular mechanism of the permanent cytotoxic effect of PGV-1 would be essential for further development of chemotherapeutic agents for HCC. The typical cytotoxic effect of PGV-1 in HCC and other cancer types is associated with G2/M arrest, especially in prometaphase or metaphase.[15,16,28] We consistently found that metaphase arrest in JHH4-treated PGV-1 led to mitotic catastrophe. Results from various cancer cells highlight the shared protein targets of PGV-1 in promoting metaphase arrest. Previous bioinformatic and molecular docking studies propose AURKA, AURKB, PLK1, CDK1, KIF11, and WEE1 as possible protein targets of PGV-1.[9,10,12] Elucidating the specific role of metaphase arrest is a crucial requirement for uncovering the precise cytotoxicity of PGV-1.

Metaphase arrest in cancer could either lead to cell death mechanisms or facilitate the promotion of PGCCs for cancer survival. Constitutive endoreplication and endomitosis at metaphase arrest resulted in centrosomal dysregulation and genomic rearrangement, generating PGCCs.[1,35] We found that PGV-1 promotes PGCCs alongside metaphase arrest cells, indicating a connection between both processes. Upon committing to mitosis, it was crucial that subsequent events, such as chromosome segregation and cytokinesis, proceeded without errors. We consider CPC as another target of PGV-1. CPC emerged as a pivotal coordinator overseeing chromosome condensation, orchestrating spindle assembly, rectifying aberrant microtubule-kinetochore interactions, impacting chromosome alignment, signaling to the spindle checkpoint, and aiding in the completion of cytokinesis. Furthermore, disrupting the interaction within the CPC emerged as a promising strategy to impede HCC growth. A prior study demonstrated that the absence of either Survivin or Borealin resulted in HCC regression after hepatocyte mitotic arrest, hypertrophy, and genome polyploidy.[36,37] mirroring the effect of PGV-1 on JHH4.

By performing molecular docking and molecular dynamic simulation of PGV-1 on the complex of CPC, we found that PGV-1 interacted with the essential amino acid sequence that contributes to the interaction of INCENP, Borealin, and Survivin protein-protein interaction, resulting in destabilization of the complex formation. New approaches in anticancer strategies, aiming to restrict CPC function by degrading CPC members or destabilizing the CPC complex, show promise.[38] Interestingly, a previous investigation emphasized the pivotal role of targeting INCENP or interrupting the interaction between INCENP and Aurora B kinase

in efficiently restraining the growth of neuroblastoma cell lines in both MYCN-WT and MYCN-amp cells.[39] Our findings align with this report, showcasing a MYCN-independent impact.

PGV-1 also induces senescence, particularly in PGCCs of JHH4. To control abnormal cell division, PGCCs enter senescence to reorganize cell division for the release of daughter cells that are more resistant to chemotherapeutic agents.[6,35] In contrast, PGV-1 triggers apoptosis in JHH4, as evidenced by the increase in cleaved PARP. These findings reveal the mechanism behind the lasting cytotoxic impact of PGV-1 in JHH4. This involves inducing mitotic arrest, forming PGCCs, increasing cellular senescence, and facilitating ultimately hindering the progression of HCC (Figure 6). Notably, no reported studies have demonstrated the promotion of PGCCs associated with irreversible cytotoxic effects.

Our findings highlight PGV-1 as a promising chemotherapeutic agent with multifaceted mechanisms that address key challenges in cancer treatment, including drug resistance, tumor recurrence, and metastasis. Unlike conventional therapies, PGV-1 demonstrates permanent cytotoxicity, even after drug withdrawal. This durable cytotoxic effect is important to improve survival rates among cancer patients, particularly in highly recurrent malignancies like HCC. As research advances toward clinical trials, PGV-1 holds promise not only for extending survival but also for transforming the therapeutic landscape of aggressive and recurrent cancers.

CONCLUSION

In conclusion, the low MYCN level in JHH4 cells established a crucial model for investigating the distinctive cytotoxic effects of PGV-1 in HCC, focusing on the observation of phenotypic changes. Our consistent findings highlighted the robust cytotoxic effect of PGV-1 in HCC cells, manifested by the induction of arrests across various mitotic phases. This suggested a potential interference with the CPC, resulting in multiple defects during mitotic arrest and the formation of PGCCs. The revelation that PGV-1 initiated senescence in PGCCs, ultimately leading to apoptotic cell death, is noteworthy. These novel insighted into the unique attributes of PGV-1 in JHH4 cells contribute to the understanding of potential therapeutic strategies, particularly in the pursuit of inducing permanent PGCCs death in HCC.

Ethics

Ethics Committee Approval: The ethical committee approval was obtained from the Medical and Health Research Ethics Committee, Faculty of Medicine, Public Health and Nursing Universitas Gadjah Mada - Dr Sardjito General Hospital (approval number: KE/FK/1045/EC/2022, dated: 10.08.2022).

Informed Consent: Not required.

Acknowledgments

This research was funded by the Ministry of Education, Culture, Research and Technology through the "Penelitian Pascasarjana Magister" 2023 scheme under number 3253/UN1/DITLIT/Dit-Lit/PT.01.05/2023 to RYU. NN also would like to thank the Indonesia Endowment Fund for Education (LPDP), Ministry of Finance of the Republic of Indonesia, through the Indonesian Education Scholarship (BPI) program [202209091880]. The authors would like to thank the scientific publication and journal department, Universitas Gadjah Mada, for their assistance in English language editing through Enago (https://www.enago.com).

Footnotes

Authorship Contributions

Concept: E.M., R.Y.U., Design: E.M., R.Y.U., Data Collection or Processing: N.N., E.M., R.Y.U., Analysis or Interpretation: B.L., E.M., R.Y.U., Literature Search: B.L., E.M., R.Y.U.

Conflict of Interest: The authors declare no conflicts of interest.

Financial Disclosure: The authors declared that this study received no financial support.

REFERENCES

1. Zhou X, Zhou M, Zheng M, Tian S, Yang X, Ning Y, Li Y, Zhang S, 2022. Polyploid giant cancer cells and cancer progression. Front Cell Dev Biol. 2022;10:1017588.
2. Zhang S, Mercado-Uribe I, Xing Z, Sun B, Kuang J, Liu J, 2014. Generation of cancer stem-like cells through the formation of polyploid giant cancer cells. Oncogene. 2014;33:116-128.
3. Niu N, Zhang J, Zhang N, Mercado-Uribe I, Tao F, Han Z, Pathak S, Multani AS, Kuang J, Yao J, Bast RC, Sood AK, Hung MC, Liu J, 2016. Linking genomic reorganization to tumor initiation *via* the giant cell cycle. Oncogenesis. 2016;5:e281.
4. Bharadwaj D, Mandal M, 2020. Senescence in polyploid giant cancer cells: a road that leads to chemoresistance. Cytokine Growth Factor Rev. 2020;52:68-75.
5. Mosieniak G, Sliwinska MA, Alster O, Strzeszewska A, Sunderland P, Piechota M, Was H, Sikora E, 2015. Polyploidy formation in doxorubicin-treated cancer cells can favor escape from senescence. Neoplasia. 2015;17:882-893.
6. Cai X, Guillot A, Liu H, 2022. Cellular senescence in hepatocellular carcinoma: the passenger or the driver? Cells, 2022;12:132.
7. Song Y, Zhao Y, Deng Z, Li Y, Hu C, Zhang Q, Liu Z, Tan H, 2021. Stress-induced polyploid giant cancer cells: unique way of formation and non-negligible characteristics. Front Oncol. 2021;11:724781.
8. Lestari B, Nakamae I, Yoneda-Kato N, Kato JY, Meiyanto E, 2019. Pentagamavunon-1 (PGV-1) inhibits ROS metabolic enzymes and suppresses tumor cell growth by inducing M phase (prometaphase) arrest and cell senescence. Sci Rep. 2019;9:14867.
9. Hasbiyani NAF, Wulandari F, Nugroho EP, Hermawan A, Meiyanto E, 2021. Bioinformatics analysis confirms the target protein underlying mitotic catastrophe of 4T1 cells under combinatorial treatment of PGV-1 and galangin. Scientia Pharmaceutica. 2021;89:38.
10. Musyayyadah H, Wulandari F, Nangimi AF, Anggraeni AD, Ikawati M, Meiyanto E, 2021. The growth suppression activity of diosmin and PGV-1 co-treatment on 4T1 breast cancer targets mitotic regulatory proteins. Asian Pac J Cancer Prev. 2021;22:2929-2938.
11. Rahmawati DR, Nurrochmad A, Jenie RI, Putri H, Sari DP, Meiyanto E, 2023. The synergistic cytotoxic effect of pentagamavunon-1 (PGV-1) and curcumin correlates with cell cycle arrest to induce mitotic catastrophe in 4T1 and T47D breast cancer cells. Indones Biomed J. 2023;15:318-327.

12. Meiyanto E, Novitasari D, Utomo RY, Fatmawati S, Putri H, Murwanti R, Astari D, Sari N, 2020. Bioinformatic and molecular interaction studies uncover that CCA-1.1 and PGV-1 differentially target mitotic regulatory protein and have a synergistic effect against leukemia cells. Indones J Pharm. 2020;11:145-158.
13. Schumacher JM, Golden A, Donovan PJ, 1998. AIR-2: An Aurora/Ipl1-related protein kinase associated with chromosomes and midbody microtubules is required for polar body extrusion and cytokinesis in Caenorhabditis elegans embryos. J Cell Biol. 1998;143:1635-1646.
14. Gassmann R, Carvalho A, Henzing AJ, Ruchaud S, Hudson DF, Honda R, Nigg EA, Gerloff DL, Earnshaw WC, 2004. Borealin. J Cell Biol. 2004;166:179-191.
15. Novitasari D, Kato J, Ikawati M, Meiyanto E, 2023. PGV-1 permanently arrests HepG2 cells in M phase and inhibits liver carcinogenesis in DMH-induced rats. J Appl Pharm Sci. 2023;8:204-211.
16. Moordiani M, Novitasari D, Susidarti RA, Putri H, Meiyanto E, 2023. Curcumin analogs PGV-1 and CCA-1.1 induce cell cycle arrest in human hepatocellular carcinoma cells with overexpressed MYCN. Indones Biomed J. 2023;15:141-149.
17. Qin XY, Gailhouste L, 2021. Non-genomic control of dynamic MYCN gene expression in liver cancer. Front Oncol. 2021;10:618515.
18. Joukov V, De Nicolo A, 2018. Aurora-PLK1 cascades as key signaling modules in the regulation of mitosis. Sci Signal. 2018;11:eaar4195.
19. Sardjiman SS, Reksohadiprodjo MS, Hakim L, Noor Z, Tanjung M, Yuwono M, 1997. 1,5-Diphenyl-1,4-pentadiene-3-ones and cyclic analogues as antioxidative agents: synthesis and structure-activity relationship. Eur J Med Chem. 1997;32:625-630.
20. Mosmann T, 1983. Rapid colorimetric assay for cellular growth and survival: application to proliferation and cytotoxicity assays. J Immunol Methods. 1983;65:55-63.
21. Debacq-Chainiaux F, Borlon C, Pascal T, Royer V, Eliaers F, Ninane N, Carrard G, Friguet B, de Longueville F, Boffe S, Remacle J, Toussaint O, 2005. Repeated exposure of human skin fibroblasts to UVB at subcytotoxic level triggers premature senescence through the TGF-beta1 signaling pathway. J Cell Sci. 2005;118:743-758.
22. Jeyaprakash AA, Klein UR, Lindner D, Ebert J, Nigg EA, Conti E, 2007. Structure of a Survivin-Borealin-INCENP core complex reveals how chromosomal passengers travel together. Cell. 2007;131:271-285.
23. Lestari B, Utomo RY, 2022. CEP55 inhibitor: extensive computational approach defining a new target of cell cycle machinery agent. Adv Pharm Bull. 2022;12:191-199.
24. Humphrey W, Dalke A, Schulten K, 1996. VMD: visual molecular dynamics. J Mol Graph. 1996;14:33-38.
25. Phillips JC, Hardy DJ, Maia JDC, Stone JE, Ribeiro JV, Bernardi RC, Buch R, Fiorin G, Hénin J, Jiang W, McGreevy R, Melo MCR, Radak BK, Skeel RD, Singharoy A, Wang Y, Roux B, Aksimentiev A, Luthey-Schulten Z, Kalé LV, Schulten K, Chipot C, Tajkhorshid E, 2020. Scalable molecular dynamics on CPU and GPU architectures with NAMD. J Chem Phys. 2020;153:044130.
26. Jo S, Kim T, Iyer VG, Im W, 2008. CHARMM-GUI: A web-based graphical user interface for CHARMM. J Comput Chem. 2008;29:1859-1865.
27. Lee KH, 2010. Discovery and development of natural product-derived chemotherapeutic agents based on a medicinal chemistry approach. J Nat Prod. 2010;73:500-516.
28. Wulandari F, Ikawati M, Widyarini S, Meiyanto E, 2023. Tumor-suppressive effects of curcumin analogs CCA-1.1 and pentagamavunone-1 in colon cancer: *In vivo* and *in vitro* studies. J Adv Pharm Technol Res. 2023;14:317.
29. Meiyanto E, Putri H, Larasati YA, Murwanti R, Sardjiman S, Fitriasari A, Kusmardi W, Utomo RY, 2019. Anti-proliferative and anti-metastatic potential of curcumin analogue, pentagamavunon-1 (PGV-1), toward highly metastatic breast cancer cells in correlation with ROS generation. Adv Pharm Bull. 2019;9:445-452.
30. Hanahan D, 2022. Hallmarks of cancer: new dimensions. Cancer Discov. 2022;12:31-46.
31. Sherr CJ, DePinho RA, 2000. Cellular senescence. Cell. 2000;102:407-410.
32. Amend SR, Torga G, Lin K, Kostecka LG, Wajapeyee N, Van Houten B, Pienta KJ, 2019. Polyploid giant cancer cells: unrecognized actuators of tumorigenesis, metastasis, and resistance. Prostate. 2019;79:1489-1497.
33. Venook AP, Papandreou C, Furuse J, de Guevara LL, 2010. The incidence and epidemiology of hepatocellular carcinoma: a global and regional perspective. Oncologist. 2010;15(Suppl 4):5-13.
34. Zeng H, Zheng R, Guo Y, Zhang S, Zou X, Wang N, Zhang L, Tang J, Chen J, Wei K, Huang S, Sun K, He J, Gu X, Jia L, Yang X, Li H, Chen W, 2015. Cancer survival in China, 2003-2005: a population-based study. Int J Cancer. 2015;136:1921-1930.
35. Zhang X, Yao J, Li X, Zhang D, Gao Y, Ding Y, Han C, 2023. Targeting polyploid giant cancer cells potentiates a therapeutic response and overcomes resistance to PARP inhibitors in ovarian cancer. Sci Adv. 2023;9:eadf7195.
36. Li L, Li D, Tian F, Zhang X, Ji S, Deng H, Zhang Y, 2016. Hepatic loss of Borealin impairs postnatal liver development, regeneration, and hepatocarcinogenesis. J Biol Chem. 2016;291:21137-21147.
37. Yue L, Li L, Li D, Ji S, Zhang Y, Deng H, 2017. High-throughput screening for Survivin and Borealin interaction inhibitors in hepatocellular carcinoma. Biochem Biophys Res Commun. 2017;484:642-647.
38. Gohard FH, St-Cyr DJ, Tyers M, Heck MM, Earnshaw WC, 2014. Targeting the INCENP IN-box-Aurora B interaction to inhibit CPC activity *in vivo*. Open Biol. 2014;4:140163.
39. Sun M, Veschi V, Bagchi S, Scher D, Annunziata M, Zhou W, Lee DW, Bollard CM, Wayne AS, Cripe TP, Houghton PJ, 2019. Targeting the chromosomal passenger complex subunit INCENP induces polyploidization, apoptosis, and senescence in neuroblastoma. Cancer Res. 2019;79:4937-4950.

Turk J Pharm Sci 2025;22(3):178-190
DOI: 10.4274/tjps.galenos.2025.56949

ORIGINAL ARTICLE

Physicochemical Characterization, Drug Release, Stability, and Cytotoxicity of Cross-Linked Curdlan-Based Nanosponges for α-Amyrin and Higenamine Delivery

Shailaja Amol DOMBE[1]*, Pramodkumar Jaykumar SHIROTE[2]

[1]Arvind Gavali College of Pharmacy, Department of Pharmaceutics, Satara, India
[2]Shivaji University, Sarojini College of Pharmacy, Department of Pharmaceutical Chemistry, Kolhapur, India

ABSTRACT

Objectives: Michigan cancer foundation-7 (MCF-7) breast-cancer cells are recognized for their resilience against conventional chemotherapy drugs and apoptosis-triggering agents. Nanosponges (NSs) have emerged as promising drug-delivery systems in cancer therapy because of their ability to encapsulate and deliver therapeutic agents efficiently. The aim of this study was to establish the combined beneficial anticancer impacts of NSs alpha-amyrin (AMY) and higenamine (HGN) on MCF-7 breast-cancer cells.

Materials and Methods: NSs were developed using a solvent-evaporation technique that used dichloromethane as the solvent and curdlan as the polymer. A comprehensive randomized 3^2 factorial design was employed to vary curdlan content (X_1) and stirring rate (revolutions per minute, X_2) and to investigate their influence on particle size (Y_1) and entrapment efficiency (EE, Y_2). The optimized formulation then underwent in-vitro investigations, encompassing apoptosis and cell-cycle studies with the MCF-7 breast-cancer cell line.

Results: The prepared NSs (F1-F9) exhibited optimal physical and chemical characteristics. Optimization produced formulation F10, which achieved a particle size of 280.9 nm and an EE of 63.00%. The model was established for all dependent variables, such as particle size and EE, at a significance level of $p<0.05$. *In vitro* studies of the prepared NSs demonstrated promising anticancer activity. The AMY + HGN combination showed synergistic effects versus AMY alone, significantly influencing the MCF-7 cell cycle, producing G1-phase arrest, and reducing cell propagation by flow-cytometry analysis.

Conclusion: The synergistic anticancer activity observed with AMY- and HGN-loaded NSs-combined with their sustained-release properties and cell-cycle modulation in MCF-7 cells-underscores the promise of this formulation as an effective cancer-treatment approach.

Keywords: Nanosponges, cancer, higenamine, synergistic, α-amyrin

INTRODUCTION

Cancer has a significant impact on global mortality, accounting for approximately 1 in every six deaths and affecting almost every household. In 2022, there were 20 million new cases of cancer and 9.7 million deaths globally ascribed to cancer. The World Health Organization projects a 77% increase in the burden of cancer by 2050, which will place additional strain on health systems and communities.[1-6]

***Correspondence:** shailaja.dombeagcop@gmail.com, **ORCID-ID:** orcid.org/0000-0002-4151-1590
Received: 08.08.2024, **Accepted:** 02.06.2025 **Publication Date:** 01.08.2025

Cite this article as: DOMBE SA, SHIROTE PJ. Physicochemical characterization, drug release, stability, and cytotoxicity of cross-linked curdlan-based. Turk J Pharm Sci. 2025;22(3):178-190

Despite these concerning statistics, there is a glimmer of hope. In the last two years, the mortality rate due to cancer has declined according to advancements in understanding tumor biology and the development of improved investigative devices and therapies.[6-7] Currently, mainstream cancer therapies include surgical intervention, radiation, and chemotherapeutic drugs. However, these interventions often harm normal cells, leading to toxicity in patients.[8] While conventional chemotherapy protocols are effective, they are also accompanied by adverse effects that can compromise biological efficacy and patient outcomes.

Exploring the principles of ancient Indian medicine, particularly Ayurveda, unveils a promising path forward. It appears that nature holds a treasure trove of potent components with anti-proliferative and anti-angiogenic properties.[9] Natural products exhibit remarkable chemical versatility and biological specificity, along with reduced toxicity. These characteristics make them valuable contenders for the creation of new and innovative medications.

The modern pharmaceutical market increasingly favors bioactive compounds obtained from natural sources due to concerns about the side effects associated with chemotherapeutic medications. Phytochemicals, valued for their nutritional benefits, not only aid in preventive measures but also hold promise in the treatment of cancer. However, many phytochemicals encounter challenges related to their hydrophilic nature, high molecular weight, and limited absorption through lipid cell membranes, leading to low bioavailability and efficacy. The current landscape of pharmacotherapy relies on traditional dosage forms, which offer therapeutic benefits to a limited extent and thus present significant obstacles in the effective treatment of cancer. As research advances, the exploration of natural compounds brings a renewed sense of optimism in the ongoing battle against this formidable disease.[10]

Alpha-amyrin (AMY) is a pentacyclic triterpene compound with the molecular formula $C_{30}H_{50}O$ isolated from the leaves of *Capparis zeylanica* L. and has reported pharmacological activities such as anti-diabetic, anticancer, anti-inflammatory, antioxidant, and antimicrobial. The molecular weight of AMY is approximately 426.71 g mol^{-1}, and its melting point falls within the range of 252-256 °C. AMY is practically water-insoluble but soluble in various solvents, including ethanol, chloroform, and acetone. Its physical properties present certain challenges-hydrophobia, high molecular weight, and low bioavailability-making it a compelling candidate for formulation development.[11]

Higenamine (HGN) is an isoquinoline derivative isolated from *Annona squamosa* L. it is also called norcoclaurine, a natural compound found in various plants, including *A. squamosa* (sitaphal). It is classified as a β_2-adrenergic receptor agonist, meaning it stimulates β_2-adrenergic receptors in the body. HGN is soluble in polar solvents such as water and ethanol due to its hydrophilic nature.[12]

So far, research has demonstrated the selective cytotoxic activity of AMY-loaded nanocapsules in leukemic cells. This study aims to combine AMY with HGN for breast-cancer treatment, to reduce side effects, enhance cytotoxicity, and improve bioavailability compared to conventional chemotherapy.[13]

Natural-polymer-based nanosystems demonstrate superior drug-loading capabilities compared with other available nanocarriers, effectively addressing issues related to physicochemical properties as well as bioavailability and stability for a wide range of therapeutic agents. Notably, natural polymers such as curdlan, hydroxypropyl cellulose, guar gum, xanthan gum, and ethylcellulose are commonly utilized to facilitate sustained release.[14]

Despite significant advancements in nanotechnology for drug delivery, no previous study has explored the combined application of AMY and HGN in nanosponge (NS)-based systems for cancer treatment. This knowledge gap highlights the novelty and importance of this investigation. The study addresses critical challenges associated with traditional chemotherapy, such as systemic toxicity, low therapeutic index, and the limitations of natural bioactive compounds, including poor solubility and bioavailability. Specifically, this work focuses on AMY and HGN—two phytochemicals known for their potent anticancer properties but whose clinical translation is hindered by these physicochemical constraints. To overcome these barriers, the study proposes the development of a curdlan-based (NS) formulation. Curdlan, a natural polymer, offers biocompatibility and biodegradability, making it an ideal candidate for nanoscale drug-delivery systems aimed at improving the therapeutic efficacy of AMY and HGN against breast cancer (MCF-7 cells).

The curdlan-based NS are designed to enable sustained drug release, reduce systemic side effects, and achieve enhanced therapeutic outcomes. To achieve these objectives, the study systematically explores the role of curdlan polymer composition and stirring rate in the fabrication of NS, assessing their influence on critical parameters such as particle size, encapsulation efficiency (EE), and therapeutic performance. The formulation is characterized and evaluated for its *in vitro* cytotoxicity against MCF-7 cells and its ability to induce cell death through flow-cytometry analysis.The rationale for this approach stems from the need to enhance the delivery, stability, and bioavailability of these compounds while leveraging their synergistic anticancer potential.[14-15] This innovative strategy aims to establish a robust, curdlan-based NS platform that addresses existing limitations in cancer drug delivery while contributing to the advancement of phytochemical-based therapeutics.

MATERIALS AND METHODS

HGN standard was obtained from Sigma-Aldrich (Bangalore, India). Dichloromethane (DCM) was procured from Thermo Fisher, while methanol was sourced from Merck. AMY was purchased from Chem-scene (China). Polyvinyl alcohol from Rankem and toluene from Qualigens (Thermo Fisher Scientific) were used.

Methodology

Preformulation study

Ultraviolet-visible (UV-visible) spectroscopy

To find the absorption maxima of HGN and AMY, standard solutions were individually scanned in a UV spectrophotometer between 200 and 400 nm, with methanol serving as a blank. The wavelength at which the spectra of the two medications overlap is known as the isosbestic point. To generate a calibration curve, working solutions were prepared, and their absorbance at the isosbestic point was measured.

Fourier transform infrared spectroscopy (FTIR)

An analytical method commonly used to identify chemical interactions is FTIR spectroscopy. In this study, the FTIR (Bruker, Germany) was used to determine the infrared spectra of HGN, AMY, curdlan polymer, physical mixture, and the optimized batch. A small quantity of the material was put on the infrared platform, and the spectra were analyzed in the wavelength range between 4000 and 400 cm^{-1}.

Differential scanning calorimetry (DSC)

The thermal behavior and thermotropic properties of the medication were assessed using DSC (SDT Q600 V20.9 Build 20, TA Instruments, New Castle, DE, USA). This method involves measuring the heat flow through the sample and reference under controlled temperature programming. DSC analyses were conducted on HGN, AMY, curdlan polymer, physical mixture, and the optimized batch. A DSC thermogram for the pure drug was obtained by heating five milligrams of the sample at a rate of 10 °C/min in a closed metal pan in a nitrogen environment with an evacuation rate of 20 mL/min. These investigations assisted in determining the thermal behavior of the drug-polymer physical mixture and the optimal batch so that their compatibility could be verified.[15-16]

Formulation and optimization of NS

Optimization of formulation parameters and process factors

A specific formula was chosen for the formulation of NS based on saturation solubility studies. As part of the preparation method optimization, various parameters were adjusted, such as polymer concentration, the stabilizer choice, volume of the aqueous phase, nature of the organic solvent, stirring time, and stirring speed. The resulting NS characteristics were comprehensively evaluated during the formulation optimization process. Different batches were formulated with varying polymer concentrations, each subjected to distinct stirring speeds of 1000, 2000, and 3000 rpm.

Factorial design

The study employed a 3^2 factorial design, where two factors, each with three levels, were investigated. Design Expert®, version 11.0 (Stat-Ease Inc., Minneapolis, MN, USA), was used to create the design. In this study, a 3^2 full factorial design was implemented, focusing on curdlan amounts (X_1) and stirring speed (X_2) chosen as independent variables. The levels of these two factors, with three different levels: low, medium, and high, were established based on a preliminary study conducted before initiating the experimental design. Throughout the study, all other formulation and processing variables remained constant. The response variables selected were particle size (Y_1) and (EE, Y_2). The prepared NS batches were evaluated and characterized across various parameters. Furthermore, the software Design Expert 11.0 advocated for a singular formulation (F10) through a multi-criterion decision strategy to optimize responses targeting various objectives. The optimal values for the variables were ascertained to be X_1 =250 mg and X_2 =1000 rpm; the formulation was counterchecked for correctness by checkpoint analysis.

Preparation of phytochemicals loaded NS

Emulsion solvent diffusion method

Various quantities of polymer can be used to produce NS as shown in Table 1. The dispersing phase, comprising a specified quantity of polyvinyl alcohol, was gently added to 100 mL of water as a continuous phase. The reaction mixture was stirred for two hours at different rpm. The generated NS were recovered by filtering, then dried for 24 hours at 40 °C in the oven. The vacuum desiccators were used to store the dried NS to make sure that any remaining solvents had been eliminated.

Evaluation of phytochemicals loaded NS

Production yield (PY)

PY was calculated using the following formula:

$$PY\ (\%) = \frac{\text{Actual wt of nanosponge}}{\text{Theoretical wt of the drug and polymer}} \times 100$$

Encapsulation efficiency (EE)

The assessment of the drug quantity encapsulated within NS is crucial, as it influences the release mechanism and ultimately the bioavailability. To determine the EE, NS (150 mg) was thawed in methanol, sonicated for 15 minutes, and then centrifuged. The resulting supernatant was filtered, appropriately diluted using pH 6.8 phosphate buffer, and subjected to analysis using a UV spectrophotometer at 219 nm. The EE was determined by the given formula provided below:

$$\%\ EE = \frac{\text{Actual drug content (NS)}}{\text{Theoretical drug taken}} \times 100$$

Scanning electron microscopy

The surface structure and morphology were examined using a scanning electron microscope (S-3400 N type II model, Hitachi Ltd., Tokyo, Japan).

Particle size and polydispersity index (PDI)

The size of AMY-HGN-loaded NS and the PDI (to assess the dispersion of particle size) were determined using dynamic light scattering at 25 °C. This method was conducted using a nanoparticle analyzer (SZ-100) from Horiba Scientific, Japan. The NS dispersion was diluted and placed into the portable measuring cuvette before being inserted into the instrument's cuvette holder for evaluation. Before measurement, any air

Table 1. Composition of nanosponges containing AMY and HGN

Components	F1	F2	F3	F4	F5	F6	F7	F8	F9
Higenamine (Ratio)	1	1	1	1	1	1	1	1	1
α-Amyrin	1	1	1	1	1	1	1	1	1
Curdlan (mg)	250	250	250	500	500	500	750	750	750
Polyvinyl alcohol (mg)	500	500	500	500	500	500	500	500	500
Dichloromethane (mL)	30	30	30	30	30	30	30	30	30
Water (mL)	100	100	100	100	100	100	100	100	100

AMY: Alpha-amyrin, HGN: Higenamine

bubbles in the capillary were removed, and the PDI was then calculated using the following formula:

$$PDI = \frac{\text{Average molecular weight in mass}}{\text{Molecular weight average numbers}}$$

Zeta potential

The measurements were conducted with a separate electrode on the same equipment. To determine the zeta potential, a transparent, single-use zeta cell was filled with 1 mL of NS solution, ensuring the absence of air bubbles. Subsequently, the system was heated to 25 °C by applying an electric field of approximately 15 V/cm, and the outcomes were documented. It is important to note that the stability of the NS preparation increases as the zeta potential becomes more negative.

Drug content

NS was taken (100 mg) and added to 10 mL of phosphate buffer (pH 6.8), then stirred for 30 minutes. Subsequently, the absorbance was measured at the highest wavelength (λmax=219 nm), using spectrophotometry following suitable dilution.

In vitro dissolution study

Dissolution studies are conducted to investigate the probable impact of formulation and process variables on the bioavailability of a medication. In this study, a paddle-shaped USP Type-II dissolution apparatus was used to assess the *in vitro* release of NS. The NS was placed into dialysis bags, followed by immersion in phosphate buffer (pH 6.8), with 900 mL serving as dissolution media. The system was kept at 37.5 °C with stirring at 100 rpm. At regular intervals, 5 mL samples were withdrawn up to 12 hours and were replaced with the same amount of the dissolution media. The absorbance of these samples was taken spectrophotometrically at 219 nm.

In vitro drug release kinetics

Plotting the following kinetic models-zero order, first order, Higuchi equations, and Hixson-Crowell, using the data gathered from *in vitro* release tests, allowed the determination of NS drug release kinetics. The Korsmeyer-Peppas equation was utilized to determine the drug release mechanism.[16,17]

MTT assay

The MCF-7 cell from the Biocyte Institute of Research & Development (Sangli, India) was cultured in DMEM-F12 medium augmented with insulin (10 µg/mL), hydrocortisone (0.5 µg/mL), and human epidermal growth factor (20 ng/mL). All culture media were supplemented with high glucose DMEM (catalog number: 11965-092), Antibiotic-Antimycotic 100X solution (Thermo Fisher Scientific, catalog number: 15240062), and fetal bovine serum (FBS) from Gibco (catalog number: 10270106). The cells were initially cultured at a concentration of 1×10^4 cells/mL for 24 hours at 37 °C with 5% CO^2. Subsequently, 104 cells per well were seeded in a 96-well plate, with 70 µl of culture medium, and 100 µl of compounds at concentrations of 10, 40, and 100 µg. Control wells contained cells with 0.2% dimethyl sulfoxide (DMSO) in phosphate-buffered saline (PBS). Following another 24-hour incubation, MTT reagent was added to evaluate cell viability by forming formazan crystals from viable cells. The absorbance at 570 nm was measured after adding DMSO to dissolve the formazan. The percentage of cell growth inhibition was calculated, and the IC_{50} value was determined using 5-Fluorouracil as a positive control.

Apoptosis study by Fluorescence microscopy

A common method for the qualitative assessment of apoptosis at the nuclear level involves using the fluorescent dye 4′,6-diamidino-2-phenylindole dichloride (DAPI), which binds to DNA and can be visualized under a fluorescence microscope. In this study, we employed a DAPI staining protocol as previously described. In brief, MCF-7 cells were seeded onto 6-well plates at a density of 5 × 10^5 cells per well, and they were left to adhere and proliferate for a full day. The cells were treated with 5-FU as the standard treatment. The cells were also treated separately using the optimized formulation. Then, they were washed with PBS, followed by being fixed with 10% formaldehyde. After that, the cells were permeabilized for 15 minutes using Triton X-100. Following additional washes, the cells were stained with DAPI for 5 minutes. Apoptotic nuclei, characterized by fragmentation or condensation, were visualized using a fluorescence microscope (Micron India). Untreated cells were used as the control in this experiment.

Cell cycle analysis

The distribution of cell cycles was assessed by flow cytometry following DAPI staining. MCF-7 cells were exposed to the optimized formulation or an equivalent amount of DMSO as a control for 24 hours. Subsequently, floating cells were gathered, while adherent cells underwent trypsinization, followed by washing with PBS containing 5% FBS, and centrifugation at

1100 g for 10 minutes. The resulting cell pellets were then suspended in 500 µl of PBS with 5% FBS, centrifuged at 200 g for 7 minutes at 4 ˚C, and stained with a solution containing PI, Triton X-100, sodium citrate, and RNase. Following an hour of incubation at 4 ˚C in the dark, flow cytometric analysis was carried out using a FACSCalibur instrument (BD Biosciences, USA).[18-20]

Stability studies

Following International Council for Harmonisation of Technical Requirements for Pharmaceuticals for Human Use guidelines, the stability testing involved subjecting the samples to conditions of 40 ˚C ± 2 ˚C and 75% relative humidity (RH) ± 5% RH for a duration of six months. Following the standard protocol, the samples were assessed at intervals of 0, 3, and 6 months. These accelerated stability tests were conducted on the ultimate optimized formulation.[21,22]

Statistical analysis

Regression analysis was performed to determine the comparative effect of the independent variables, X1 (polymer concentration) and X2 (stirring rate), on the dependent variables, R1 (particle size) and R2 (EE). The final regression equations were presented in terms of coded factors. These equations help quantify the impact of the independent variables on the dependent variables. The statistical significance of the coefficients in the equations demonstrates the reliability of the results.[22]

RESULTS

Preformulation studies

Ultraviolet-visible (UV-visible) spectroscopy

HGN and AMY exhibited (λ max) of 254 nm and 208 nm, respectively, when dissolved in methanol. Figure 1 displays an overlay plot of these two drugs. The isosbestic point of the two drugs was found to be 219 nm. Calibration curves and graphs for a mixture of HGN and AMY were constructed using methanol. These exhibited a regression coefficient of 0.998, with a slope value of 0.143 and a Y-intercept value of 0.0049.

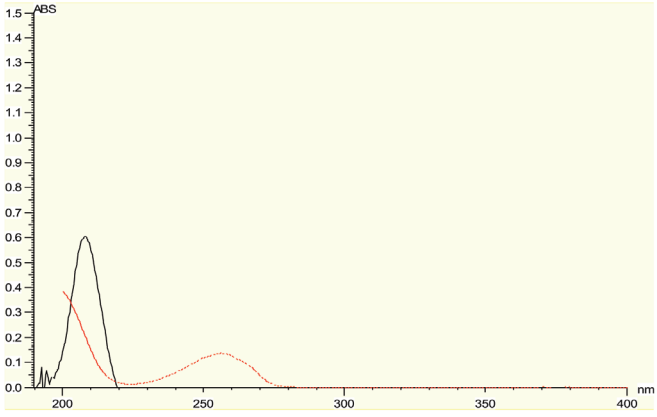

Figure 1. Overlay spectrum of HGN and AMY mixture in methanol
HGN: Higenamine, AMY: alpha-amyrin, ABS: Absorption,

This suggests a linear relationship between concentration and absorbance within the range of 10-60 µg/mL for the HGN and AMY in methanol.

Fourier transforms infrared spectroscopy (FTIR)

FTIR spectroscopy was used to capture the infrared spectrum of HGN and AMY, with the findings presented in Figure 2. The FT-IR spectrum displayed all the characteristic IR peaks corresponding to the functional groups associated with HGN and AMY in the drug mixture and the optimized formulation, as illustrated in Table 2.

DSC analysis

The thermogram of HGN exhibited two endothermic peaks, *i.e.*, 98.94 ˚C and another at 246.07 ˚C, which may represent the loss of water or solvent molecules and the melting of the sample, respectively. The melting point of the sample is reported to be 258-260 ˚C, which is consistent with the observed peak at 246.07 ˚C. The thermogram of AMY showed a peak at 170.67 ˚C, representing a melting point (theoretically 186 ˚C). The polymer can be accredited with its peak melting point at 282.77 ˚C. The physical mixture exhibited the endothermic peak at 304.34 ˚C for curdlan polymer. This DSC analysis indicated that

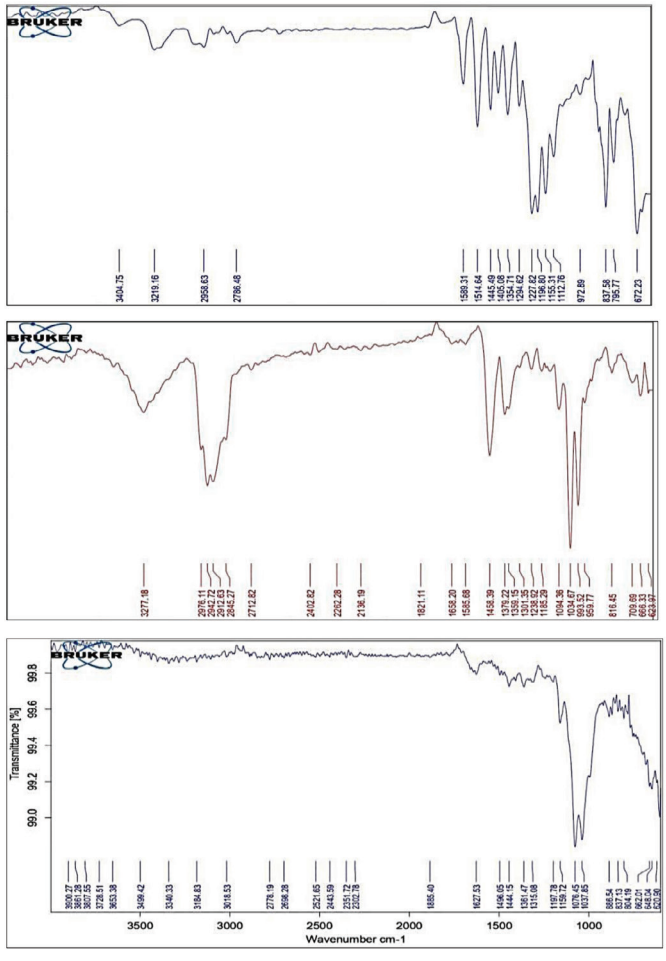

Figure 2. FTIR spectrum of (A) HGN, (B) AMY, (C) optimized formulation
FTIR: Fourier transform infrared spectroscopy, HGN: Higenamine, AMY: alpha-amyrin

Table 2. Interpretation of FT-IR spectrum of HGN and AMY physical mixture

Sr. no.	Frequency (cm^{-1})	Peak observed	Interpretation
1	3550-3220	3222,3217.8	Phenol O-H Stretch
2	3000-2850	2943,2958	Alkane C-H Stretch
3	1480-1350	1357.93,1411,1447	Aromatic C=C stretching vibrations
4	3500-3300	3184.83	Amine N-H Stretch
5	1360-1080	1315.08	Amine C-N Stretch
6	1640-1550	1599.04	Amide N-H bending
7	1000-650	885.54	Alkene=C-H bending

Sr. no.: Serial number, FT-IR: Fourier transform infrared spectroscopy, HGN: Higanamine, AMY: alpha-amyrin

no noteworthy change was perceived in the melting points of both drugs in combination. The thermogram of DSC is shown in Figure 3.

Formulation and optimization of NS

Compatibility study for Nanosponges

FT-IR analysis

The spectra of HGN and AMY, as well as the physical mixture, were analyzed. The functional groups identified in the physical mixture of drugs and polymer were found to align with the peaks observed for the pure drugs. Notably, Figure 2 demonstrates the significant peaks of the drug mixture-including 3018.53 cm-1 for Alkane C-H stretching, 837.13 cm-1 for alkene C-H bending, 1361.47 cm-1 for amine C-N-stretching, and 1627.53 cm-1 for amide N-H bending, in the FT-IR spectra of the physical mixture.

DSC analysis

The DSC Thermograms of HGN and AMY, as well as the drug-polymer physical mixture, are presented in Figure 3. The drug mixture displayed endothermic peaks of HGN and alpha-amyrin at 246.07 ˚C and 170.67 ˚C, respectively. In contrast, the physical mixture of drugs and the polymer demonstrated an endothermic peak at 304.34 ˚C for the curdlan polymer.

Evaluation alpha-amyrin and higenamine loaded NS

Production yield and EE

The production yields of the prepared formulations varied between 41.53% and 70.36%. The proportion of drug to polymer was identified as having a crucial role in determining production yield, indicating that increased polymer concentrations resulted in higher yields. On the other hand, the EE of all formulations ranged from 59.23% to 81.79% as shown in Table 3.

Particle size and PDI

Measurements were made of the formulation of NS particle size analysis as reported in Table 4. The results indicate that the particle size of the various formulations ranged from 241.3 nm to 622.2 nm. The PDI across the formulations ranged from 0.382 to 0.960, which suggests a considerable variance in particle size distribution. Notably, the relatively high PDI values suggest a range in the distribution of particle sizes, with some formulations exhibiting a more uniform distribution than others.

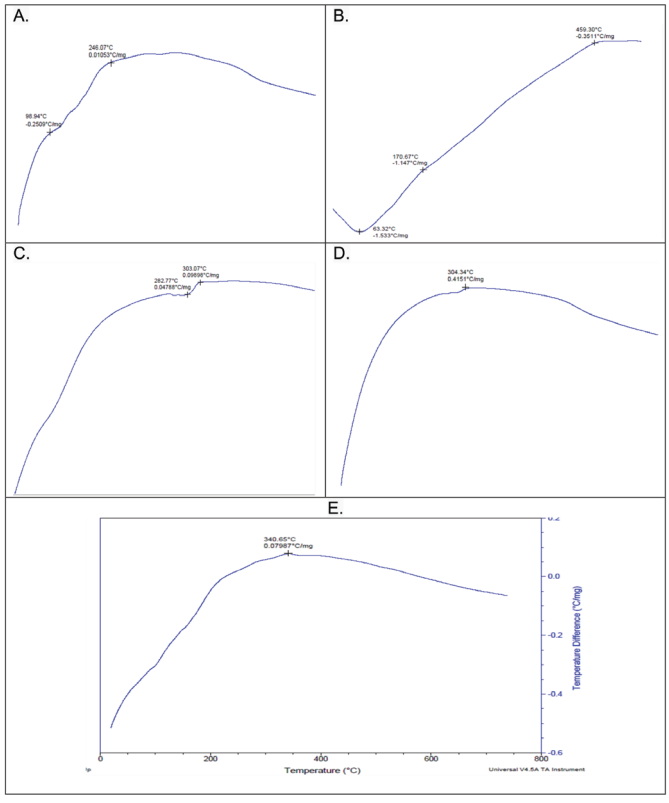

Figure 3. DSC thermogram of (A) HGN, (B) AMY, (C) polymer, (D) physical mixture, (E) optimized formulation

DSC: Differential scanning colorimetry, HGN: Higenamine, AMY:alpha-Amyrin

This might have implications for the stability and performance of these formulations, potentially influencing their suitability for specific applications and delivery systems.

Zeta potential

The zeta potential values of formulations ranged from -5.5 mV to -23.3 mV, a range that is crucial for maintaining physical stability among nanoparticles (NS) by promoting electrostatic repulsion and preventing aggregation. Furthermore, the reduction in particle size results in an increased surface area,

which in turn contributes to higher zeta potential values, as observed in Table 5.

In vitro drug release studies

NS were produced and evaluated, utilising an emulsion solvent diffusion method, providing several key outcomes for the effective creation of NS. The *in vitro* drug release profile ranged from 79.60 to 91.58% CDR for 12 hours, which revealed that the formulation with a higher coded value for the polymer and a lower coded value for stirring rate exhibited the highest *in vitro* drug release compared to the other formulations (Figure 4) as detailed in Table 6.

Experimental design for NS formulations

The outcomes obtained for selected software responses are detailed in Table 7. The particle size of all runs ranged from 241.3 nm to 622.2 nm, and entrapment efficiency (%) was observed ranging from 79.60% to 91.80%.

Table 3. Data for production yield and EE for NS formulation

Sr. no.	Batch	PY (%)	EE (%)
1	F1	45.60±0.75	62.00±0.81
2	F2	47.43±0.50	60.00±1.63
3	F3	41.53±0.55	65.45±0.41
4	F4	51.26±0.57	66.00±0.81
5	F5	55.70±0.36	80.24±0.50
6	F6	50.51±0.42	79.63±1.73
7	F7	70.63±0.49	81.79±0.57
8	F8	66.63±0.54	59.23±0.32
9	F9	62.83±0.60	69.63±1.73

Data are mean values (n=3) ± SD. SD: Standard deviation, Sr. no.: Serial number, PY: Production yield, EE: Entrapment efficiency

Table 4. Particle size and PDI of NS formulation

Sr. no.	Batches	Particle size (nm)	PDI
1	F1	280.9±0.82	0.496±0.0005
2	F2	290.7±0.12	0.381±0.0630
3	F3	389.9±0.91	0.557±0.0035
4	F4	420.1±0.58	0.960±0.0026
5	F5	241.3±0.28	0.559±0.0024
6	F6	349.5±0.89	0.589±0.0026
7	F7	502.3±0.42	0.493±0.0024
8	F8	613.5±0.41	0.596±0.0008
9	F9	622.2±0.71	0.685±0.0670

Data are mean values (n=3) ± SD. SD: Standard deviation, Sr. no.: Serial number, PDI: Polydispersity index

Regression analysis

The regression equations represented the comparative effect of the independent variables X1: polymer concentration (mg) and X2: stirring rate on dependent variables R1: particle size (nm) and R2: EE (%).

The final equation in coded factors terms

The equation for response R1 has shown that both factors have a significant positive effect on the particle size of NS formulations.

$$R1 = +412.27+129.43X1+26.38X2 \quad (1)$$

The equation for response R2 has shown that factor X1 has a positive effect, whereas factor X2 has a negative effect on EE of NS formulations.

$$R2 = +69.33 +4.69\ X1 - 16.38\ X2 \quad (2)$$

The experimental runs of the nine trials are listed in Table 7. The effects of the main factors on the formulation responses are noted in the regression equations. An increase in the independent variable X1 led to an increase in particle size and EE. While an increase in X2 resulted in a larger particle size, it caused a decrease in EE.

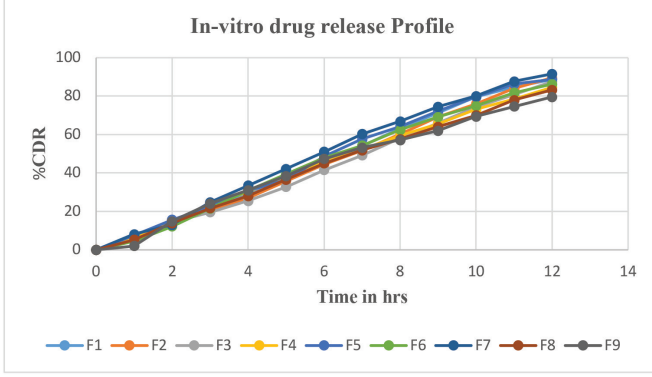

Figure 4. *In vitro* drug release profiles of F1 to F9 batches

Table 5. Zeta potential of NS formulation

Sr. no.	Batch code	Zeta potential (mV)
1	F1	-5.5±0.32
2	F2	- 5.6±0.22
3	F3	-11±0.42
4	F4	-23.3±0.26
5	F5	-13±0.39
6	F6	-15±0.20
7	F7	-6.4±0.25
8	F8	-10.5±0.31
9	F9	-12.7±0.28

Data are mean values (n=3) ± SD. NS: Nanosponge, SD: Standard deviation, Sr. no.: Serial number

Response-surface analysis

The primary objective of optimization is to determine the most effective levels of the variables that impact the process, enabling the smooth and consistent production of a product with desired attributes. The effects of various independent variables on the dependent variables were expressed using 3D graphics. The polymer concentration and stirring speed had a significant effect on particle size, whereas polymer concentration had a significant impact on entrapment efficiency. The response surface graphs the most statistically significant variables for the evaluated responses as shown in Figure 5.

Analysis of variance (ANOVA)

The model was established for all dependent variables, such as particle size and entrapment efficiency, at a significance level of $p<0.05$. The linear model showed the best fit for both responses.

Checkpoint analysis and optimization of design

Through the Design of Experiments (DOE) methodology to optimize responses targeting various objectives, the software Design Expert 11.0 advocated for a singular formulation (F10) through a multi-criterion decision strategy. The optimal values for the variables were ascertained to be X1=250 mg and X2 =1000 rpm. The final formulation was developed by applying optimal factor values and subsequently evaluated for particle size and entrapment efficiency. The optimized formulation, represented by F10, exhibited a particle size measuring 280.9 nm alongside an entrapment efficiency of 63.00%. Comparing the predicted and observed outcomes revealed a desirability

Table 6. *In vitro* drug release profiles of F1 to F9 batches

Time (Hours)	% CDR								
	F1	F2	F3	F4	F5	F6	F7	F8	F9
0	0	0	0	0	0	0	0	0	0
1	5.50	6.80	7.60	6.20	7.56	4.53	8.19	5.20	2.06
2	14.33	15.56	14.55	14.85	15.6	12.16	13.03	13.90	14.88
3	22.66	20.15	19.56	23.45	22.63	21.60	24.83	21.70	24.15
4	29.63	27.00	25.45	30.12	30.89	30.90	33.5	28.00	31.02
5	38.23	35.78	32.74	38.40	36.45	39.35	42.16	36.57	38.41
6	46.06	44.56	41.58	45.61	48.56	47.88	51.03	45.00	47.28
7	54.00	51.74	49.12	52.19	57.65	54.26	60.23	51.79	53.21
8	63.23	60.12	58.07	59.46	64.23	62.45	66.85	57.60	57.18
9	71.28	69.24	66.05	65.58	72.24	69.12	74.52	64.12	62.00
10	79.55	76.00	74.24	73.12	79.57	75.00	80.05	70.00	69.35
11	84.72	83.99	80.70	80.40	84.26	81.76	87.69	77.91	74.59
12	88.69	86.56	87.21	88.58	87.69	86.26	91.58	83.26	79.60

CDR: Cummulative drug release

Table 7. 3^2 full factorial design layout and responses noted for NS formulation

Trial	Polymer conc (X1)	Stirring time (X2)	Particle size Y1	Entrapment efficiency Y2
1	250	1000	280.9±0.82	62.00±0.81
2	250	2000	290.7±0.12	60.00±1.63
3	250	3000	389.9±0.91	65.45±0.41
4	500	1000	420.1±0.58	66.00±0.81
5	500	2000	241.3±0.28	80.24±0.50
6	500	3000	349.5±0.89	79.63±1.73
7	750	1000	502.3±0.42	81.79±0.57
8	750	2000	613.5±0.41	59.23±0.32
9	750	3000	622.2±0.71	69.63±1.73

Data are mean values (n=3) ± SD. NS: Nanosponge, SD: Standard deviation

value of 0.656 with minimal relative errors, endorsing the dependability of the optimization process. Additionally, the strong coherence between the projected and observed values was evidenced in Table 8, underscoring the efficiency and accuracy of the optimization process employed. Factors X1 and X2, determined as 250 mg and 1000 rpm, respectively, were recognized as the optimum parameters for the NS drug delivery system.

Characterization of optimized NS formulation

Scanning electron microscopy (SEM)

SEM analysis was conducted on the prepared NS to examine their morphology and surface texture. The NS were found to be approximately spherical, displaying an uneven surface and a porous, spongy nature, as depicted in Figure 6.

Particle size analysis, zeta potential measurement

The measured particle size closely matched the predicted value obtained from the DOE. Table 8 illustrates that the predicted and observed particle size values for the NS were similar, with a residual value of 24.44 existing between them. A reduction in particle size enhances the interfacial area available for drug diffusion, potentially leading to improved drug release. Additionally, the narrow size distribution helped increase bioavailability.

The zeta potential of the NS formulation was determined to be -5.8 mV, contributing to the physical stability of the NS particles through electrostatic repulsion, thereby preventing aggregation. Moreover, the decrease in particle size resulted in an increased surface area, leading to a higher zeta potential. A zeta potential of -5.8 mV signifies a slight negative charge on the particle surface, indicating a tendency for repulsion between particles and supporting the stability of the colloidal system.

Entrapment efficiency

The achieved EE closely aligned with the predicted value derived from the DOE. As detailed in Table 8, the predicted and observed values of drug entrapment in the NS were nearly identical, with a residual value of 6.33.

FT-IR analysis of NS

FT-IR spectroscopy was conducted on the optimized formulation to confirm the entrapment of the drug mixture within NS. The absence of major peaks associated with the drug mix, such as phenolic OH group stretch (3510.56 cm-1), amine N-H stretch (3112.26 cm-1), and alkene=C-H bonding (740.69 cm-1), in the NS formulation spectra, confirms the drug mixture's entrapment within the polymer system of NS in Figure 2. Furthermore, characteristic peaks present in the pure drug mix and the drug and polymer physical mixture, including alkane C-H stretch, alkene C-H bending, amine C-N stretch, and amide N-H bending, were found in the optimized formulation, indicating the presence of the drug in the NS.

DSC analysis of NS

The DSC thermogram of the optimized NS formulation, depicted in Figure 3, revealed an endothermic peak at 340.03 °C, indicating the presence of Curdlan polymer. The absence of peaks related

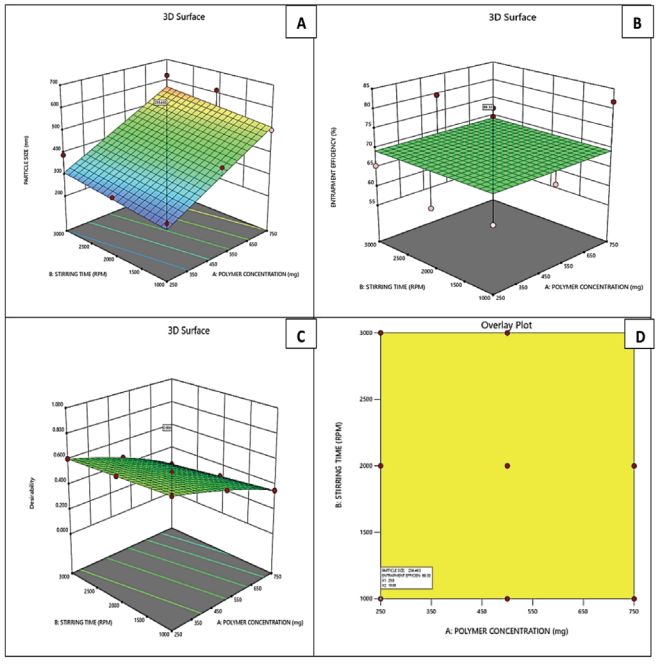

Figure 5. (A) 3D surface plot for particle size, (B) entrapment efficiency, (C) Desirability plot, (D) Overlay plot for polymer concentration and stirring rate

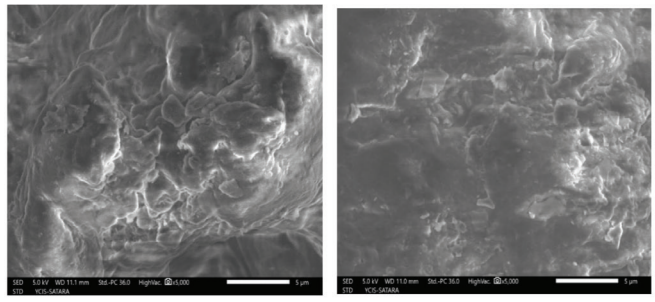

Figure 6. SEM micrograph of optimized formulation
SEM: Scanning electron microscopy

Table 8. Check point analysis of optimized NS formulation F10

Response	Expected	Observed	Residual	Desirability
Particle size (nm)	256.46	280.9	24.44	0.656
EE (%)	69.33	63	6.33	0.656

NS:Nanosponge, EE: Entrapment Efficiency

to drugs indicated that the drug mixture is encapsulated within the polymer system, demonstrating its compatibility.

Drug release kinetic study of optimized formulation

For the assessment of release kinetics, the drug release data underwent analysis using various kinetic equations. This analysis involved evaluating key parameters, correlation coefficient (R), and release exponent (n)-to explore the release mechanism. Table 9 presents the correlation coefficient (R) for the optimized formulation.

The model that gave a high 'R' value was considered the best fit for the release data. The Korsmeyer-Peppas model best described the sustained release of the optimized formulation: the diffusion exponent (n) value. From the result, the best fit model for optimized formulation is zero zero-order model (Figure 7).

Super Case II transport specifically refers to the situation where the release exponent (n=0.9210) is greater than 0.89. In this scenario, the drug release mechanism is considered to be more dominated by polymer relaxation or erosion compared to the standard "anomalous transport" in the range of 0.45 to 0.89. It implies that the release kinetics are significantly influenced by the swelling, relaxation, or erosion of the polymeric matrix.

MTT assay

Prior research has highlighted the anticancer properties of *Annona squamosa* L. the leaves extract. Hence, this study seeks to explore the anticancer activity of isolated HGN specifically on breast cancer cells.

Different doses ranging from 10 µg to 100 µg of various compounds were evaluated for their anti-tumor effects on the MCF-7 cell line. Notably, HGN demonstrated an IC_{50} value of 42.39 µg/mL in MCF-7 breast cancer cells, exceeding the IC_{50} of 5-fluorouracil at 39.22 µg/mL, indicating promising activity compared to the standard compound, as depicted in Figure 8. Similarly, AMY derived from *Capparis zeylanica* L. was evaluated at different doses (ranging from 10 µg to 100 µg) for its antitumor activity against the MCF-7 cell line. An IC_{50} value of 34.54 µg/mL for AMY was observed in MCF-7 breast cancer cells. AMY outperformed 5-fluorouracil, which has an IC_{50} of 39.22 µg/mL. The samples demonstrated noteworthy activity compared to the standard compound, as illustrated in Figure 9. Moreover, the combination of both HGN and AMY yielded an IC_{50} value of 43.03 µg/mL, whereas the optimized NS formulation showed an IC_{50} value of 33.71 µg/mL.

Apoptosis analysis

In the study to evaluate the apoptotic effects of the optimized batch, DAPI staining was conducted. The results from the control group in Figure 10A revealed normal nuclear morphology with intact and evenly distributed chromatin. Figure 10B displayed significant DNA alterations in cells treated with fluorouracil, which indicates apoptosis or cell death, characterized by condensed or fragmented nuclei. Moreover, changes in nuclear architecture, such as membrane blebbing and apoptotic body formation, were observed, which is characteristic of apoptotic cells. The optimized formulation depicted in Figure 10C demonstrated a notable decrease in the MCF-7 cell population, primarily showing mitotic morphology suggestive of effective G2/M cell cycle arrest. The images exhibited highly fragmented cell nuclei, substantial cell loss, and extensive cellular damage.

Table 9. Release kinetics of optimized formulation

Model		Formulation code
Zero order	R^2	0.9981
First order	R^2	0.9877
Higuchi model	R^2	0.8925
Hixson-Crowell	R^2	0.9929
Korsmeyer Peppas	R^2	0.9618
Best fit model	Zero order model	

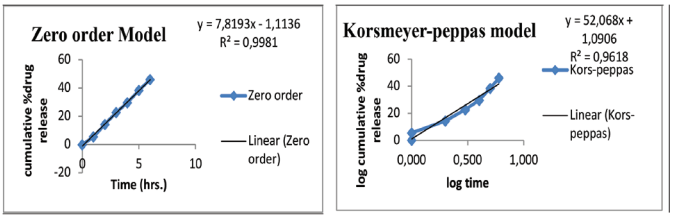

Figure 7. Release kinetics graph of optimized formulation

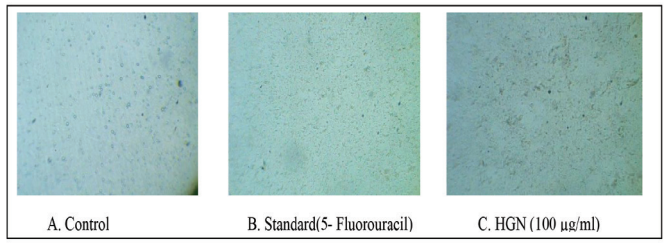

Figure 8. Cell line study with MCF-7 breast cancer cell line (A) control, (B) standard, (C) HGN

MCF: Michigan Cancer Foundation, HGN: Higenamine

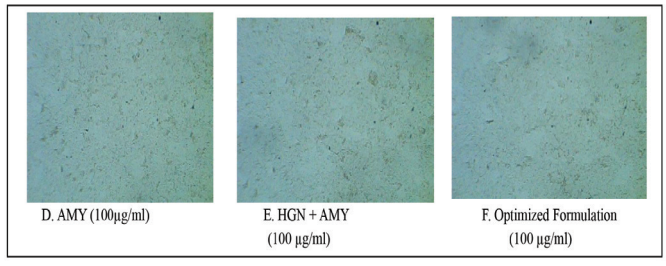

Figure 9. Cell line study with MCF-7 breast cancer cell line (D) AMY, (E) HGN + AMY, (F) optimized formulation

MCF: Michigan Cancer Foundation, AMY: alpha-amyrin, HGN: Higenamine

Cell cycle analysis

Figure 11A illustrates the distribution of cells treated with the optimized formulation based on granularity and APC fluorescence. The percentages of cells in different cell cycle phases were observed as follows: G0 (24.56%), G1 (48.21%), S (25.26%), G2 (15.36%), and M (3.25%). A red box marked with a star highlights a region with no events (0%). Figure 11B demonstrates a clear correlation between cell size and granularity, with the majority of cells (88%) falling within the red-boxed region, indicating a specific population of cells with consistent size and granularity properties. Figures 11C and 11D show the relationship between cell size (diameter) and APC fluorescence. In these plots, only a small number of events were detected in the red-boxed region (4.33 counts in plot C and 3.89 counts in plot D), which represents near 0% of the total events.

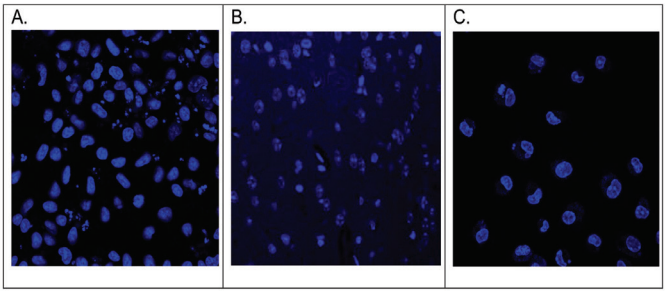

Figure 10. Nuclear morphology of MCF-7 cells after DAPI staining. (A) control, (B) Std. 5-FU, (C) optimized formulation

MCF: Michigan Cancer Foundation, DAPI: 4',6-diamidino-2-phenylindole, Std.: Standard, 5-FU: 5-Fluorouracil

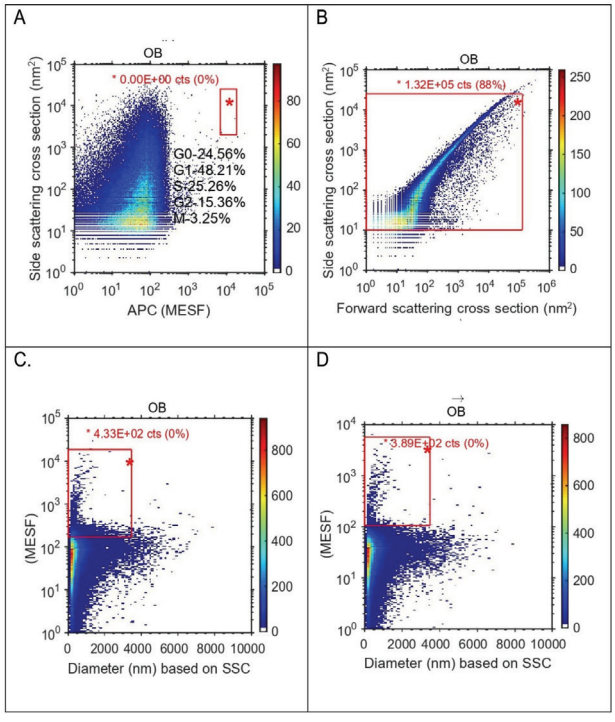

Figure 11. Flow cytometry analysis of optimized formulation with following plots (A) side scattering cross section vs. APC (MESF), (B) side scattering cross section vs. forward scattering cross section, (C) diameter (nm) based on SSC vs. APC (MESF), (D) diameter (nm) based on SSC vs. APC (MESF). Colour Scale: The colour scale on the right indicates the density of cells, with blue representing lower density and red representing higher density

APC: Allophycocyanin, MESF: Molecules of equivalent soluble fluorochrome, SSC: Side scattering cross, OB: Optical block

Stability studies

The stability of the optimized formulation was investigated in accordance with ICH guidelines, evaluating parameters such as drug content and *in vitro* drug release. The outcomes of these investigations are outlined in Table 10. The results indicated that there was no substantial change in the parameters mentioned when subjected to increased temperature and humidity during the stability assessments.

DISCUSSION

The preformulation studies and formulation optimization for the NS loaded with AMY and HGN yield results that provide valuable insights into the physicochemical properties and performance of the developed formulations.

The UV-Visible spectroscopy analysis established the λ max values for HGN and AMY, enabling reliable quantification. Crucial for stability, FTIR spectra confirmed the compatibility between the drug mixture and the polymer, as no interactions were observed. Additionally, DSC analysis showed no significant interactions affecting melting points, underlining the stability of the drug-polymer system and affirming the compatibility of the drug mixture with the polymer.

Variations in production yields and EE were observed based on the drug-to-polymer ratio. Particle size analysis revealed differences in size distribution impacting formulation stability. Negative zeta potential values indicated enhanced stability and minimized aggregation in the NS formulation. *In vitro* drug release profiles highlighted parameter-dependent variations, with optimization potential for improved therapeutic effectiveness.

The experimental design outcomes showcased consistent particle size and EE across formulations, providing a comprehensive overview of the formulation characteristics and highlighting the importance of controlling parameters for desired drug release behavior and efficacy.

Analysis of the SEM micrographs indicated the presence of numerous fine surface voids on the formed NS, presumably attributed to solvent diffusion. Additionally, no residual or intact drug crystals were observed on the NS surface, suggesting the formation of an NS matrix through the interaction of the

Table 10. Stability studies for optimized formulation

Time (Months)	Drug content (%)	*In vitro* drug release (%)
0	81.79±0.68	89.69±0.23
3	81.74±0.99	89.70±0.34
6	81.76±0.78	89.59±0.40

Data are mean values (n=3) ± SD. SD: Standard deviation

drug with the polymer. The FT-IR spectroscopy analysis of the optimized formulation verified the successful entrapment of the drug mixture within the NS. It was validated that the drug mixture had been effectively encapsulated within the polymer structure of the NS. In addition, the presence of characteristic peaks specific to the pure drug mix and the physical mixture of the drug and polymer in the optimized formulation further supported the presence of the drug within the NS matrix in the DSC study. From the result of release kinetics, the best-fit model for the optimized formulation is the zero-order model. The release kinetics are significantly influenced by the swelling, relaxation, or erosion of the polymeric matrix.

The MTT analysis indicated a synergistic effect of HGN and AMY in their anticancer activity, enhanced by their encapsulation into the NS formulation, which promotes increased bioavailability. DAPI staining analysis demonstrated that the optimized formulation induced apoptotic effects on MCF-7 cells, evidenced by DNA alterations, membrane blebbing, apoptotic body formation, and effective G2/M cell cycle arrest, showcasing the formulation's potential for targeted cancer therapy through apoptosis induction and cell cycle modulation.

The cell cycle analysis results offer a comprehensive view of the distribution patterns and characteristics of cells treated with the optimized formulation, shedding light on the formulation's impact on cell cycle progression and highlighting the complexity of cellular responses to the treatment. Consequently, the findings from the stability studies validate that the developed formulation is minimally affected by elevated humidity and temperature.

Overall, the combined results offer a holistic understanding of the physicochemical characteristics, compatibility, stability, and performance of the alpha-amyrin-loaded higenamine-loaded NS formulations, forming a solid foundation for further development and optimization in pharmaceutical applications.

CONCLUSION

Natural polymer-based NS comprising AMY and HGN proved successful in a meticulous 32 full factorial design, with batch F10 serving as their optimal batch. These NS demonstrated superior performance, particularly in their remarkable ability to exhibit enhanced therapeutic effects for combating cancer, offering sustained drug release extending up to 12 hours. *In vitro* studies further illuminated the potential of NS in cancer treatment, marking it as a beacon of promise in the realm of carriers. The development of NS is tailored for breast cancer treatment. Key components like curdlan and DCM were used in the formulation process, with varying polymer concentrations to obtain different NS types. Optimization through a factorial design study identified the ideal combination for results. The NS exhibited controlled drug release patterns, confirmed by a zero-order kinetic model, highlighting consistent release rates. Testing on MCF-7 cell lines, stability assessments, and the inclusion of AMY and HGN in the NS all showcased enhanced anticancer effects and sustained release benefits. Flow cytometry results indicated a significant impact on MCF-7 cell cycles, including cell cycle arrest in the G1 phase and decreased proliferation, underscoring the potential of this NS combination as an innovative and efficient cancer treatment.

Ethics

Ethics Committee Approval: Not required.

Informed Consent: Not required.

Footnotes

Authorship Contributions

Concept: S.A.D., Design: S.A.D., Data Collection or Processing: S.A.D., Analysis or Interpretation: S.A.D., Literature Search: P.S.J., Writing: P.S.J.

Conflict of Interest: The authors declare no conflicts of interest.

Financial Disclosure: The authors declared that this study received no financial support.

REFERENCES

1. Devendra Prajapati, Arindam Chatterjee, Mayank Bansal, Saurabh Pandey. Formulation and evaluation Tolbutamide liposomes for a sustained drug delivery system. J Biomed Pharma Res. 2022;11:16-27.
2. Ali MR, Osmani, Thirumaleshwar S, Rohit R, Bhosale, Parthasarathi K. Nanosponges: The spanking accession in drug delivery - an updated comprehensive review. Der Pharmacia Sinica. 2014;5:7-21.
3. Penjuri SCB, Ravouru N, Damineni S, BNS S, Poreddy SR. Formulation and evaluation of Lansoprazole loaded nanosponges. Turk J Pharm Sci. 2016;13:304-310.
4. SG V, Vaishnav GA, Joshi AS, Girbane YR. Preparation and *in-vitro* assessment of Tolbutamide loaded nanosponges. Ind J Res Methods Pharm Sci. 2022;1:15-20.
5. Iriventi P, Gupta NV, Osmani RAM, Balamuralidhara V. Design & development of nanosponge loaded topical gel of curcumin and caffeine mixture for augmented treatment of psoriasis. DARU J Pharma Sci. 2020;28:489-506.
6. Sathishkumar K, Chaturvedi M, Das P, Stephen S, Mathur P. Cancer incidence estimates for 2022 & projection for 2025: Result from National Cancer Registry Programme, India. Indian J Med Res. 2022;156:598-607.
7. Mizrahy S, Hazan-Halevy I, Landesman-Milo D, Ng BD, Peer D. Advanced strategies in immune modulation of cancer using lipid-based nanoparticles. Front Immunol. 2017;8:69.
8. Lefranc F, Tabanca N, Kiss R. Assessing the anticancer effects associated with food products and/or nutraceuticals using *in vitro* and *in vivo* preclinical development-related pharmacological tests. Semin Cancer Biol. 2017;46:14-32.
9. Choudhari AS, Mandave PC, Deshpande M, Ranjekar P, Prakash O. Phytochemicals in cancer treatment: from preclinical studies to clinical practice. Front Pharmacol. 2020;10:1614.
10. Dombe SA, Shirote PJ. Phytonutraceuticals in cancer prevention and therapeutics. Curr Nutr Food Sci. 2023;19:209-228.
11. Kim SS, Rait A, Kim E, DeMarco J, Pirollo KF, Chang EH. Encapsulation of temozolomide in a tumor-targeting nanocomplex enhances anticancer efficacy and reduces toxicity in a mouse model of glioblastoma. Cancer Lett. 2015;369:250-258.

12. Dombe SA, Shirote PJ. Isolation, *in-silico* studies, and biological evaluation of higenamine from *Annona squamosa* L. against breast cancer. Int J Pharma Qual. 2023;14:1039-1047.

13. SF Neto, AL Prada, LDR Achod, HFV Torquato, CS Lima, EJ Paredes-Gamero, MOS de Moraes, ES Lima, EH Sosa, TP de Souza, JRR Amado. α-amyrin-loaded nanocapsules produce selective cytotoxic activity in leukemic cells. Biomed Pharmacother, 2021;139:111656.

14. Dhimmar B, Pokale R, Rahamathulla M, Hani U, Alshahrani MY, Alshehri S, Shakeel F, Alam P, Osmani RAM, Patil AB. Newfangled topical film-forming solution for facilitated antifungal therapy: design, development, characterization, and *in vitro* evaluation. Polymers (Basel). 2023;15:1003.

15. Darandale SS, Vavia PR. Cyclodextrin-based nanosponges of curcumin: formulation and physicochemical characterization. J Incl Phenom Macrocycl Chem. 2013;75:315–322.

16. Dingwoke E, Felix SY. Development and evaluation of nanosponges loaded extended release tablets of lansoprazole. Univ J Pharma Res. 2019;4.

17. Osmani RAM, Kulkarni PK, Shanmuganathan S, Hani U, Srivastava A, Prerana M, Shinde CG, Bhosale RR. A 3^2 full factorial design for development and characterization of a nanosponge-based intravaginal in situ gelling system for vulvovaginal candidiasis. RSC Adv. 2016;6:18737-18750.

18. Anwer MK, Fatima F, Ahmed MM, Aldawsari MF, Alali AS, Kalam MA, Alshamsan A, Alkholief M, Malik A, Az A, Al-Shdefat R. Abemaciclib-loaded ethylcellulose based nanosponges for sustained cytotoxicity against MCF-7 and MDA-MB-231 human breast cancer cells lines. Saudi Pharm J. 2022;30:726-734.

19. Pathak N, Singh P, Singh PK, Sharma S, Singh RP, Gupta A, Mishra R, Mishra VK, Tripathi M. Biopolymeric nanoparticles based effective delivery of bioactive compounds toward the sustainable development of anticancerous therapeutics. Front Nutr. 2022;9:963413.

20. Yang HB, Song W, Chen LY, Li QF, Shi SL, Kong HY, Chen P. Differential expression and regulation of prohibitin during curcumin-induced apoptosis of immortalized human epidermal HaCaT cells. Int J Mol Med. 2014;33:507-514.

21. Osmani RA, Hani U, Bhosale RR, Kulkarni PK, Shanmuganathan S. Nanosponge carriers- an archetype swing in cancer therapy: a comprehensive review. Curr Drug Targets. 2017;18:108-118.

22. Baburaj R, Veerabhadrappa RS, Das K. Alpha amyrin nano-emulsion formulation from stem bark of *Ficus benghalensis* and its characterization for neuro-behavioral studies. Turk J Pharm Sci. 2024;21:42-51.

Turk J Pharm Sci 2025;22(3):191-206
DOI: 10.4274/tjps.galenos.2025.70718

ORIGINAL ARTICLE

Simultaneous Quantification of Doravirine, Lamivudine, and Tenofovir Disoproxil Fumarate in Human Plasma by UPLC-MS/MS: Method Development and Validation

Narasimha KANJARLA, Balaraju KATTA*

Chaitanya (Deemed to be University), Department of Pharmacy, Hyderabad, Telangana, India

ABSTRACT

Objectives: A novel, high-throughput liquid chromatography tandem mass spectrometry (UPLC–MS/MS) technique has been developed that uses Etravirine (ETR) as the internal standard (IS) to simultaneously quantify Doravirine (DOR), Lamivudine (LAM), and Tenofovir Disoproxil Fumarate (TDF) in human plasma. The procedure employs a precipitation extraction technique to analyze analytes from human plasma. This study aims to develop and validate a novel and reliable stability-indicating UPLC–MS/MS method for the simultaneous determination of DOR, LAM, and TDF in human plasma, using ETR as the IS.

Materials and Methods: ETR, based on its stable-isotopic nature and structural and physicochemical similarity to the analytes of interest, was used as an IS. Precipitation extraction was the technique used to prepare samples. An agilent zorbax XDB C18 analytical column (2.1 × 50 mm, 3.5 µm) was used for chromatographic separation, and its isocratic mobile phase consists of acetonitrile and buffer (5 mM of ammonium formate with 0.1 % formic acid) in the ratio 80:20, *v/v*, at a flow rate of 0.120 mL/min.

Results: The parent-to-product ion transitions for the drugs were as follows : LAM: m/z 231.08 amu → 112.00 amu, TDF: m/z 288.33 amu → 176.17 amu, DOR: m/z 426.38 amu → 112.02 amu, and IS ETR: m/z 437.36 amu → 164.97 amu. These transitions were observed using a triple quadrupole mass spectrometer in the multiple reaction monitoring (MRM) positive ion mode. The compound's basic group content determined which positive mode to choose. For DOR, LAM and TDF, the method was validated throughout concentration ranges of 2.5–1000 ng/mL with correlation coefficients (r^2) values obtained were found to be 0.99. From spiked plasma samples, the mean recovery outcomes were observed and found to be DOR, LAM, and TDF was 83.39%, 87.33%, and 85.56%. With a 3.0-minute total run time, the approach was shown to be reliable and quick.

Conclusion: A triple quadrupole mass spectrometer running in the MRM positive ion mode was used to track these transitions. The compounds' functional group content served as the basis for choosing the positive mode. The mean recovery values were obtained for three APIs from spiked plasma samples. The run times were found to be both reliable and quick. The method was proven to produce precise and specific results for the determination of selected drugs through the current study. The method is stable when exposed to various stress conditions, demonstrating minimal degradation. The current method was validated as per the ICH M10 guidelines and was found to meet the desired acceptance criteria. The developed bioanalytical method, validated in accordance with ICH M10 guidelines, demonstrated high accuracy, precision, and reproducibility for the simultaneous quantification of DOR, LAM, and TDF. Its streamlined design and reliable performance make it a valuable tool for routine analysis.

Keywords: Doravirine, Tenofovir Disoproxil Fumarate, lamivudine, UPLC-MS/MS, quantification

***Correspondence:** balrajkatta@gmail.com, **ORCID-ID:** orcid.org/0009-0002-8297-0934

Received: 19.05.2024, **Accepted:** 02.06.2025 **Publication Date:** 01.08.2025

Cite this article as: KANJARLA N, KATTA B. Simultaneous quantification of Doravirine, Lamivudine, and Tenofovir Disoproxil Fumarate in human plasma BY UPLC-MS/MS: method development and validation. Turk J Pharm Sci. 2025;22(3):191-206

INTRODUCTION

In the domain of pharmaceutical research, the creation of precise and efficient analytical methods for quantifying drug compounds in biological matrices is crucial for ensuring the effectiveness and safety of therapeutic interventions. Human immunodeficiency virus (HIV) represents one of the most pressing global health issues of our time, impacting millions worldwide. HIV belongs to the lentivirus family, a type of retrovirus known for its ability to target and debilitate the immune system, particularly CD4 cells (T-helper cells), which are vital for coordinating the body's immune response against infections.[1,2]

The US Food and Drug Administration approved the tablet [containing Doravirine (DOR), Lamivudine (LAM), and Tenofovir Disoproxil Fumarate (TDF): 100 mg/300 mg/300 mg] on August 30, 2018 to treat HIV-1 infection in adults who have never received antiretroviral therapy. Alternatively, they were be used to replace an existing antiretroviral regimen in people who were virologically suppressed for at least six months on a stable antiretroviral regimen, had no history of treatment failure, and had no known substitutions linked to resistance to these tablets.[2]

Data from clinical trials showing the effectiveness of combining DOR, LAM, and TDF in lowering HIV virus type 1 (HIV-1) viral load and raising cluster of differentiation four positive ($CD4^+$) cell counts served as the foundation for the approval. With this approval, HIV treatment has advanced significantly, and patients now have a powerful, well-tolerated choice for treating their condition.[3-6] The fixed-dose combination pill was meant to be taken orally once a day, with or without meals. It functions by inhibiting the replication of HIV, thereby decreasing the viral load in the body and delaying the advancement of the disease.

This research aimed to develop and validate a novel and reliable stability-indicating high-throughput liquid chromatography–tandem mass spectrometry (UPLC–MS/MS) method for the simultaneous determination of DOR, LAM, and TDF (Figure 1-3) in human plasma. Developing and validating such a method is pivotal for facilitating accurate pharmacokinetic studies, monitoring therapeutic drug levels, and ensuring compliance with regulatory standards.

It is observed that no methods are available for the "Simultaneous Quantification of DOR, LAM, and Tenofovir Disoproxil Fumarate in Human Plasma by UPLC-MS/MS". Different publications were available for the simultaneous estimation of these drugs using HPLC and HPTLC methods in tablet formulation.[13-20] While HPLC methods are indeed well-established, UPLC-MS/MS offers superior sensitivity, specificity, and the ability to detect and quantify analytes at lower concentrations, which is critical for the simultaneous estimation of DOR, LAM, and TDF in a biological matrix. These advantages make UPLC-MS/MS a more suitable choice for the objectives of our work. Hence, the current experimental study will be beneficial for the simultaneous estimation of the aforementioned drugs in a biological matrix.

MATERIALS AND METHODS

Resources and techniques

Working standards and references

The samples of LAM, TDF, and DOR (with 99% *w/w* purity) were obtained from Hetero Labs Limited, Hyderabad. The same supplier provided the 99% *w/w* pure ETR, which was used as an internal standard (IS).

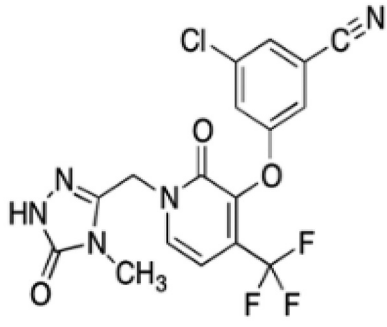

Figure 1. Structure of Doravirine

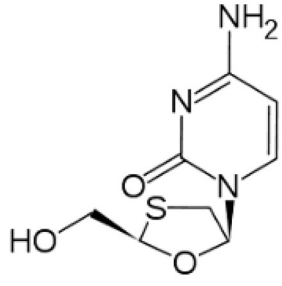

Figure 2. Structure of Lamivudine

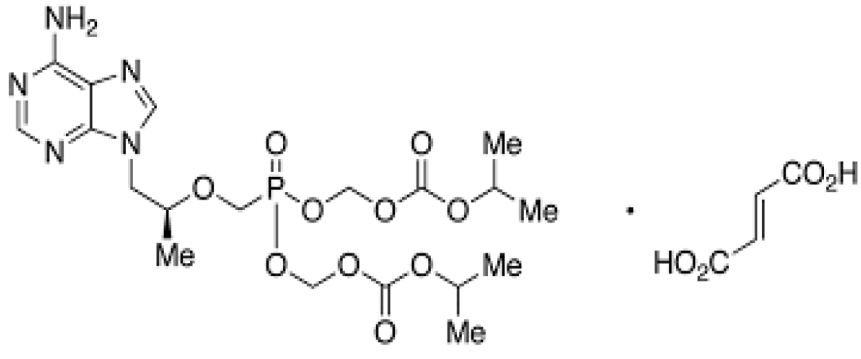

Figure 3. Structure of Tenofovir Disoproxil Fumarate

Chemicals-reagents

The research employed the following reagents and chemicals: HPLC-grade methanol (from Merck), K2EDTA human plasma, Milli-Q water (from Merck), and acetonitrile (from Merck).

Instruments utilized

Waters Acquity UPLC and Waters Quattro Premier XE Mass Spectrometer systems were utilized for method development and validation of the simultaneous quantification of DOR, LAM, and TDF. The UPLC system comprised a tunable UV detector, a quaternary pump, and an auto-injector. The MS/MS system, featuring a heated electrospray ionization (ESI) probe, delivers high sensitivity and ultra-fast detection. Designed to minimize contamination, the mass spectrometer incorporates a high-temperature heating block, heated ESI probe, drying gas, and heated desolvation line. Data analysis and interpretation were performed using MassLynx software (Version 4.1). Collectively, this instrumentation provides a robust platform for accurate and efficient quantification of the target compounds.

Equipment and UPLC-MS/MS assay conditions

In this study, a SIL HTC, a high-performance autosampler, a column oven (CTO-AS), a degasser DGU-20A3, and an Acquity UPLC system from Waters were used. The Quattro Premier XE type mass analyzer from Waters was the apparatus used for mass spectrometric detection in multiple reaction monitoring (MRM) mode. The data processing was performed using MassLynx, version 4.1, and the analysis was performed using a positive ionization interface.

Conditions of MS

The fundamental principle of MS revolves around the generation and detection of ions separated based on their mass-to-charge (m/z) ratios. In the method developed for this study, 500 ng/mL solutions of analytes and IS were prepared using a mixture of acetonitrile and buffer in an 80:20 ratio. These solutions were then infused into the mass spectrometer with an injection volume of 10 µL. Initially, full scan mode was employed to scan the parent and corresponding fragment ions for each analyte and IS pair. Subsequently, following the parent ion's identification, scanning was performed through MS/MS to obtain the resultant ions. Nitrogen gas was utilized as the collision gas, while zero air served as the sheath gas. Unit mass was used to measure the resolution. The fragment ion with the highest intensity, which was used for multiple reaction monitoring, was chosen for quantification.

Tuning of MS

The process confirmed the successful identification of parent ions and daughter ions for all analytes based on their molecular weights. Therefore, the analytes have been proved to be polar and ionizable. Consequently, for the investigation, the ESI method was chosen.

Optimized conditions

Instrument Setup: The analysis was performed using the Waters ACQUITY UPLC System coupled with a QUATTRO PREMIER XE mass spectrometer.

Ionization Conditions: Positive ion mode was selected as the polarity, with Electron Ion Spray (EIS) used as the ion source.

Detected Ions:

DOR: Parent ion at 426.38 amu; Daughter ion at 112.02 amu

TDF: Parent ion at 288.33 amu; Daughter ion at 176.17 amu

LAM: Parent ion at 231.08 amu; Daughter ion at 112.00 amu

Etravirine (ETR) (used as IS): Parent ion at 437.36 amu; Daughter ion at 164.97 amu

Chromatographic Conditions: Separation was achieved using an Agilent Zorbax XDB C18 column (2.1 × 50 mm, 3.5 µm particle size). The column oven temperature was maintained at 30 °C, and the Peltier temperature was set to 10 °C.

Mobile Phase & Flow Parameters: The mobile phase consisted of acetonitrile and buffer in an 80:20 *(v/v)* ratio, delivered at a flow rate of 0.120 mL/min. A sample volume of 5.0 µL was injected using a partial loop with needle overfill technique.

Retention Times & Run Duration: Tenofovir DF: 1.11 min, LAM: 1.00 min, DOR: 1.20 min and ETR (IS): 1.72 min. Total run time was 3.0 minutes. The mass spectra are illustrated in Figures 4-11.

Extraction procedure

Protein precipitation serves as a method to mitigate matrix interference in the analyte. Precipitating agents like trichloroacetic acid and perchloric acid are employed for this purpose. The precipitating agent is diluted with the sample matrix before it is vortexed. Subsequent centrifugation and filtration were employed to eliminate high-molecular-weight proteins. The obtained filtrate was analyzed. It's essential that the reconstituted solvent easily dissolve any protein precipitated during the precipitation process.

Procedure for extracting samples

Each sample was placed into a 5 mL polypropylene tube and weighed at approximately 200 milligrams. To this, the sample was mixed with 1 mL of acetonitrile (a precipitating agent) and 50 µL of Internal Standard (ISTD) solution (1 µg/mL ETR). Vortexing thoroughly mixed the materials to aid in precipitation. Eight-tenths milliliters of the liquid supernatant were collected after precipitation, placed in vials, and then injected into the UPLC-MS/MS for examination.

Procedure optimization

The ideal chromatographic conditions were established by analyzing the standard solutions of the three analytes.

Preparation of mobile phase

0.1% formic acid solution

Precisely dispense 1.0 mL of formic acid. Dissolve the dispensed formic acid in 1000 mL of water (HPLC grade). Filter and sonicate the solution for 10 minutes to ensure complete mixing and dissolution.

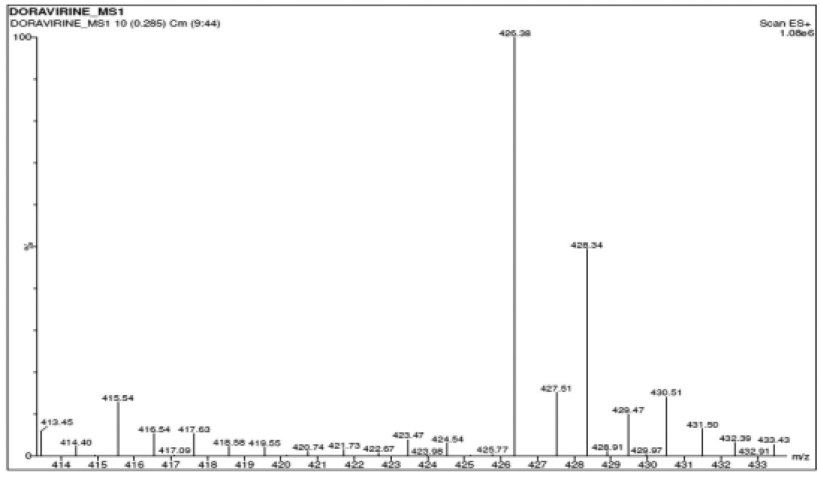

Figure 4. Parent ion of Doravirine

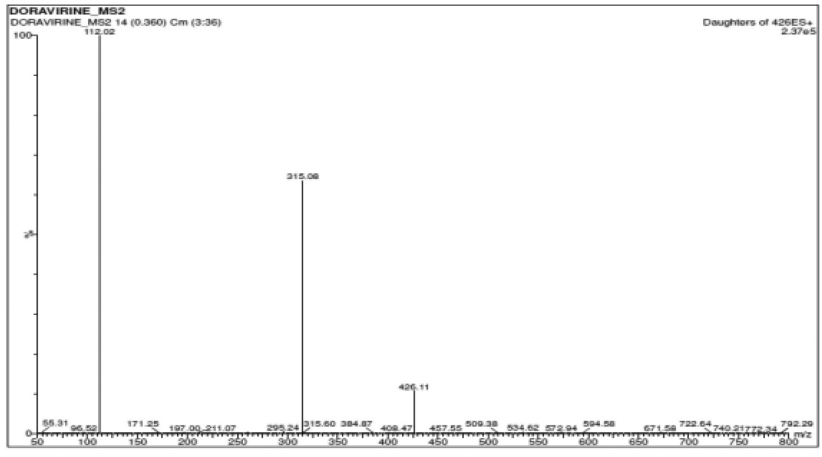

Figure 5. Daughter ion of Doravirine

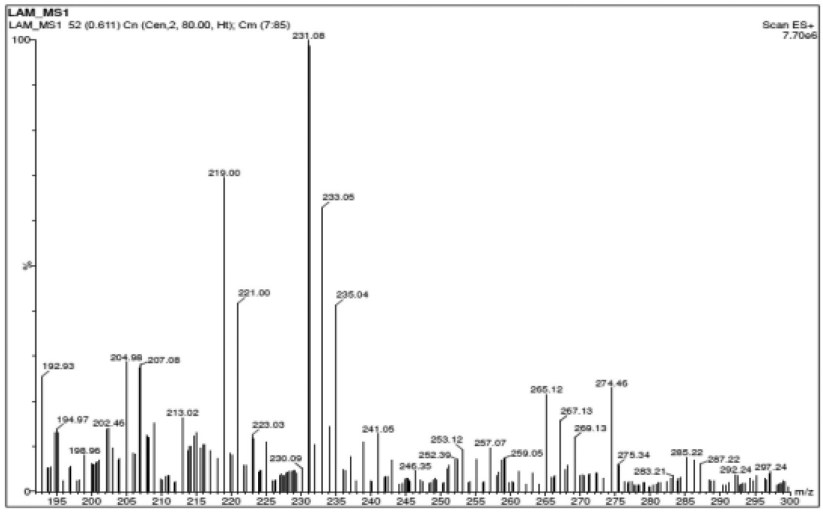

Figure 6. Parent ion of Lamivudine

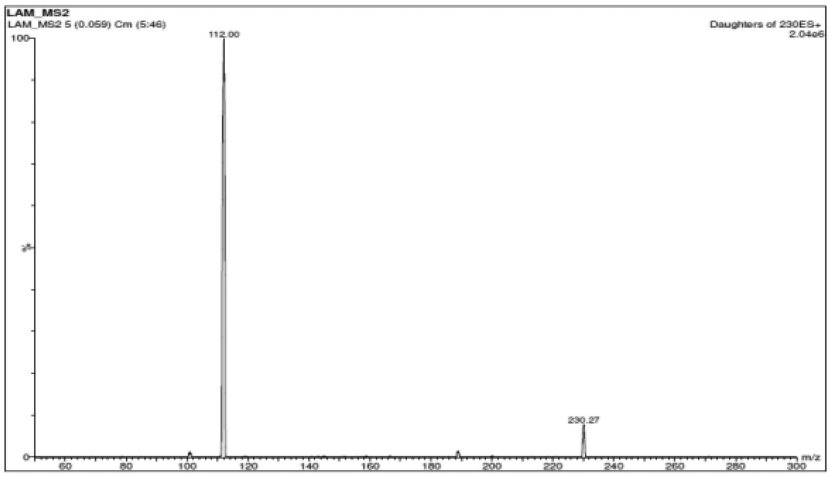

Figure 7. Daughter ion of Lamivudine

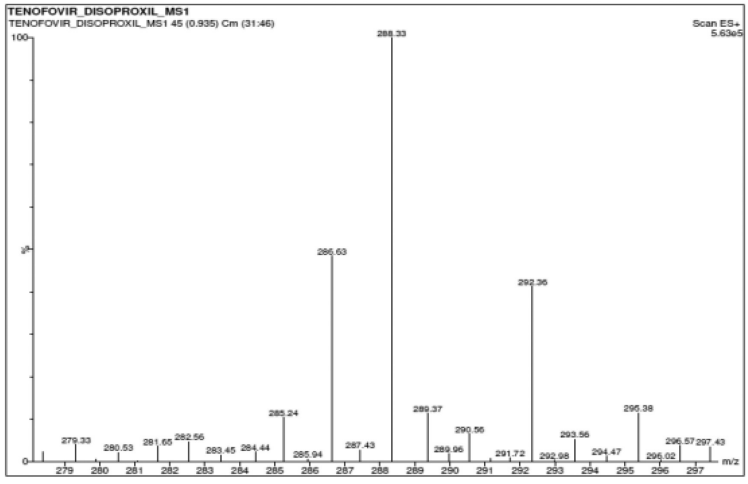

Figure 8. Parent ion of Tenofovir Disoproxil Fumarate

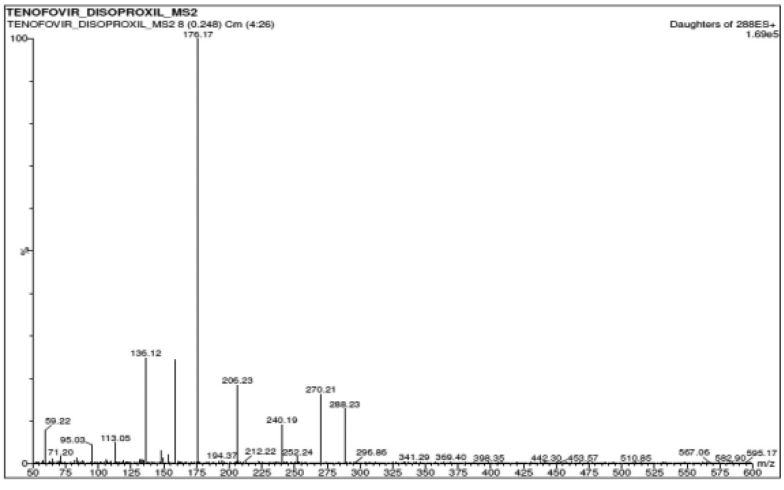

Figure 9. Daughter ion of Tenofovir Disoproxil Fumarate

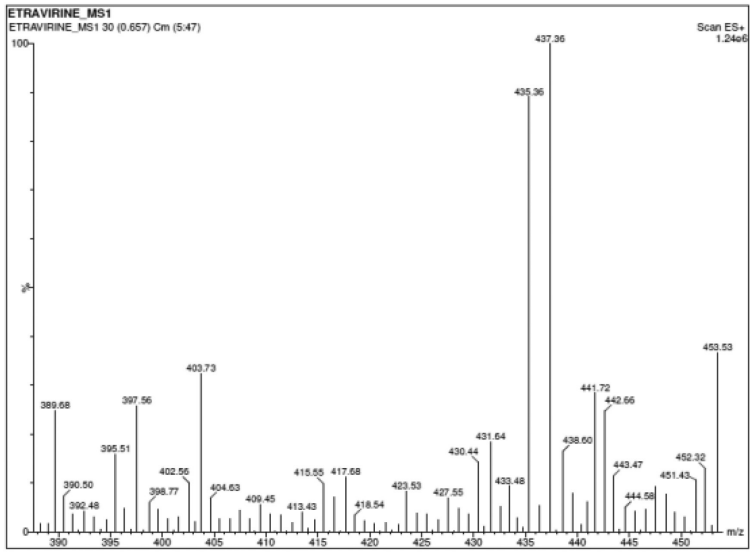

Figure 10. Parent ion of

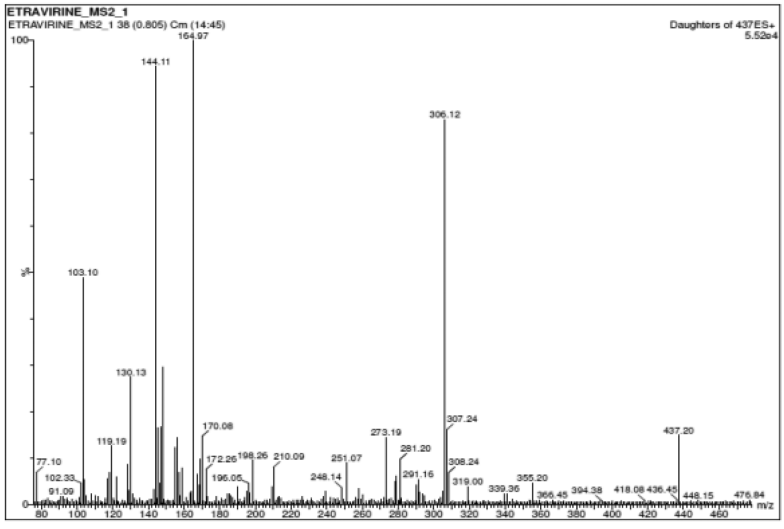

Figure 11. Daughter ion of Etravirine

Preparation of buffer

Combine 5 mM of ammonium formate with 0.1% formic acid.

Preparation of mobile phase

Accurately measure 800 mL (80%) of acetonitrile and 200 mL (20%) of buffer. Mix the components thoroughly and filter using the vacuum.

Diluent preparation

Measure 800 mL of acetonitrile and 200 mL of water to obtain an 80% acetonitrile solution. Filter the mixture using a vacuum (0.45 µm).

Needle wash & seal wash solutions

Diluent solution (80% acetonitrile).

Internal standard solution

Mix ETR to achieve a concentration of 1 µg/mL using a combination of methanol: water in a 50:50 volume ratio (*v/v*).

Preparation of standard solutions of DOR, LAM, & TDF

Typical stock resolutions

Weigh 1.0 mg of each analyte (DOR, LAM, TDF) and ISTD (ETR) in 10.0 mL flasks. Add 5.0 mL methanol, and then dilute each solution to the mark with methanol/water in the ratio 50:50 (*v/v*).

Mixed standard solution

Accurately weigh 1 mg of each analyte (DOR, LAM, TDF) into a 1 mL diluent. Vortex the solution thoroughly to dissolve. This results in a concentration of 1000 µg/mL for each analyte. This solution constitutes the mixed stock solution containing DOR, LAM, and TDF at a concentration of 1000 µg/mL each.

Working solutions

Pipette 20 µL of each solution into a 2 mL diluent, achieving a concentration of 10 µg/mL or 10000 ng/mL. Pipette 200

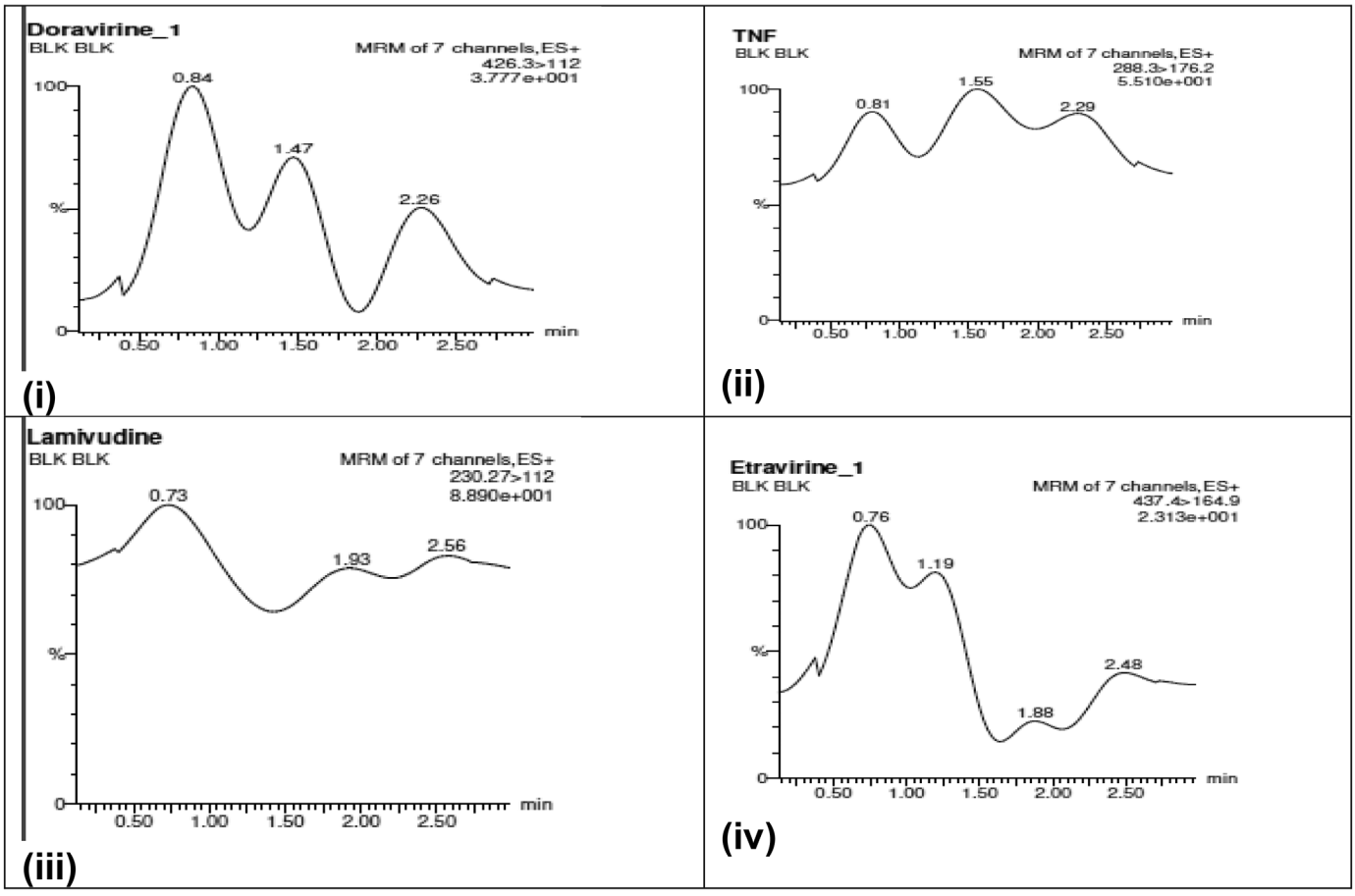

Figure 12. Blank Chromatograms of (i) DOR, (ii) TDF, (iii) LAM & (iv) ETR

DOR: Doravirine, TDF: Tenofovir disoproxil fumarate, LAM: Lamivudine, ETR: Etravirine

µL of each resulting solution into a 2 mL diluent to obtain a concentration of 1000 ng/mL using a methanol:water mixture in the ratio 50:50 (*v/v*).

Preparing quality control samples and plasma-spiked calibration standards

Calibration standards were prepared at 2.5, 10, 50, 250, 500, and 1000 ng/mL concentrations for the combination of DOR, LAM, and TDF. Quality control (QC) samples were prepared at concentrations of 7.4 ng/mL for Low-Quality Control (LQC), 480 ng/mL for Middle-Quality Control (MQC), and 900 ng/mL for High-Quality Control (HQC) for DOR, LAM & TDF.

Sample extraction

To guarantee uniformity, 950 µL of human plasma was used in each analyte sample. After adding 1 mL of acetonitrile (ACN) to the mixture, the centrifugation was run for 10 min, followed by vortexing for 5 min. After centrifugation, 0.8 mL of the solution's supernatant was carefully taken from the supernatant, put into vials, and then injected into the UPLC-MS/MS apparatus for examination.

Criteria for system suitability and mobile phase

Each composition was determined, resulting in the preparation of a large volume of mobile phase combining 800 mL of acetonitrile with 200 mL of buffer. This was done to ensure comparable outcomes throughout the study and validation. For System Suitability Testing (SST), a mobile phase was prepared to achieve the Lower LLOQ concentration, which was 2.5 ng/mL in this case. The System Suitability Test (SST) should be assessed.

Method development

After injecting the analyte solution, each analyte's parent ion weight was scanned. Furthermore, the parent ions were examined to determine the product ions in MS/MS mode. Scanning was conducted in the range of 100 to 600 atomic mass units. All ion peaks were eluted accurately. During the optimization of compound parameters for all three analytes, TDF required relatively high collision energy to achieve an appropriate response, and the respective mass chromatograms are detailed in Figures 12 and 13 below.

Method validation

The concentration of a medication, and possibly its metabolites, in biological samples, including blood, urine, plasma, serum, and tissue extracts, can be quantitatively measured using a bioanalytical technique. The process of method validation guarantees that the analytical approach yields precise results for the quantitative evaluation of drugs.

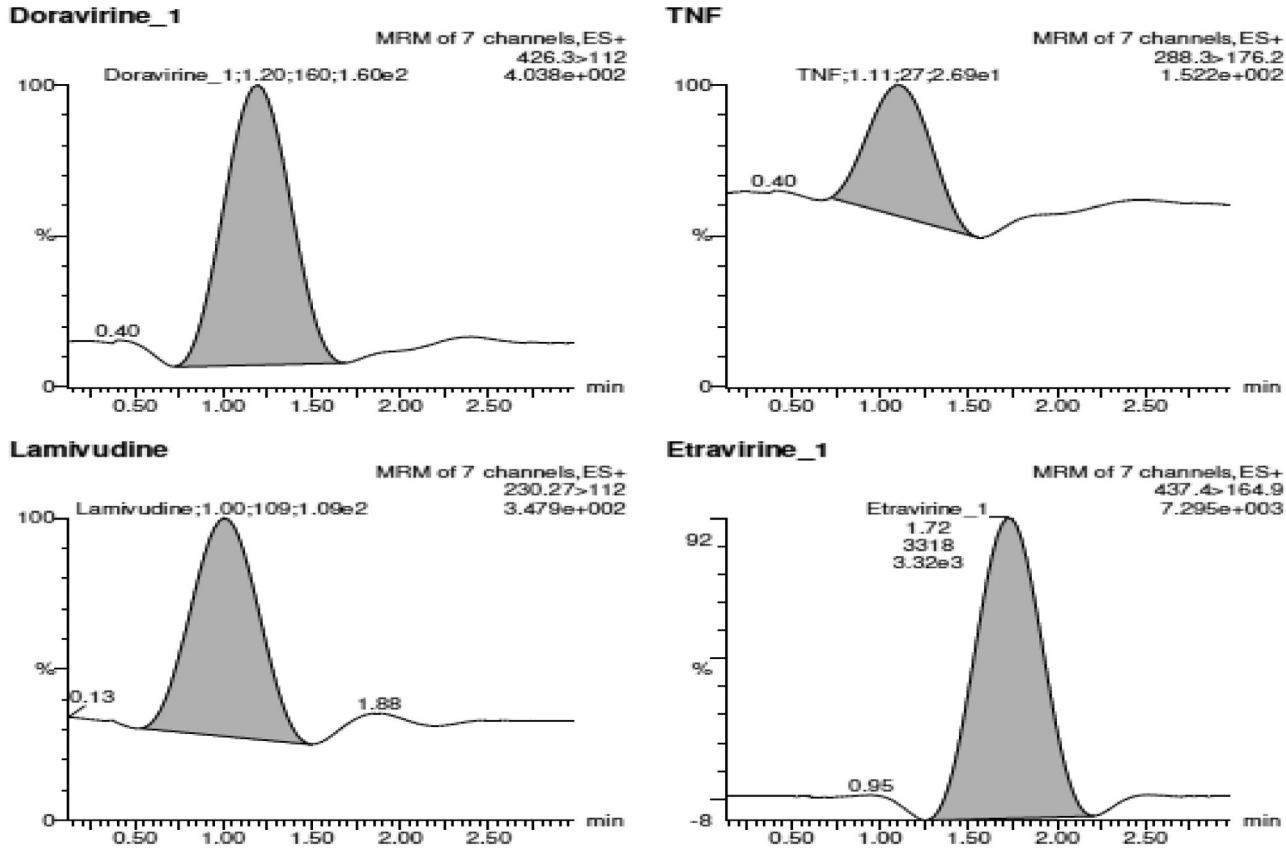

Figure 13. Sample Chromatograms of (i) DOR, (ii) TDF, (iii) LAM & (iv) ETR
DOR: Doravirine, TDF: Tenofovir disoproxil fumarate, LAM: Lamivudine, ETR: Etravirine

Method validation encompasses various parameters, including:

Specificity-sensitivity

The capacity to measure and distinguish the analyte signal when the sample contains the expected constituents or excipients. The capacity to measure and distinguish the analyte signal when the sample contains the expected constituents or excipients. *Procedure:* Six replicates were used to analyze a blank sample of 200 µL of human plasma at the LLOQ value of 2.5 ng/mL.

Selectivity

The capacity of the analysis technique to detect the presence of endogenous components in the matrix, such as metabolites, impurities, or decomposition products.

Procedure: Analysis was performed on plasma, LLOQ sample, and blank human plasma using an IS.

Calibration curve

Constructed by testing within the same biological matrix sample solutions that were intended, and spiking the matrix with known analyte concentrations.

Linearity

The ability of the bioanalytical procedure to yield outcomes that are exactly proportionate to the concentration of the sample within the standard curve's range.

Procedure: To find the linear range, concentration levels containing at least five to eight standards are used. The details for the preparation of spiked plasma are given in Table 1. The calibration curves for DOR, LAM, and TDF were determined to be linear, with correlation coefficients (r^2) exceeding 0.99 across the concentration range of 2.5 to 1000 ng/mL.

Quantification range

In this study, 2.5 ng/mL was found to be the LLOQ based on the established linearity range, and the Upper Limit of Quantification (ULOQ) was determined to be 1000 ng/mL for DOR, LAM, and TDF samples.

Fresh samples

Fresh sample QCs are essential for assessing the accuracy and stability of analyte molecules. They help evaluate method performance and analysis stability, ensuring the correctness and accuracy of the technique. These performance QCs play a crucial role in validating the reliability and precision of the analytical method.

Procedure: The study's QC samples are chosen to assess the precision and stability of an established method. They are prepared in duplicate and cover a minimum of three concentrations, including the LLOQ, the mid-range, and the high end. The methods used to prepare spiking plasma samples of the three subject analytes (DOR, LAM, TDF) are detailed in Table 2 as follows.

Table 1. Information on how to prepare spiked plasma

Plasma spiking preparations					
Concentration of stock (µg/mL)	Stock volume (mL)	Plasma volume (mL)	Final volume (mL)	Final concentration (ng/mL)	Details
20.00	0.1	0.90	1.000	1000	CC6
10.00	0.1	0.90	1.000	500	CC5
5.00	0.1	0.90	1.000	250	CC4
1.00	0.1	0.90	1.000	50	CC3
0.10	0.1	0.90	1.000	10	CC2
0.04	0.1	0.90	1.000	2.5	CC1

Table 2. The specifics of the three QC sample preparation stages for Doravirine, Lamivudine, and Tenofovir Disoproxil Fumarate

Plasma spiking preparations – Doravirine, Lamivudine, and Tenofovir Disoproxil Fumarate					
Concentration of stock (µg/mL)	Stock volume (mL)	Plasma volume (mL)	Final volume (mL)	Final concentration (ng/mL)	Details
18.00	0.1	0.9	1	900	HQC
9.50	0.1	0.9	1	480	MQC
0.08	0.1	0.9	1	7.4	LQC

HQC: High-Quality Control, MQC: Middle-Quality Control, LQC: Low-Quality Control

Accuracy

Samples spiked with known concentrations of the analyte, such as QC samples, should be used to assess accuracy. Five concentration measurements and at least three levels should be included in this evaluation. The accuracy of the developed method is assessed using its percentage coefficient of variation.

Precision

The precision of a developed method refers to the agreement between individually obtained results under predefined experimental conditions. Precision is evaluated using QC samples, including the Lower Limit of Quantification QC (LLOQC), Lower-Quality Control (LQC), Medium Quality Control (MQC), and High-Quality Control (HQC), each analyzed in six replicates.

Recovery

This paper describes the contrast between the detector response derived from a pure standard nominal concentration and the response derived from an analyte extraction quantity from plasma (biological matrix). It is sufficient that the analyte recovery be consistent, precise, and reproducible for both the analyte and the IS; 100% recovery is not necessary.

Procedure: Extraction recoveries for DOR, LAM, and TDF were assessed by comparing the responses obtained from plasma samples spiked before extraction to those spiked after extraction. The mean recoveries for DOR, LAM, and TDF were determined to be within the specified range (80-120%).

Matrix factor

The "matrix effect" refers to the combined influence of all components present in the sample solution, except for the analytes being measured during the sample quantification process. It is assessed by determining the "matrix factor," which measures the degree of this effect. It is calculated for each analyte in the study to assess the extent of matrix interference. *Procedure:* Blank plasma was collected from six sources, including one hemolytic and one lipemic lot, in order to study the matrix effect. To construct post-extracted samples, the residue was reconstituted using a mobile phase that contained an ISTD and a set amount of analyte (LQC level). These samples, in addition to aqueous samples, were then assessed. The matrix factor for each analyte/ISTD was determined by comparing the peak response in the presence of matrix ions to the peak response in their absence. Each response ratio of the post-extracted matrix samples was compared to the mean response of the aqueous samples to assess the matrix effect.

Stability

Stability is evaluated to determine the chemical or physical compatibility of analytes under specific conditions and intervals, ensuring their reliability in a particular matrix. Furthermore, the stability analysis encompasses evaluating the impact of sample preparation, handling procedures, and analytical runtime over a specified period.

Procedure:

BT, short-term stability, and long-term stability are among the situations that are tested for stability. To evaluate the stability of each analyte, the data obtained on the percentage stability (% Stability) was determined. Details of the stability study are presented in Tables 3 and 4.

RESULTS

System suitability

The specificity serves as an indicator of the system's optimal performance during analysis, ensuring accurate results. The analyte peaks demonstrated specific elution with optimal resolution, affirming the method's specificity and sensitivity.

Selectivity

The method exhibited selectivity, as the analyte peaks were eluted without interference from other components present, as shown in Figure 14, ensuring accurate detection and quantification.

Table 3. Details of the production of stability samples for Doravirine, Lamivudine, and Tenofovir Disoproxil Fumarate (Benchtop and Long-Term)

Preparations of spiked plasma – Doravirine and Tenofovir Disoproxil Fumarate Benchtop and Long-Term Stability study					
Concentration of stock in µg/mL	**Stock volume (mL)**	**Plasma volume (mL)**	**Final volume (mL)**	**Final concentration (ng/mL)**	**Details**
0.08	0.1	0.9	1	7.4	LQC (Old)
0.08	0.1	0.9	1	7.4	LQC (Fresh)
18.00	0.1	0.9	1	900	HQC (Old)
18.00	0.1	0.9	1	900	HQC (Fresh)

HQC: High-Quality Control, LQC: Low-Quality Control

Table 4. The stability sample preparation details for Doravirine, Lamivudine, and Tenofovir Disoproxil Fumarate (Short-Term)

Preparations – Doravirine, Lamivudine, and Tenofovir Disoproxil Fumarate Short Term Stability Study					
Concentration of stock (µg/mL)	**Stock volume (mL)**	**Diluent volume (mL)**	**Final volume (mL)**	**Final concentration (ng/mL)**	**Details**
Old stock (9.5)	0.1	0.9	1	480	MQC - Old
Fresh stock (9.5)	0.1	0.9	1	480	MQC - Fresh

MQC: Middle-Quality Control

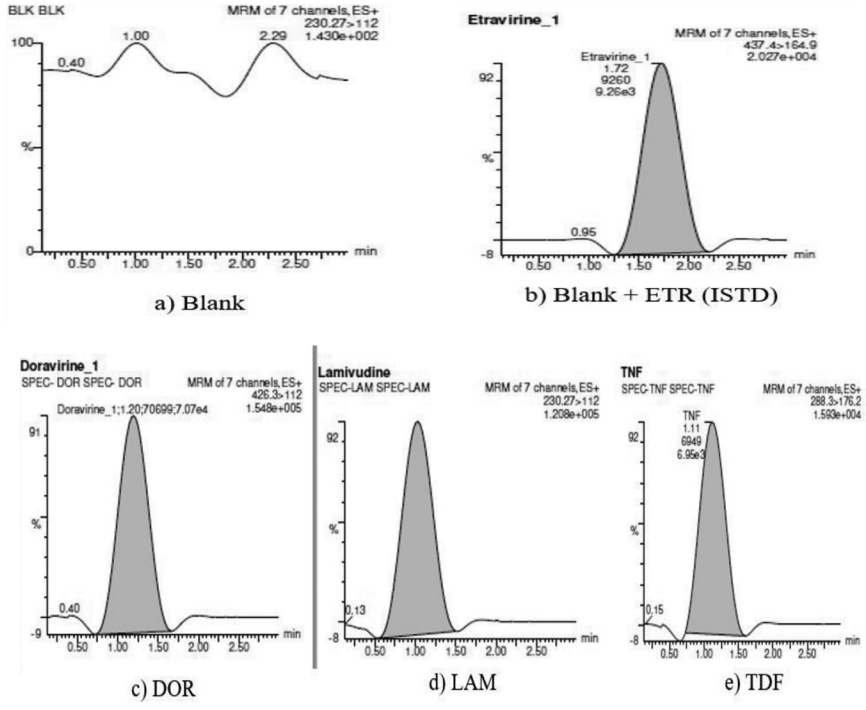

Figure 14. Chromatograms of a) Blank, b) Blank + ETR (ISTD), c) DOR, d) LAM & e) TDF

DOR: Doravirine, TDF: Tenofovir disoproxil fumarate, LAM: Lamivudine, ETR: Etravirine

Linearity range and calibration curve

A calibration curve with a matrix basis was constructed and applied to determine the analyte concentrations in unknown samples. The calibration curves for DOR, LAM, and TDF were found to be linear, with r^2 0.99 within the concentration range of 2.5 to 1000 ng/mL. Detailed results are provided in Table 5, and calibration curves are displayed in Figure 15.

QCs samples:

Three concentration levels of fresh QC samples were prepared: one in the center, one at the top end of the range, and one at three times the Lower Limit of Quantification (LLOQ). The precision and stability of these watery samples were evaluated.

Precision and accuracy:

The Upper and Lower Quantification Limits, which together constitute the range for the Limit of Quantification (LOQ), must each exhibit appropriate precision and accuracy. Table 6 displays the precision findings.

Extraction recovery

In contrast to the response derived from a pure, genuine standard concentration, recovery describes the detector response obtained from the amount of analyte supplied, which is then extracted from the matrix. The recovery of DOR, TDF, and LAM at low, medium, and high concentrations was ascertained by comparing the pre-extraction reaction plasma samples (n=6) with the post-extraction plasma samples. With a coefficient of variation (CV) ranging from 1.2 to 13.9 %, the mean recovery for DOR, LAM, and TDF was 83.39%, 87.33%, and 85.56%, respectively. Table 7 displays the results.

Matrix effect

Co-eluting matrix components may have a positive or negative effect on ionization, but they may not impact the outcome. By comparing each post-extracted matrix lot's response ratio to the corresponding aqueous samples, the matrix effect was evaluated using samples from six distinct lots. By contrasting the peak response in the presence and absence of matrix ions, the matrix factor for each analyte or the ISTD was determined. Results are presented in Tables 8, 9, and 10.

Benchtop stability

Benchtop stability (BT) was evaluated to make sure the analytes do not degrade during sample analysis or extraction. Six QC samples were removed from the freezer and allowed to come to room temperature, or around 25 °C. In fewer than six hours, stability standards and QC samples were produced, and the outcomes were compared to control samples. By contrasting the concentrations of the stability and control samples, the percentage stability of the sample concentrations was computed.

Long-term stability

Storage stability was evaluated to ensure that the analytes stay stable in the matrix throughout the study. After six hours at –20

Table 5. Calibration curve outcomes

Analyte	Nominal concentration (ng/mL)	Mean found concentration (ng/mL)	CV%	Parameters
DOR	2.5	2.1	00%	• Slope: 0.00875556 • Y-intercept: 0.015462 • r^2: 0.99929 • Regression equation: y = 0.00875556x + 0.015462 • Linearity range: 2.5 - 1000 ng/mL
	10	11.1	11%	
	50	49.8	6.8%	
	100	107.3	7.3%	
	500	476.3	-4.74%	
	1000	992.2	-0.78%	
TDF	2.5	2.2	-12.0%	• Slope: 0.00321555 • Y-intercept: 0.00158833 • r^2: 0.993768 • Regression equation: y = 0.00321555x + 0.00158833 • Linearity range: 2.5 - 1000 ng/mL
	10	9.2	-8.0%	
	50	51.1	4.2%	
	100	111.5	11.5%	
	500	481.6	-3.68%	
	1000	1007.1	0.71%	
LAM	2.5	2.6	4%	• Slope: 0.000851902 • Y-intercept: 0.00409457 • r^2: 0.998670 • Regression equation: y = 0.000851902x + 0.00409457 • Linearity range: 2.5 - 1000 ng/mL
	10	8.7	-13%	
	50	50.4	4.4%	
	100	109.4	9.4%	
	500	445.9	-10.82%	
	1000	1040.9	4.09%	

DOR: Doravirine, LAM: Lamivudine, TDF: Tenofovir Disoproxil Fumarate, CV: Coefficient of variation

± 5 °C, samples were examined using calibration standards and QC samples. Percentage stability was determined by comparing the average concentration of the stability sample with that of the control samples.

Short-term stability

A shorter storage stability study was carried out from sample collection to sample analysis in order to verify the stability of the analytes within the test system matrix. After keeping the samples at room temperature in a laboratory setting, six replicates of each sample were processed and assessed using freshly made calibration standards and QC samples (aqueous comparison samples). The percent stability was ascertained by contrasting the average concentration of the stability samples with that of the comparison samples.

All the outcomes obtained from the stability studies of DOR, LAM, and TDF are presented in Table 11. MRM chromatograms of DOR, TDF, LAM and ETR are shown in Figure 16.

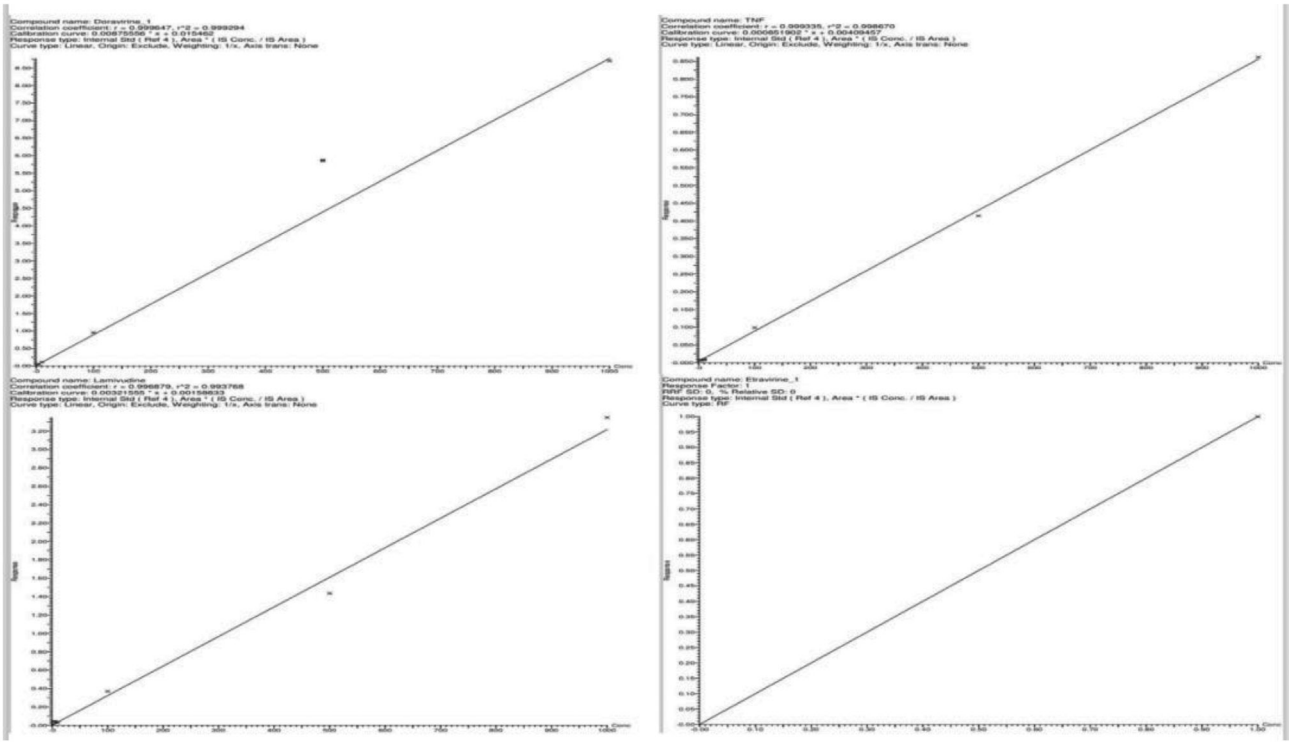

Figure 15. Calibration curves of DOR, TDF, LAM & ETR

DOR: Doravirine, TDF: Tenofovir disoproxil fumarate, LAM: Lamivudine, ETR: Etravirine

Table 6. Outcomes of precision

Analyte	Level of QC	Nominal concentration (ng/mL)	Intra batch		Inter batch	
			Mean found concentration (ng/mL)	CV%	Mean found concentration (ng/mL)	CV%
DOR	LQC	7.4	6.8	-1.08	6.5	-1.18
	MQC	480	439.9	-4.23	423.4	-5.31
	HQC	900	991.3	5.06	1070.2	7.01
LAM	LQC	7.4	8.5	5.23	8.8	6.54
	MQC	480	501.9	8.8	521.4	5.6
	HQC	900	986.7	5.23	1026.1	7.1
TDF	LQC	7.4	7.9	2.1	8.5	2.6
	MQC	480	501.4	4.2	522.8	6.2
	HQC	900	912.1	2.2	1005.6	5.9

DOR: Doravirine, LAM: Lamivudine, TDF: Tenofovir Disoproxil Fumarate, CV: Coefficient of variation, HQC: High-Quality Control, MQC: Middle-Quality Control, LQC: Low-Quality Control

Table 7. Results of extraction recovery

Analyte	QC level	Extracted samples	Extracted spiked samples (post)	% of recovery	% of mean recovery	Standard deviation	CV%
DOR	LQC	978	1169	83.66	83.39	1.84	2.21
	MQC	17327	20365	85.08			
	HQC	32625	40063	81.43			
LAM	LQC	538	623	86.36	87.33	2.30	2.64
	MQC	7704	8564	89.96			
	HQC	12380	14451	85.67			
TDF	LQC	149	174	85.63	85.56	1.92	2.25
	MQC	1893	2165	87.44			
	HQC	3231	3865	83.60			

Internal standard		Extracted samples	Extracted spiked samples (post)	% of recovery	% of mean recovery
Etravirine	LQC	3871	4618	83.82	81.75
MQC	3587	4423	81.10		
HQC	4168	5189	80.32		

DOR: Doravirine, LAM: Lamivudine, TDF: Tenofovir Disoproxil Fumarate, CV: Coefficient of variation, HQC: High-Quality Control, MQC: Middle-Quality Control, LQC: Low-Quality Control

Table 8. Outcomes of Doravirine Matrix Effect

Analyte	Doravirine		
	Analyte MF	ISTD MF	IS normalized factor
Lot-I	0.791	0.720	1.099
Lot-II	0.747	0.606	1.233
Lot-III	0.637	0.620	1.027
Lot-IV	0.762	0.712	1.070
Lot-V	0.711	0.696	1.022
Lot-VI	0.667	0.709	0.941
Mean	-	-	**1.065**
SD%	-	-	0.098
CV%	-	-	9.204

MF: Matrix factor, ISTD: Internal standard, CV: Coefficient of variation, SD: Standard deviation

Table 9. Outcomes of Lamivudine matrix effect

Analyte	Lamivudine		
	Analyte MF	ISTD MF	IS normalized factor
Lot-I	0.410	0.720	0.569
Lot-II	0.574	0.794	0.723
Lot-III	0.488	0.750	0.651
Lot-IV	0.533	0.774	0.689
Lot-V	0.441	0.852	0.518
Lot-VI	0.497	0.821	0.605
Mean	-	-	**0.626**
SD%	-	-	0.077
CV%	-	-	12.24

MF: Matrix factor, ISTD: Internal standard, CV: Coefficient of variation, SD: Standard deviation

Table 10. Outcomes of Tenofovir Disoproxil Fumarate matrix effect

Analyte	Tenofovir Disoproxil Fumarate		
	Analyte MF	ISTD MF	IS normalized factor
Lot-I	0.627	0.720	0.871
Lot-II	0.722	0.690	1.046
Lot-III	0.768	0.680	1.129
Lot-IV	0.762	0.678	1.124
Lot-V	0.653	0.714	0.916
Lot-VI	0.691	0.691	1.000
Mean	-	-	**1.014**
SD%	-	-	0.106
CV%	-	-	10.49

MF: Matrix factor, ISTD: Internal standard, CV: Coefficient of variation, SD: Standard deviation

Table 11. Outcomes of stability studies of all three analytes

Stability	Analyte	QC level	Mean concentration of fresh stability sample	Mean concentration of old comparison sample	Stability %
Bench top (6 hrs @ 25 °C)	DOR	LQC	978	1107	88.35
		HQC	32625	34706	94.00
	LAM	LQC	538	600	89.67
		HQC	12380	12339	100.33
	TDF	LQC	149	178	83.71
		HQC	3231	3533	91.45
Long-term (6 hrs @ -20 °C)	DOR	LQC	971	1198	81.05
		HQC	29103	32400	89.82
	LAM	LQC	856	976	87.70
		HQC	13988	13561	103.15
	TDF	LQC	172	163	105.52
		HQC	3654	3403	107.38
Short-term (25°C @ room temperature)	DOR	MQC	3330	3261	102.12
	LAM	MQC	17675	18421	95.95
	TDF	MQC	25498	24958	102.16

DOR: Doravirine, LAM: Lamivudine, TDF: Tenofovir Disoproxil Fumarate, HQC: High-Quality Control, MQC: Middle-Quality Control, LQC: Low-Quality Control

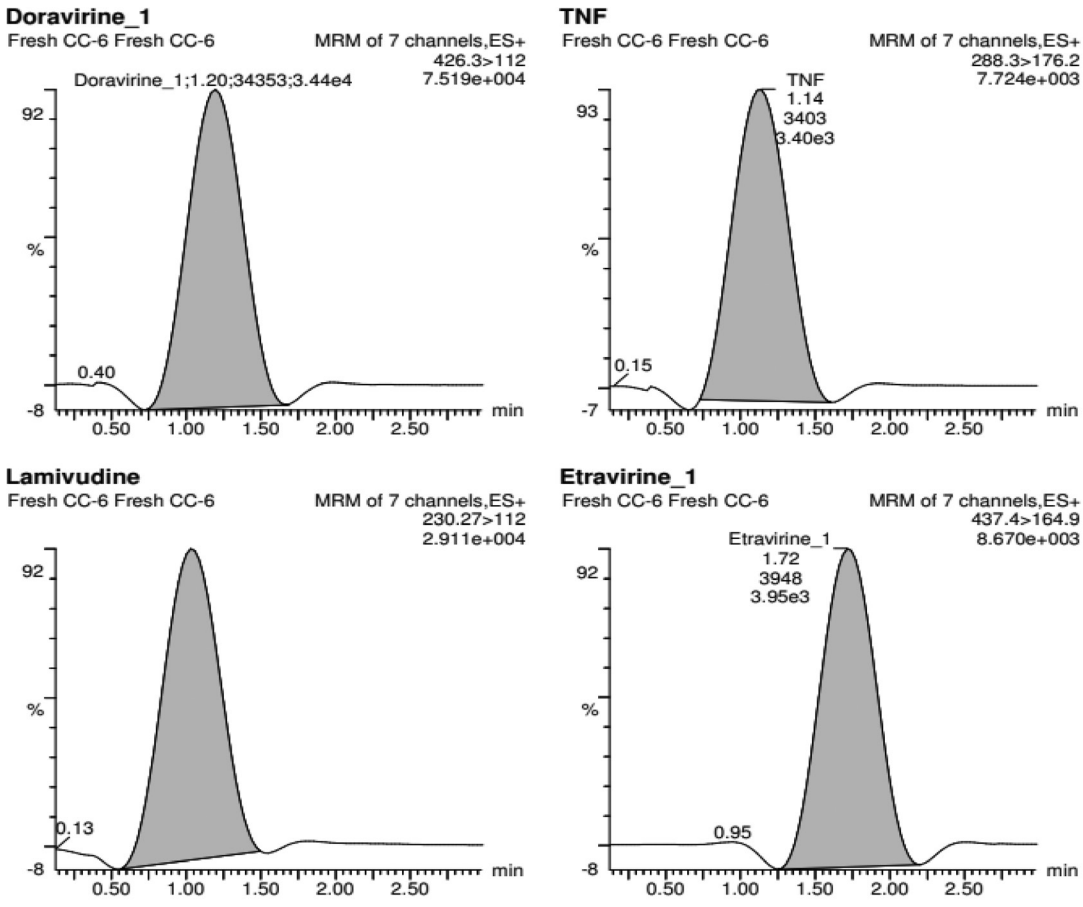

Figure 16. MRM Chromatograms of (i) DOR, (ii) TDF, (iii) LAM & (iv) ETR

DOR: Doravirine, TDF: Tenofovir disoproxil fumarate, LAM: Lamivudine, ETR: Etravirine

DISCUSSION

The bioanalytical method developed in this study demonstrates robust specificity and selectivity for the quantification of DOR, LAM, and TDF in human plasma. Method development, validation, and stability assessments adhered to regulatory standards outlined by the FDA, EMA, and ICH M10, thereby ensuring global applicability and reliability of the results. The strategic use of cost-effective solvents not only enhanced the method's economic viability but also contributed to reproducible outcomes with no observable interferences or impurities.

Compared to conventional analytical methods, particularly traditional HPLC, the newly optimized approach via UPLC-MS/MS offers superior sensitivity and specificity. The inclusion of tandem mass spectrometry enables the detection of analytes at lower concentration levels, a critical aspect of therapeutic drug monitoring. Validation parameters such as accuracy, precision, and percent recovery consistently fell within acceptable limits across the defined linearity range, substantiating the method's robustness.

Additionally, the method exhibited a minimal matrix effect, and stability studies revealed that the analytes remained stable under various conditions, affirming the method's suitability for routine clinical application. Notably, the use of columns with smaller particle sizes and high-pressure tolerance allowed for significantly shorter retention times and enhanced resolution. This translated into improved compound separation and reduced risk of co-elution, which is particularly beneficial when analyzing complex biological matrices. The increased throughput of the method presents a valuable advantage for clinical laboratories requiring rapid sample processing without compromising analytical performance.

CONCLUSION

We developed and validated a highly sensitive, reproducible, and robust bioanalytical method using the UPLC-MS/MS technique. The method demonstrated excellent performance across all parameters and complied fully with ICH guidelines. Given its reliability and consistency, this approach is well-suited for routine quantification of LAM, DOR, and TDF in analytical applications.

Ethics

Ethics Committee Approval: Not required.

Informed Consent: Not required.

Acknowledgments

The authors would like to express their profound thanks to M/S KSHETRA ANALYTICALS, Hyderabad, for providing crucial research facilities and direction during the progression and completion of this study. We would also like to thank "Hetero Labs Ltd.", Hyderabad, for kindly providing gift samples of the drug compounds used in this investigation.

Footnotes

Authorship Contributions

Concept: N.K., B.K., Design: N.K., B.K., Data Collection or Processing: N.K., B.K., Analysis or Interpretation: N.K., B.K., Literature Search: N.K., B.K., Writing: N.K., B.K.,

Conflict of Interest: The authors declare no conflicts of interest.

Financial Disclosure: The authors declared that this study received no financial support.

REFERENCES

1. Bekker LG, Beyrer C, Mgodi N, Lewin SR, Delany-Moretlwe S, Taiwo B, Masters MC, Lazarus JV. HIV infection. Nat Rev Dis Primers. 2023;9:42.
2. Full Prescribing Information (PIL) of Delstrigo Tablets, US FDA.
3. Colombier MA, Molina JM. Doravirine: a review. Curr Opin HIV AIDS. 2018;13:308-314.
4. Boyle A, Moss CE, Marzolini C, Khoo S. Clinical pharmacodynamics, pharmacokinetics, and drug interaction profile of Doravirine. Clin Pharmacokinet. 2019;58:1553-1565.
5. Blevins SR, Hester EK, Chastain DB, Cluck DB. Doravirine: a return of the NNRTI class? Ann Pharmacother. 2020;54:64-74.
6. Johnson MA, Moore KH, Yuen GJ, Bye A, Pakes GE. Clinical pharmacokinetics of Lamivudine. Clin Pharmacokinet. 1999;36:41-66.
7. Taylor K, Fritz K, Pellegrini MV, Parmar M. Lamivudine. 2024 Feb 28. In: StatPearls [Internet].
8. Kumar PN, Patel P. Lamivudine for the treatment of HIV. Expert Opin Drug Metab Toxicol. 2010;6:105-114.
9. Gallant JE, Deresinski S. Tenofovir Disoproxil Fumarate. Clin Infect Dis. 2003;37:944-950.
10. Miller MD. K65R, TAMs and tenofovir. AIDS Rev. 2004;6:22-33.
11. Nastri BM, Pagliano P, Zannella C, Folliero V, Masullo A, Rinaldi L, Galdiero M, Franci G. HIV and drug-resistant subtypes. Microorganisms. 2023;11:221.
12. Johnson M, Kumar P, Molina JM, Rizzardini G, Cahn P, Bickel M, Mallolas J, Zhou Y, Morais C, Kumar S, Sklar P, Hanna GJ, Hwang C, Greaves W; DRIVE-SHIFT Study Group. Switching to Doravirine/Lamivudine/Tenofovir Disoproxil Fumarate (DOR/3TC/TDF) maintains HIV-1 virologic suppression through 48 weeks: results of the DRIVE-SHIFT trial. J Acquir Immune Defic Syndr. 2019;81:463-472.
13. Kokkirala TK, Kancherla P, Alegete P, Suryakala D. A simple alternative and improved HPLC method for the estimation of Doravirine, Lamivudine, and Tenofovir Disoproxil Fumarate in solid oral dosage form. Biomed Chromatogr. 2021;35:e5121.
14. Attaluri T, Seru G, Varanasi SNM. Development and validation of a stability-indicating RP-HPLC method for the simultaneous estimation of Bictegravir, Emtricitabine, and Tenofovir Alafenamide Fumarate. Turk J Pharm Sci. 2021;18:410-419.
15. Tanuja A, Ganapaty S. Bio-analytical method development and validation for simultaneous determination of bictegravir, emtricitabine, and tenofovir alafenamide fumarate in human plasma by LC-MS/MS. Indian Journal of Pharmaceutical Education and Research. 2022;56:1190-1205.
16. Schauer AP, Sykes C, Cottrell ML, Imaz A, Podzamczer D, Kashuba AD. Validation of an LC-MS/MS assay for the simultaneous determination of bictegravir, Doravirine, and raltegravir in human plasma. J Pharm Biomed Anal. 2022;220:115010.
17. Marakatham S, Shanmugapandiyan P. Bioanalytical method development and validation of Doravirine, Lamivudine and Tenofovir Disoproxil Fumarate using HPLC in human plasma. Research Journal of Pharmacy and Technology. 2021;14:4087-4091.
18. Godela R, Gummadi S. A simple stability indicating RP-HPLC-DAD method for concurrent analysis of Tenofovir Disoproxil Fumarate, Doravirine and Lamivudine in pure blend and their combined film coated tablets. Ann Pharm Fr. 2021;79:640-651.
19. Rathod SM, Patel NC, Patel PU. Simultaneous determination of emtricitabine, tenofovir alafenamide fumarate and dolutegravir sodium by validated stability-indicating RP-HPLC-DAD method. Ann Pharm Fr. 2023;81:94-106.
20. Anderson MS, Gilmartin J, Fan L, Yee KL, Kraft WK, Triantafyllou I, Reitmann C, Guo Y, Liu R, Iwamoto M. No meaningful drug interactions with Doravirine, Lamivudine and Tenofovir Disoproxil Fumarate coadministration. Antivir Ther. 2019;24:443-450.

Turk J Pharm Sci 2025;22(3):207-216
DOI: 10.4274/tjps.galenos.2025.49840

ORIGINAL ARTICLE

Anticancer and Anti-Inflammatory Effects of Benzothiazole Derivatives Targeting NF-κB/COX-2/iNOS in a Hepatocellular Carcinoma Cell Line

Muhammed Mehdi ÜREMİŞ[1]*, Nuray ÜREMIŞ[1], Mustafa CEYLAN[2], Yusuf TÜRKÖZ[1]

[1]İnönü University Faculty of Medicine, Department of Medical Biochemistry, Malatya, Türkiye
[2]Gaziosmanpaşa University Faculty of Arts and Sciences, Department of Chemistry, Tokat, Türkiye

ABSTRACT

Objectives: Benzothiazole compounds, characterized by their diverse biological and pharmacological properties, have emerged as promising molecules for suppressing cancer cell proliferation and invasion due to their antiproliferative attributes. Prior research from our laboratory revealed that 2-substituted benzothiazole compounds inhibit the proliferation of glioma and cervical cancer cells and induce apoptosis in pancreatic cancer cells. However, there is limited research on the effectiveness of benzothiazoles against hepatocellular carcinoma cells (HCC). This study sought to elucidate the anticancer potential of 2-substituted benzothiazole derivatives through their modulation of oxidative stress and inflammation mediators.

Materials and Methods: Antiproliferative effects of two-step synthesized 2-substituted benzothiazole derivatives were evaluated on HepG2 cells via MTT assay. Apoptosis induction was assessed using Annexin V/PI staining; cell cycle arrest effects were determined through cell cycle analysis; cell migration was examined via wound healing assay; and mitochondrial membrane damage was quantified using JC-1 staining. Spectrophotometric measurements of total antioxidant status (TAS), total oxidant status, superoxide dismutase (SOD), total thiol, and native thiol levels were used to assess cellular redox status. Expression of nuclear factor kappa B (NF-κB), an inflammatory marker, was assessed by western blot, while inflammation-related cyclooxygenase-2 (COX-2) and inducible nitric oxide synthase levels were measured using ELISA.

Results: This investigation unveiled benzothiazole derivatives' antiproliferative and cytotoxic properties against HepG2 cells (IC_{50} values of 56.98 μM and 59.17 μM at 24 h, and 38.54 μM 29.63 at 48 h). The synthesized compounds exhibited the ability to suppress cell migration and induce apoptosis, mediated by mitochondrial membrane potential loss (wound-closure rates of 84.0 and 90.4% vs. 51.7% control at 48 h, apoptosis rates of 10.70% and 45.22% vs. 1.02% control). Furthermore, these derivatives reduced SOD activity (A and B at 100 μM $p<0.001$), TAS levels (A and B at 100 μM, $p < 0.05$, $p < 0.001$), and dynamic disulfide content. Notably, a decrease in NF-κB protein levels, closely associated with inflammation, was observed, along with a subsequent reduction in downstream effectors COX-2 (A and B at 100 μM, $p<0.001$) and iNOS (A and B at 100 μM, $p < 0.001$).

Conclusion: The findings of this study underscore the antiproliferative effects of benzothiazole derivatives in human HCCs, coupled with their anti-inflammatory potential by diminishing NF-κB levels.

Keywords: Benzothiazole, cyclooxygenase-2, inflammation, inducible nitric oxide synthase, nuclear factor kappa B, oxidative stress

INTRODUCTION

Hepatocellular carcinoma (HCC), a primary liver cancer, arises from a complex interplay of factors, including viral hepatitis, fatty liver disease, alcohol consumption, and the ingestion of aflatoxin-containing foods, ultimately resulting in liver inflammation, cirrhosis, fibrosis, and aberrant regeneration.[1] Among these factors, chronic hepatitis B and C virus infections inflict cellular damage, chronic alcohol consumption triggers steatohepatitis, and obesity fosters triglyceride accumulation, alters the hepatocyte microenvironment, and incites inflammation.[2]

***Correspondence:** mmuremis@hotmail.com, **ORCID-ID:** orcid.org/0000-0003-2296-2422
Received: 02.05.2024, **Accepted:** 02.06.2025 **Publication Date:** 01.08.2025

Cite this article as: ÜREMİŞ MM, ÜREMİŞ N, CEYLAN M, TÜRKÖZ Y. Anticancer and anti-inflammatory effects of benzothiazole derivatives targeting NF-κB/COX-2/INOS in a hepatocellular carcinoma cell line. Turk J Pharm Sci. 2025;22(3):207-216

Nuclear factor kappa B (NF-κB) is an essential transcription factor in regulating cell proliferation, survival, and inflammation.[3] Inducible nitric oxide synthase (iNOS) and cyclooxygenase-2 (COX-2) are the primary enzymes involved in the inflammatory response, and their expression levels are elevated in response to NF-κB activation.[4] The increased production of these enzymes leads to an accumulation of intracellular reactive oxygen species (ROS) and reactive nitrogen species (RNS), which exacerbate inflammation, disrupt redox homeostasis, induce DNA damage, and promote cellular transformation toward malignancy.[5] Given the intimate link between cancer development and pro-inflammatory factors, a primary objective in pharmaceutical chemistry is to devise cost-effective synthetic compounds that mitigate the molecular consequences of inflammation and restrain tumor cell proliferation.[6]

Benzothiazoles, whose diverse biological activities are dependent on the substituents and structural arrangement within their heterocyclic nucleus, have garnered significant interest in synthetic and pharmaceutical chemistry.[7] Our previous investigations revealed that benzothiazole compounds with 2-substituted groups can induce apoptosis in pancreatic adenocarcinoma cells (PANC-1), reduce cell viability, and decrease antioxidant levels.[8] This highlights the potential therapeutic effectiveness of these compounds. In addition, we observed that these compounds have antiproliferative effects in cervical cancer and glioma cells.[9,10] Given these positive results, understanding how 2-substituted benzothiazole compounds may affect inflammation and oxidative stress modulation in HCCs has become particularly important, shedding light on their potential therapeutic effects in liver cancer treatment. Due to their diverse biological roles, encompassing anticancer, anti-inflammatory, antimicrobial, and anticonvulsant properties, benzothiazole derivatives have emerged as subjects of keen exploration.[9-12] Clinical trials have scrutinized benzothiazole-containing compounds for neurological and psychiatric disorders, affirming their therapeutic potential.[11,13,14] Furthermore, select benzothiazole derivatives, distinguished by their anticancer prowess, have undergone clinical assessment as chemotherapeutic agents against recurrent melanoma, exhibiting promising results during phase I clinical trials.[15]

While there exists a body of research highlighting the utilization of benzothiazoles in the development of new drugs for various ailments, the anticancer attributes of 2-substituted benzothiazole derivatives against hepatocellular carcinoma, their interplay with inflammation, and the molecular mechanisms governed by the NF-κB/COX-2/iNOS signaling pathway remain incompletely understood. In light of this, the present study endeavors to elucidate the mechanisms underlying the anticancer and anti-inflammatory effects of synthesized 2-substituted benzothiazole derivatives on HCC.

MATERIALS AND METHODS

Synthesis of 2-substituted benzothiazole derivatives

The synthesis of 2-substituted benzothiazole compounds (A and B) was performed in two steps, following previously established protocols.[8-10,12] Chalcone analogs were synthesized via an aldol condensation reaction in the first step. Specifically, 4-fluorobenzaldehyde or 4-nitrobenzaldehyde (2.3 mmol) was reacted with cis-bicyclo[3.2.0]hept-2-en-6-one, in a basic medium containing sodium hydroxide (NaOH, 2.3 mmol) at room temperature. This reaction yielded chalcone analogs. In the second step, the chalcone analogs (1 mmol) were refluxed with 2-amino-thiophenol (1 mmol) in the presence of a catalytic amount of *p*-toluenesulfonic acid (*p*-TsOH) to produce benzothiazole compounds (Figure 1). Chloroform was added to the reaction mixture, and the organic phase was washed, dried with sodium sulfate, and filtered. The final products (A and B) underwent purification via chromatography, using hexane mixed with a gradually increasing concentration of ethyl acetate (0-15%). This procedure resulted in a solid compound with a waxy consistency. After purification, the compounds were kept under cold storage conditions (-20 °C). The structure of the compounds was explained based on spectroscopic methods (NMR, IR, and elemental analysis), and comparisons with authentic samples.[8-10]

Cell culture and cell viability assay

Culturing, passaging, incubation of cells, and preparation of compounds were conducted as defined previously.[16] Cell proliferation was measured using the MTT test, one of the most commonly used cell viability tests. HepG2 and L929 cells were seeded and treated with compounds A and B at concentrations of 10, 25, 50, 75, and 100 μM. Sorafenib, which is used in the treatment of HCC in the clinic, was also applied to HepG2 cells as a positive control at concentrations of 0.1, 0.5, 1, 5, and 10 μM. After treatment, the medium was removed from the plates containing the compounds, and the MTT solution (0.5 mg/mL, Sigma) was added to the cells. After incubating the plates for 4 hours, dimethyl sulfoxide was added. At the end of this period, the absorbance values of the samples at 570 nm and 650 nm wavelengths were measured.

Apoptosis assay

The Annexin Apoptosis kit (BD Biosciences) assessed apoptosis in HepG2 cells.[17] Compounds A and B were applied at 100 μM doses in experiments exclusively designed to induce apoptosis. After incubation for 48 hours, the cells were subjected to trypsinization and rinsed in phosphate-buffered saline (PBS). Subsequently, the cells were suspended in a binding buffer, and 5 μL of fluorescein isothiocyanate (FITC) and propidium iodide (PI), dyes, were mixed in the suspensions. A Beckman Coulter flow cytometer was used to evaluate samples within 15 minutes, with the Kaluza Analysis software (Beckman Coulter) employed to analyze the data.

Cell cycle test

The Propidium Iodide Flow Cytometry Kit (Abcam, ab139418) was used to study the cell cycles.[18] HepG2 cells were treated with 100 μM compounds A and B for 48 hours. After trypsinization, washing, and suspension in PBS, the cells were kept in a mixture of PBS and ethanol at 4 °C for at least two hours. Next, they were resuspended in PBS and stained with PI.

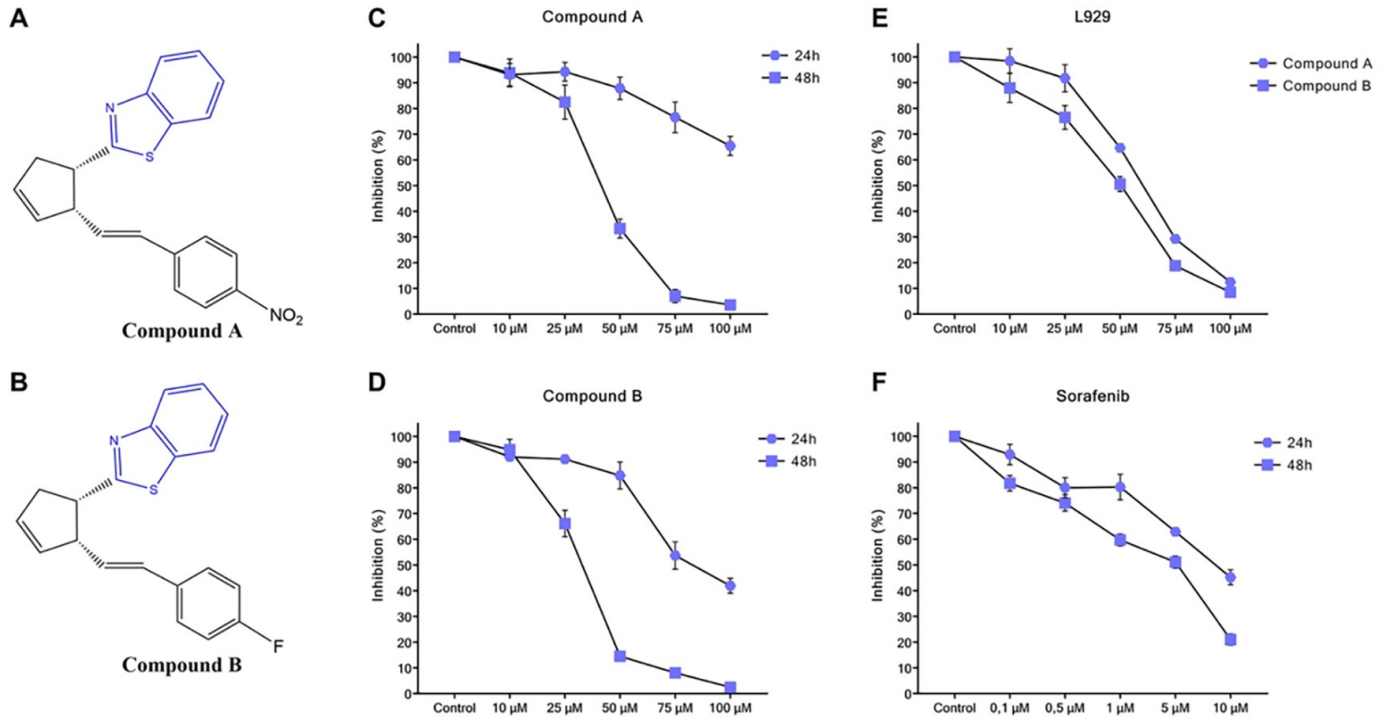

Figure 1. Synthesized 2-substituted benzothiazole compounds and inhibition effects of A and B on HepG2 and L929 cell lines

(A, B) In the initial step, chalcone derivatives were synthesized by combining cis-bicyclo[3.2.0]hept-2-en-6-one with benzaldehyde (4-nitro or 4-fluoro) compounds in the presence of NaOH. Subsequently, the chalcone compounds obtained in the second step were subjected to a reaction with 2-amino-thiophenol in the presence of p-toluene sulfonic acid, forming benzothiazole compounds.

The inhibition rates of A and B administrations on HepG2 and L929 cell lines were evaluated. The control groups, where no drug administration took place, showed an inhibition rate of 0%. (C) Cell viability of compound A in HepG2 cell line at 24 and 48 hours. (D) Cell viability of compound B in HepG2 cell line at 24 and 48 hours. (E) Cell viability of compounds A and B for 48 hours in the normal cell line (L929). (F) Cell viability of compound Sorafenib in HepG2 cell line at 24 and 48 hours

The data were analyzed using Kaluza Analysis software after examining the samples with a Beckman Coulter flow cytometer.

Mitochondrial membrane potential assay (ΔΨM)

Once the HCCs had reached confluence in a 96-well plate, they were treated with various doses (50, 75, and 100 µM) of compounds A and B. This was done by adding the compounds directly to the cell culture media. The cells were then incubated for 48 hours to allow the compounds to take effect. Subsequently, 100 µL of a JC-1 solution (Abcam, ab113850-JC1) was added to each well.[19] The plate was incubated at 37 °C for 10 minutes in the dark. A fluorescent microscope was used to capture an image of the plate with a Texas red filter, with excitation/emission at 590/610 nm.

Wound healing analysis

The Ibidi brand wound healing culture apparatus was used to evaluate wound width.[20] Cells were seeded in split wells, and the apparatus was removed after confluency. Zero-time images (T0) of the cells were photographed under the microscope. Cells were photographed again 48 hours (T48) after administering compounds A and B (50, 75, and 100 µM). Cell migration rates were determined by evaluating the gap closure after A and B administration.

Western blot analysis

Protein analysis by Western blot was performed as previously described in.[21] Briefly, analyses were performed in supernatants obtained from cells lysed with Radioimmunoprecipitation Assay (RIPA) buffer. Samples subjected to sodium dodecyl sulfate-polyacrylamide gel electrophoresis were electrophoresed and transferred to the polyvinylidene difluoride membrane. The bands were imaged and analyzed after incubation with the appropriate primary and secondary antibodies.

Oxidative stress parameters and COX-2 and iNOS activity

Compound A and B concentrations (50, 75, and 100 µM) were used to treat both types of cancer cells and the cells were allowed to incubate for 48 h. The culture medium was removed from the incubated cells, and the cell pellets were lysed. After centrifuging the mixture at 14,000 × g for 10 min, the supernatant was obtained and used to measure oxidative stress parameters. Total antioxidant status (TAS), total oxidant status (TOS), and total and native thiol concentrations in the supernatant were determined using a spectrophotometer (microplate reader, Synergy H1). The TOS to TAS ratio was acknowledged as an oxidative stress index (OSI) at a fixed ratio. The OSI=TOS/TAS formula was used to calculate the OSI value. The activity of superoxide dismutase (SOD) was measured by assessing the decrease of nitroblue tetrazolium generated by xanthine and

xanthine oxidase according to the procedure described by Sun et al.[22]. COX-2 and iNOS were measured by an ELISA kit according to the manufacturer's procedure (SunRed Biotechnology).

Statistical Analysis

The statistical analyses used GraphPad Prism 9 (GraphPad Software, San Diego, CA, USA). Shapiro-Wilk tests were used to assess the normality of the data. One-way ANOVA was used for group statistical comparisons, followed by Dunnett's multiple comparison tests.[23] If the data did not follow a normal distribution, the Kruskal-Wallis and Dunn's post-hoc tests were used. The data were expressed as means and standard deviations. A p-value less than 0.05 was considered significant and denoted with * for $p < 0.05$, ** for $p < 0.01$, or *** for $p < 0.001$.

RESULTS

Cytotoxic effects of 2-substituted benzothiazole compounds

To assess the cytotoxic effects of compounds A and B on hepatocellular carcinoma, we determined the percentage viability of HepG2 cells. It was evident that the proliferation of hepatocellular cells decreased in a dose-dependent manner when exposed to 10, 25, 50, 75, and 100 µM of compounds A and B, as well as 0.1, 0.5, 1, 5, and 10 µM of the positive control, sorafenib. Notably, the inhibitory properties of these compounds varied, with compound B (a benzothiazole derivative with a fluorine substituent) displaying higher inhibitory activity compared to compound A (a benzothiazole derivative with a nitro substituent), particularly at the 24-hour time point (Figure 1C, D).

Although significant inhibition of the benzothiazole compounds was observed at the 48-hour time point, with 100 µM of compound A inhibiting HepG2 cell growth by 96.4%, 100 µM of compound B exhibiting a growth inhibition of 97.5%, and 10 µM of sorafenib displaying a 79% growth inhibition, further investigation is necessary to understand the mechanism of inhibition. When evaluating the obtained MTT data, the IC50 values for compound A were determined to be 56.98 µM after 24 hours and 38.54 µM after 48 hours, respectively. The IC50 values for compound B after 24 hours and 48 hours were 59.17 µM and 29.63 µM, respectively.

To further evaluate the antiproliferative effects of these compounds, we conducted experiments using the L929 mouse fibroblast cell line. In normal cells (L929), the IC_{50} concentrations for compound A and compound B at 48 hours were 53.84 µM and 40.16 µM, respectively (Figure 1E, F).

Effects of 2-substituted benzothiazole compounds on apoptosis

The apoptotic cell ratios were assessed following the treatment of HepG2 cells with 100 µM compounds, which exhibited significant cytotoxic effects. The apoptotic cell population was compared to the control group after administering benzothiazole compounds to the cells for 48 hours. In the control group, the apoptotic cell rate was 1.02%. However, following treatment with 100 µM concentrations of compounds A and B, the apoptotic cell rates were 10.70% and 45.22%, and the necrotic cell rates were 48.70% and 23.49%, respectively (Figure 2).

Effect of 2-substituted benzothiazole compounds on the cell cycle

Our research on the effects of compounds A and B, which are 2-substituted benzothiazole compounds, on the cell cycle has promising implications for cancer treatment and drug development. Through our analysis of the distribution of cell cycle phases in PI-labeled cells, we discovered that a significant proportion of HepG2 cells treated with these compounds at a concentration of 100 µM were in the sub-G1 phase. This indicates apoptosis and DNA fragmentation. After treatment with compounds A and B, the percentage of the cell population in the sub-G1 phase was found to be 42.23% and 55.53%, respectively (Figure 3). These findings suggest that the compounds have the potential to be used in cancer therapy and drug design.

Effect of 2-substituted benzothiazole compounds on mitochondrial membrane potential

The impact of 2-substituted benzothiazole compounds on ΔΨm was evaluated using a cationic dye called JC-1 and fluorescence microscopy. The control group exhibited intense red fluorescent staining, indicating the aggregation of JC-1 dye within the mitochondria. To assess the effect of benzothiazole compounds, concentrations of 50, 75, and 100 µM were applied; the red fluorescence intensity of JC-1 dye was analyzed. It was observed that both substituents A and B caused a dose-dependent reduction in the red fluorescence intensity (Figure

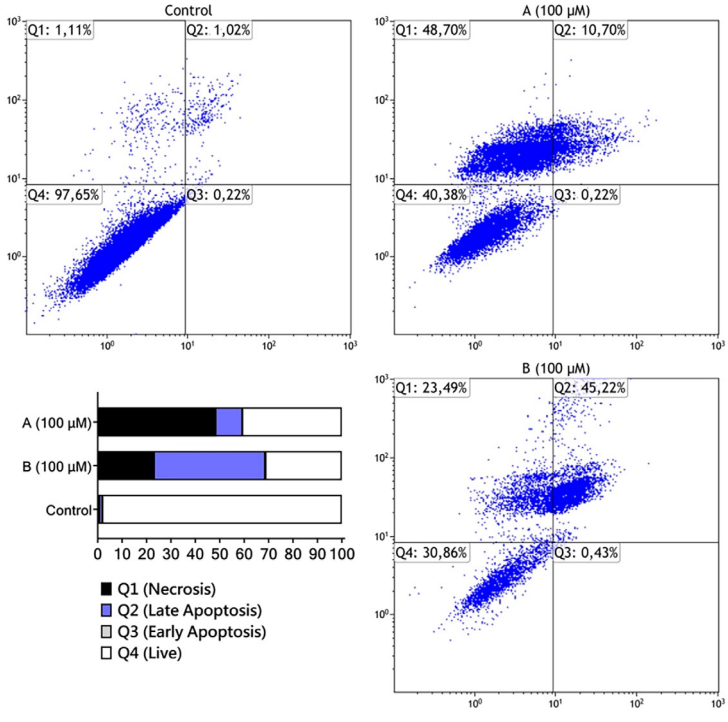

Figure 2. Annexin V flow cytometry analysis of the effects of A and B on HepG2 cell line. 100 µM concentration of A and B can cause apoptosis. FITC-Annexin V was utilized to evaluate apoptosis in HepG2 cells following a treatment period of 48 hours with 100 µM each of compounds A and B. The total number of Annexin V+/PI+ quadrants reflects the degree of apoptosis

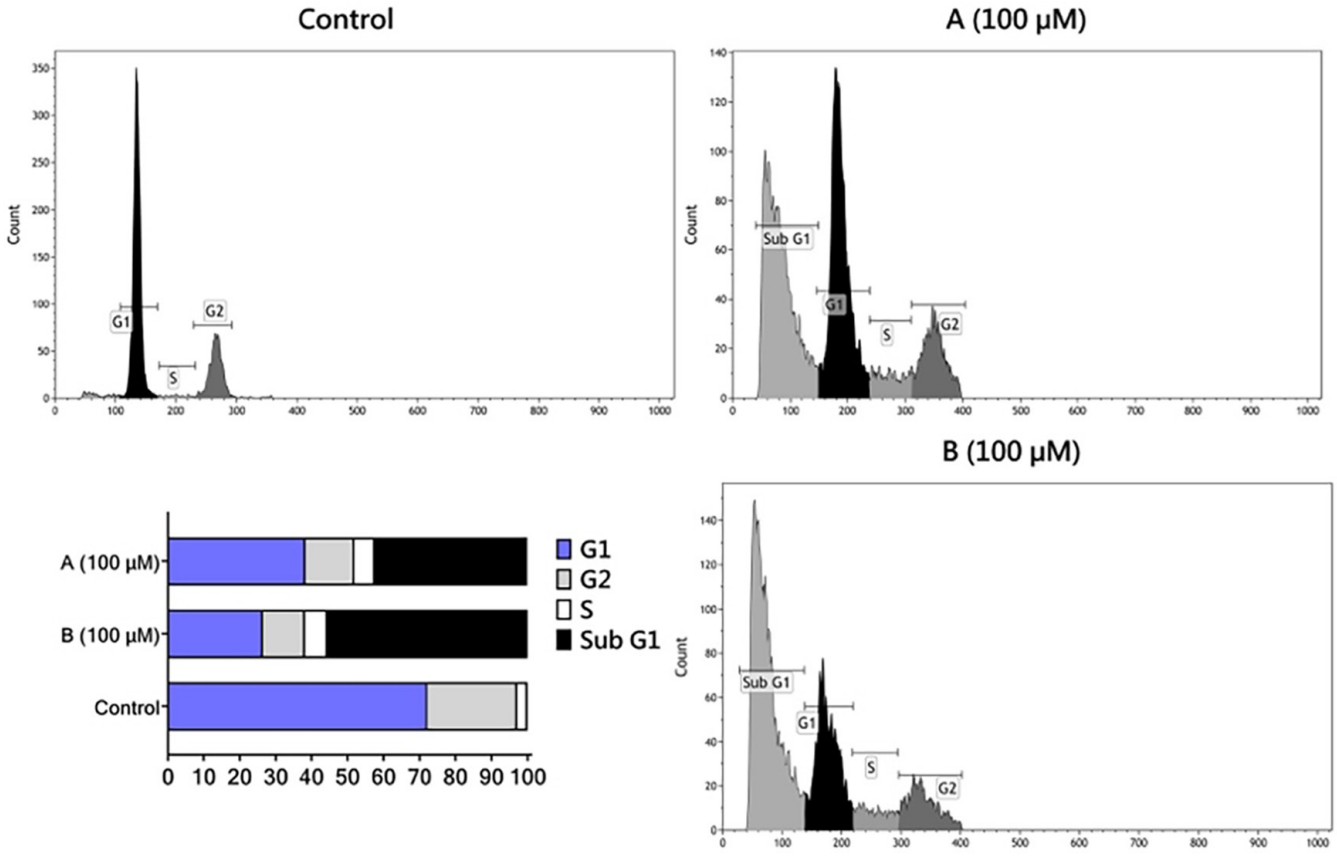

Figure 3. Effects of A and B on cell cycle. The effects of A and B on the cell cycle of HepG2 cells were examined. Administration of 100 µM doses of A and B each caused the cells to shift to the sub-G1 phase

4). These findings suggest that 2-substituted benzothiazole compounds induce apoptosis by disrupting the ΔΨm.

Effect of 2-substituted benzothiazole compounds on wound healing

To assess the influence of 2-substituted benzothiazole compounds on the migration of HepG2 cells, we evaluated T0, T24, and T48 images to measure changes in wound widths. The wound width of HepG2 cells after 48 hours was 51.7% in the control group. In contrast, treatment with 50 and 100 µM of compound A resulted in wound widths of 80.6% and 84.0% in HepG2 cells, respectively, while compound B led to wound widths of 89.2% and 90.4%, respectively. These observations indicate that 2-substituted benzothiazole compounds effectively suppress cell migration in a dose-dependent manner (Figure 5).

Effects of 2-substituted benzothiazole compounds on NF-κB, COX-2, and iNOS

The inflammation and cell proliferation processes in cancer formation are intricately linked to the effects of inflammatory mediators, including NF-κB activation, COX-2, and iNOS, on transcriptional regulation.[24] Consequently, we evaluated NF-κB, COX-2, and iNOS levels to investigate the underlying inflammatory mechanisms influenced by 2-substituted benzothiazole compounds in liver cancer.

When HepG2 cells were treated with 50 and 100 µM concentrations of compounds A and B, we observed a dose-dependent decrease in NF-κB protein expression levels (Figure 6A, B). The Western blot results underscore the anticancer effects of 2-substituted benzothiazole compounds, highlighting their role in mediating a reduction in NF-κB protein expression levels, a pivotal mediator of inflammation.

We also scrutinized the impact of benzothiazole compounds on COX-2 and iNOS enzymes, which are critical players in the inflammatory process. Our observations indicated that 2-substituted benzothiazole compounds, when applied to HepG2 cells, led to a dose-dependent inhibition of COX-2 and iNOS (Figure 6C, D). These findings suggest that compounds A and B effectively reduce COX-2 and iNOS levels by operating downstream from NF-κB inhibition and consequently mitigate heightened inflammation associated with carcinogenesis.

Effect of 2-substituted benzothiazole compounds on oxidative stress

Previous studies have demonstrated that drugs employed in cancer treatment induce cell death by either causing cellular damage or disrupting the redox balance, through oxidative stress mechanisms in tumor cells.[25] Consequently, in this study, we assessed the levels of, TOS, TAS, OSI, SOD, total thiol, and native thiol to elucidate the pro-oxidant effect of 2-substituted benzothiazole compounds on HepG2 cells.

In HepG2 cells treated with doses of 50, 75, and 100 µM of compounds A and B, TAS, SOD, total thiol, and native thiol

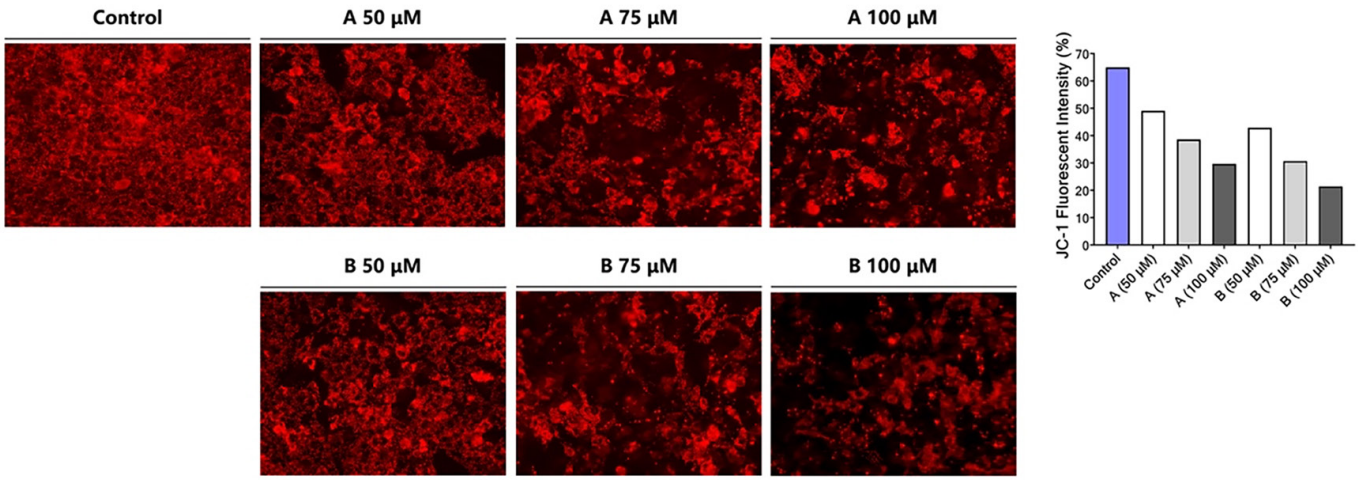

Figure 4. Effect of A and B on mitochondrial membrane potential. A red fluorescence image of HepG2 cells stained with JC-1 was taken after administering varying concentrations of compounds A and B, with each at concentrations of 50, 75, and 100 µM. The aggregation of JC-1 dye in cells decreased in a dose-dependent manner with the administration of A and B

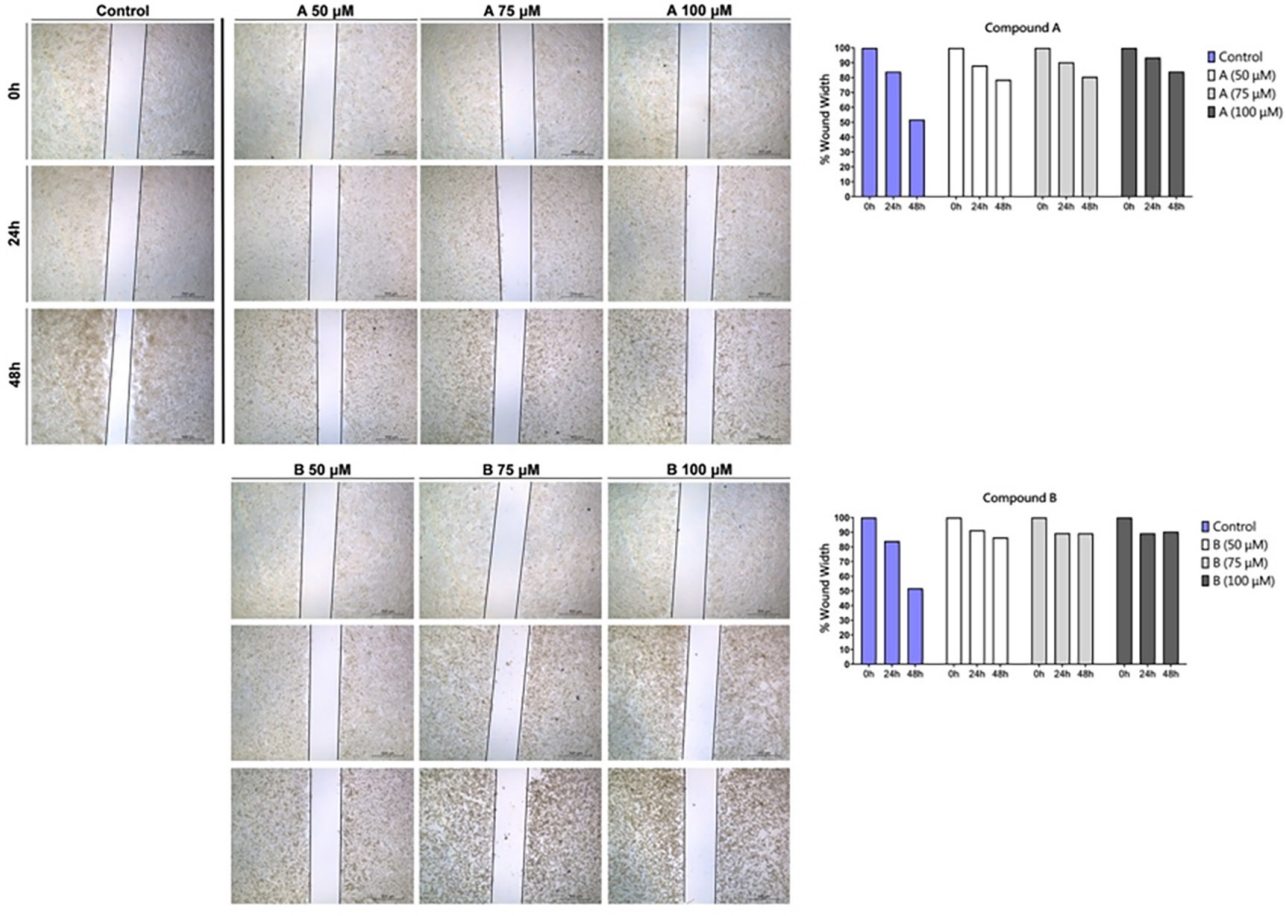

Figure 5. Effect of A and B on wound healing in HepG2. Images of wound width in cells treated with A and B at 0, 24, and 48 hours. Treatment with benzothiazole derivatives decreased the closure of wound width in cells in a dose-dependent manner

levels exhibited a dose-dependent decrease (Figure 7A, D-F). Notably, the most pronounced increase in TOS level and OSI was observed at a concentration of 100 µM (Figure 7B, C). These findings indicate that the elevated oxidant levels induced cell death in HepG2 cells through the actions of 2-substituted benzothiazole compounds.

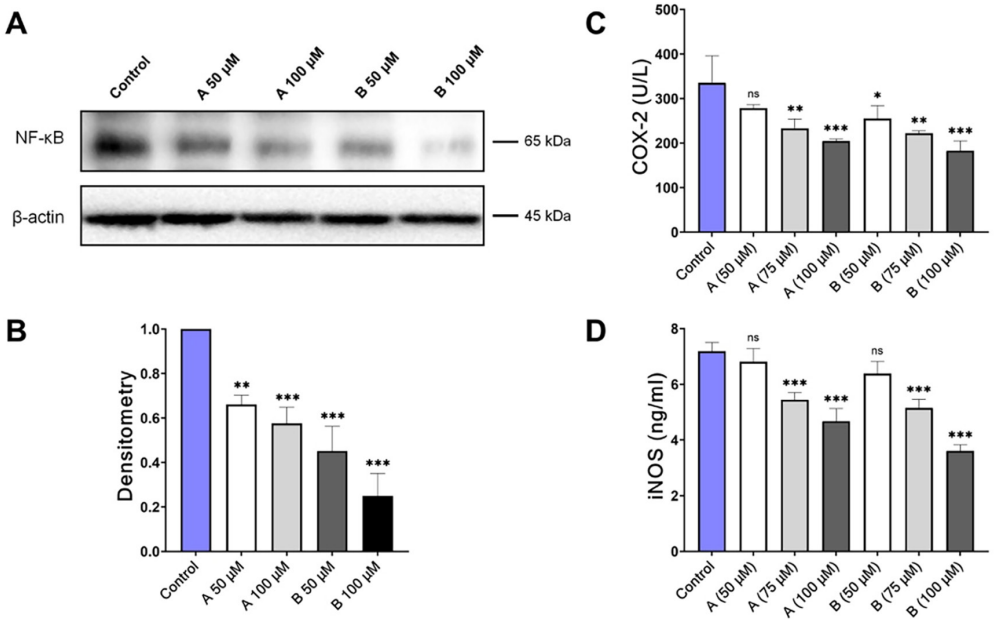

Figure 6. Effects of A and B on NF-κB protein expression and COX-2 and iNOS activity. Western blot bands showing NF-κB protein expression levels after administration of A and B at 50 and 100 µM doses (A). Densitometric analysis of NF-κB protein levels (B). Different concentrations of compounds A and B affect COX-2 (C) and iNOS (D) levels in HepG2 cells

NF-κB: Nuclear factor kappa B, COX-2: Cyclooxygenase-2

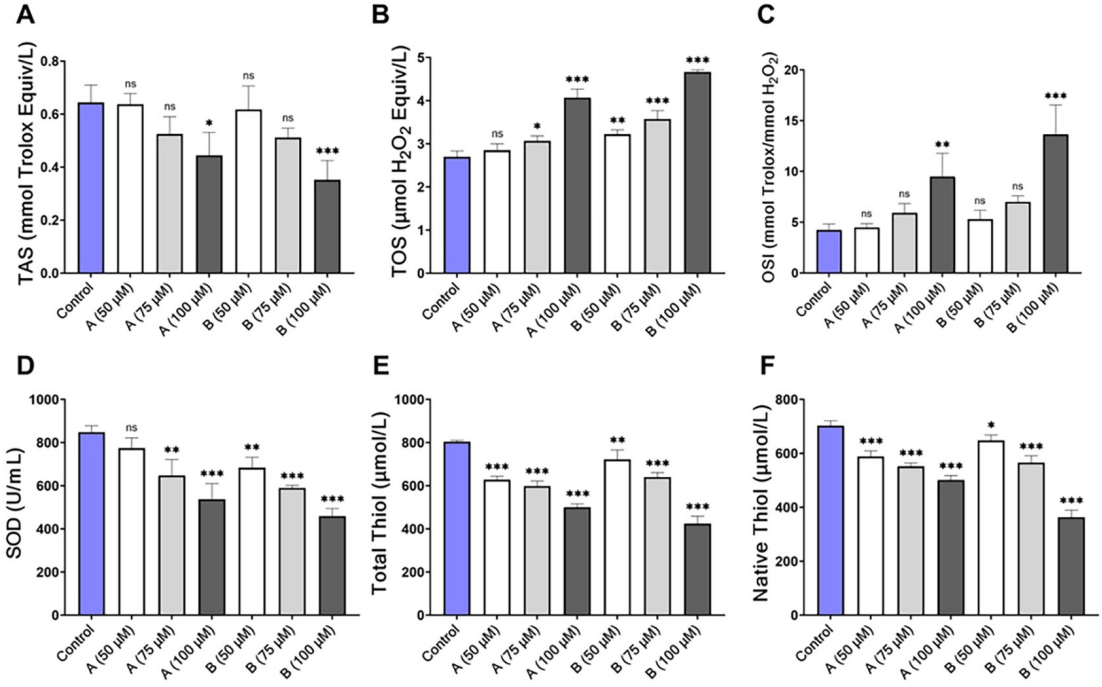

Figure 7. Effect of A and B on oxidative stress parameters in HepG2. HepG2 cells were treated with 50, 75, and 100 µM of A and B for 48 hours; TAS (A), TOS (B), OSI (C), SOD (D), total thiol (E), and native thiol (F) levels were measured

TAS: Total antioxidant status, TOS: Total oxidant status, OSI: Oxidative stress index, SOD: Superoxide dismutase

DISCUSSION

HCC is a significant health problem worldwide, leading to impaired control of fundamental processes such as cellular differentiation, proliferation, and metastasis.[26] In our study, we evaluated the antiproliferative and anti-inflammatory effects of 2-substituted benzo[d]thiazole derivatives on HepG2 cells and demonstrated that these effects are mediated through the NF-κB/COX-2/iNOS signaling pathway. Our findings align with previous studies supporting the potential of synthetic compounds with similar structures to suppress proliferation and target inflammation-related signaling pathways in different cancer types.[27] The cost-effective production and development of synthetic compounds; their easy accessibility; low toxicity; high selectivity; and potential for combination therapy offer significant advantages in the fight against cancer.[28] However, despite extensive research on the molecular mechanisms of signaling pathways in hepatocytes associated with liver cancer, chemotherapeutic approaches to target these signals remain limited.

Our study aimed to assess the impact of 2-substituted benzothiazole compounds on the proliferation of hepatocarcinoma cells. We employed a concentration range of 10 to 100 μM for our experiments. Following a 24-hour treatment with compounds that contained nitro (A) and fluorine (B) substituents, we determined IC_{50} values of 56.98 μM and 59.17 μM, respectively. Notably, we observed that benzothiazole compounds with both substituents exhibited similar effects in suppressing the proliferation of HepG2 cells. This discovery implies that 2-substituted benzothiazole compounds possess inhibitory properties against hepatocarcinoma cell growth. Furthermore, our findings indicate that benzothiazole compounds have a more significant inhibitory effect on HepG2 cancer cells than healthy mouse fibroblast L929 cells. This observation suggests that these compounds may exhibit selectivity in their action, offering a promising avenue for further investigation in developing targeted cancer therapeutics.

The induction of apoptosis and cell cycle arrest are two critical mechanisms commonly employed to elucidate the ability of anticancer drugs to inhibit tumor growth.[29] Numerous studies have demonstrated that benzothiazole-based derivatives induce apoptosis in vitro in various cancer types, such as prostate, stomach, lung, breast, colon, and glioblastoma.[30] Modi et al.[31] reported that a phenyl derivative benzothiazole compound initiated caspase-dependent apoptosis in cervical cancer (SiHa) cells and enhanced the tumor suppressor effect of the p53 protein. Peng et al.[32] demonstrated that a small molecule, 2-substituted benzothiazole compound, increased DNA fragmentation in human melanoma cells' sub-G1 phase of the cell cycle (A375). Li et al.[33] discovered that a 2-substituted benzothiazole compound mediated apoptosis induction in B lymphoma cells (Ramos) by arresting the cell cycle in the G0/G1 phase, inducing loss of ΔΨm, and elevating caspase-9/8 and caspase-3 protein levels. In line with previous studies, our flow cytometry analysis of AnnexinV/FITC and PI-labeled cells revealed an increase in the percentage of apoptotic cells and an accumulation of cells in the sub-G1 phase with increasing concentrations of compounds A and B in HepG2 cells. Additionally, the red fluorescence signal of JC-1 dye within the cells was progressively diminished in a dose-dependent manner. These findings suggest that benzo[d]thiazole derivatives may induce apoptosis through ΔΨm loss and exhibit anticancer effects in HepG2 cells.

NF-κB is a pivotal nuclear transcription factor that regulates gene expression in the cell cycle. It plays a crucial role in controlling normal cellular functions and contributes to the onset of diseases such as cancer. Viral infections (such as hepatitis B or C) and liver tissue inflammation lead to sustained NF-κB activation.[34] This prolonged activation promotes cell proliferation, angiogenesis, and invasion and simultaneously inhibits apoptosis. Understanding the regulation of NF-κB and its impact on COX-2 and iNOS enzymes is vital for cancer research.[35] Therefore, our study aims to investigate the impact of synthesized 2-substituted benzothiazole derivatives on NF-κB protein expression and COX-2 and iNOS enzyme inhibition, which are critical factors in inflammation and cancer progression. Previous research suggests that the ability of certain compounds containing a thiazole ring to induce apoptosis and suppress inflammation is associated with the regulation of NF-κB/mTOR/PI3K/Akt signaling activity.[36] However, our study is the first to establish a link between the anti-inflammatory effect of benzothiazole-derived compounds and their potential to inhibit COX-2 and the iNOS enzymes, which are involved in downstream inflammation. Our findings demonstrate that benzothiazole compounds with fluorine and nitro substituents suppress COX-2 and iNOS activation in HepG2 cells by inhibiting NF-κB, subsequently leading to apoptosis through the anti-inflammatory mechanistic signaling pathway. These results suggest that benzothiazole-derived compounds could be a novel therapeutic approach for hepatocellular carcinoma characterized by inflammation.

It is well-known that elevated levels of ROS within cells can function as a mechanism to target cancer cells. The initiation of oxidative stress in cancer cells may prompt programmed cell death via DNA damage, mitochondrial damage, and activation of apoptosis. Consequently, researchers are currently investigating ROS regulators or drugs that can reduce ROS production in cancer cells as a prospective strategy for cancer therapy. Our study assessed the impacts of 2-substituted benzothiazole compounds on HepG2 cells to induce apoptosis by promoting oxidative stress and ROS accumulation. Our findings reveal that compounds A and B diminish the antioxidant defense in hepatocarcinoma cells through reductions in TAS, dynamic disulfide levels, and SOD enzyme activity. Moreover, they induce oxidative stress by elevating TOS and OSI levels. Previous investigations have documented that a benzothiazole core compound can produce cellular damage by inhibiting SOD and glutathione reductase enzymes, thereby increasing oxidative stress in breast cancer.[37] Another study has shown that a water-soluble benzothiazole derivative compound can induce loss of function and cell death by accumulating ROS in B-lymphoma cells.[33] These studies underscore the potential of oxidative stress as a targeted attack mechanism in cancer

cells and propose that benzothiazole-derived compounds might induce damage in cancer cells due to their pro-oxidant effect.

CONCLUSION

This study shows that compounds containing 2-substituted benzothiazole effectively reduce the cell viability of hepatocarcinoma cells. Furthermore, these compounds cause cellular damage, resulting in increased oxidative stress, fragmentation of DNA, and loss of $\Delta\Psi m$. Additionally, these compounds suppress the activation of the inflammation-inducing NF-κB/COX-2/iNOS signaling pathway, which plays a critical role in developing hepatocellular carcinoma. Our study is the first to establish a connection between the apoptotic effects of benzothiazole-derived compounds and the proteins and enzymes NF-κB, COX-2, and iNOS. Moreover, our study sheds light on the inhibitory effects of these compounds on inflammation. These findings offer valuable insights into the potential utilization of 2-substituted benzothiazole compounds in therapy for cancer and inflammation.

Ethics

Ethics Committee Approval: This study was conducted exclusively on established HepG2 and L929 cell lines and did not involve human participants or animal subjects; therefore, ethics committee approval and informed consent were not required.

Informed Consent: Not required.

Footnotes

Authorship Contributions

Concept: M.M.**Ü**., N.**Ü**., M.C., Design: M.M.Ü., N.Ü., M.C., Data Collection or Processing: M.M.Ü., N.Ü., M.C., Y.T., Analysis or Interpretation: M.M.Ü., N.Ü., M.C., Y.T., Literature Search: M.M.Ü., N.Ü., Writing: M.M.Ü., N.Ü.

Conflict of Interest: The authors declare no conflicts of interest.

Financial Disclosure: The authors declared that this study received no financial support.

REFERENCES

1. Llovet JM, Zucman-Rossi J, Pikarsky E, Sangro B, Schwartz M, Sherman M, Gores G. Hepatocellular carcinoma. Nat Rev Dis Primers. 2016;2:16018.
2. Hernandez-Gea V, Toffanin S, Friedman SL, Llovet JM. Role of the microenvironment in the pathogenesis and treatment of hepatocellular carcinoma. Gastroenterology. 2013;144:512-527.
3. Lee CH, Jeon YT, Kim SH, Song YS. NF-kappaB as a potential molecular target for cancer therapy. Biofactors. 2007;29:19-35.
4. Ohshima H, Tazawa H, Sylla BS, Sawa T. Prevention of human cancer by modulation of chronic inflammatory processes. Mutat Res. 2005;591:110-122.
5. Sivandzade F, Prasad S, Bhalerao A, Cucullo L. NRF2 and NF-κB interplay in cerebrovascular and neurodegenerative disorders: molecular mechanisms and possible therapeutic approaches. Redox Biol. 2019;21:101059.
6. Garofalo M, Grazioso G, Cavalli A, Sgrignani J. How computational chemistry and drug delivery techniques can support the development of new anticancer drugs. Molecules. 2020;25:1756.
7. Law CSW, Yeong KY. Current trends of benzothiazoles in drug discovery: a patent review (2015-2020). Expert Opinion on Therapeutic Patents. 2022;32:299-315.
8. Uremis N, Uremis MM, Tolun FI, Ceylan M, Doganer A, Kurt AH. Synthesis of 2-substituted benzothiazole derivatives and their *in vitro* anticancer effects and antioxidant activities against pancreatic cancer cells. Anticancer Res. 6389-37:6381;2017.
9. Ceylan M, Erkan S, Yaglioglu AS, Akdogan Uremis N, Koç E. Antiproliferative evaluation of some 2-[2-(2-Phenylethenyl)-cyclopent-3-en-1-yl]-1,3-benzothiazoles: DFT and molecular docking study. Chem Biodivers. 2020;17:e1900675.
10. Üremiş MM, Yağlıoğlu A, Budak Y, Ceylan M. Synthesis, characterization, in vitro antiproliferative and cytotoxicity effects of a new class of 1))-2R,2S)-2-((E)-4-substitutedstyryl) cyclooctyl)benzo[d]thiazole derivatives. Organic Communications. 2017;10:190-200.
11. Tariq S, Kamboj P, Amir M. Therapeutic advancement of benzothiazole derivatives in the last decennial period. Arch Pharm (Weinheim). 2019;352:e1800170.
12. Şahin B, Yağlıoğlu AS, Ceylan M. Synthesis and cytotoxic activities of novel -1,5)-2bis(aryl) penta-1,4-dien-2-yl) benzo[d]thiazol derivatives. Organic Communications. 2016;9:65-72.
13. Van Meter AR, Perez-Rodriguez MM, Braga RJ, Shanahan M, Hanna L, Malhotra AK, Burdick KE. Pramipexole to improve cognition in bipolar disorder: a randomized controlled trial. J Clin Psychopharmacol. 2021;41:421-427.
14. Hametner EM, Seppi K, Poewe W. Role and clinical utility of pramipexole extended release in the treatment of early Parkinson's disease. Clin Interv Aging. 2012;7:83-88.
15. Spencer KR, Portal DE, Aisner J, Stein MN, Malhotra J, Shih W, Chan N, Silk AW, Ganesan S, Goodin S, Gounder M, Lin H, Li J, Cerchio R, Marinaro C, Chen S, Mehnert JM. A phase I trial of riluzole and sorafenib in patients with advanced solid tumors: CTEP #8850. Oncotarget. 2023;14:302-315.
16. Mehdi Üremiş M, Üremiş N, Tosun E, Durhan M, Çiğremiş Y, Baysar A, Türköz Y. Cucurbitacin D inhibits the proliferation of HepG2 cells and induces apoptosis by modulating JAK/STAT3, PI3K/Akt/mTOR and MAPK signaling pathways. Curr Cancer Drug Targets. 2022;22:931-944.
17. Vermes I, Haanen C, Steffens-Nakken H, Reutelingsperger C. A novel assay for apoptosis. Flow cytometric detection of phosphatidylserine expression on early apoptotic cells using fluorescein labelled Annexin V. J Immunol Methods. 1995;184:39-51.
18. Carbonari M. New use for an old reagent: cell cycle analysis of DNA content using flow cytometry in formamide treated cells. Cytometry A. 2016;89:498-503.
19. Smiley ST, Reers M, Mottola-Hartshorn C, Lin M, Chen A, Smith TW, Steele GD Jr, Chen LB. Intracellular heterogeneity in mitochondrial membrane potentials revealed by a J-aggregate-forming lipophilic cation JC-1. Proc Natl Acad Sci U S A. 1991;88:3671-3675.
20. Cappiello F, Casciaro B, Mangoni ML. A novel in vitro wound healing assay to evaluate cell migration. J Vis Exp. 2018:56825
21. Üremiş N, Üremiş MM, Çiğremiş Y, Tosun E, Baysar A, Türköz Y. Cucurbitacin I exhibits anticancer efficacy through induction of apoptosis and modulation of JAK/STAT3, MAPK/ERK, and AKT/mTOR signaling pathways in HepG2 cell line. J Food Biochem. 46;2022:e14333.

22. Sun Y, Oberley LW, Li Y. A simple method for clinical assay of superoxide dismutase. Clin Chem. 1988;34:497-500.

23. Kim TK. Understanding one-way ANOVA using conceptual figures. Korean J Anesthesiol. 2017;70:22-26.

24. Gupta R, Kadhim MM, Turki Jalil A, Obayes AM, Aminov Z, Alsaikhan F, Ramírez-Coronel AA, Ramaiah P, Tayyib NA, Luo X. Multifaceted role of NF-κB in hepatocellular carcinoma therapy: molecular landscape, therapeutic compounds and nanomaterial approaches. Environ Res. 2023;228:115767.

25. Marioli-Sapsakou GK, Kourti M. Targeting production of reactive oxygen species as an anticancer strategy. Anticancer Res. 2021;41:5881-5902.

26. Keibel A, Singh V, Sharma MC. Inflammation, microenvironment, and the immune system in cancer progression. Curr Pharm Des. 2009;15:1949-1955.

27. Xu X, Zhu Z, Chen S, Fu Y, Zhang J, Guo Y, Xu Z, Xi Y, Wang X, Ye F, Chen H, Yang X. Synthesis and biological evaluation of novel benzothiazole derivatives as potential anticancer and antiinflammatory agents. Front Chem. 2024;12:1384301.

28. Ceylan M, Zorlu B, Şahin Yağlıoğlu A, Akdoğan Üremiş N, Gürdere MB, Keçeci Sarıkaya M, Budak Y. Synthesis of (E)-7-arylidene-5-(hydroxy(aryl)methyl)bicyclo[3.2.0] heptan-6-one derivatives as anti-cancer agents. JNRS. 2023;12:149-156.

29. Ouyang L, Shi Z, Zhao S, Wang FT, Zhou TT, Liu B, Bao JK. Programmed cell death pathways in cancer: a review of apoptosis, autophagy and programmed necrosis. Cell Prolif. 2012;45:487-498.

30. Haider K, Rehman S, Pathak A, Najmi AK, Yar MS. Advances in 2-substituted benzothiazole scaffold-based chemotherapeutic agents. Arch Pharm (Weinheim). 2021;354:e2100246.

31. Modi A, Singh M, Gutti G, Shanker OR, Singh VK, Singh S, Singh SK, Pradhan S, Narayan G. Benzothiazole derivative bearing amide moiety induces p53-mediated apoptosis in HPV16 positive cervical cancer cells. Invest New Drugs. 2020;38:934-945.

32. Peng X, Xie G, Wang Z, Lin H, Zhou T, Xiang P, Jiang Y, Yang S, Wei Y, Yu L, Zhao Y. SKLB-163, a new benzothiazole-2-thiol derivative, exhibits potent anticancer activity by affecting RhoGDI/JNK-1 signaling pathway. Cell Death Dis. 2014;5:e1143.

33. Li MH, Yang P, Yang T, Zhang K, Liu Y, Liu J, Li LM, Luo XY, Yang SX, Zou Q, Zhang CJ. A novel water-soluble benzothiazole derivative BD926 triggers ROS-mediated B lymphoma cell apoptosis via mitochondrial and endoplasmic reticulum signaling pathways. Int J Oncol. 2016;49:2127-2134.

34. Luedde T, Schwabe RF. NF-κB in the liver--linking injury, fibrosis and hepatocellular carcinoma. Nat Rev Gastroenterol Hepatol. 2011;8:108-118.

35. Park MH, Hong JT. Roles of NF-κB in cancer and inflammatory diseases and their therapeutic approaches. Cells. 2016;5:15.

36. Sahil, Kaur K, Jaitak V. Thiazole and related heterocyclic systems as anticancer agents: a review on synthetic strategies, mechanisms of action and SAR studies. Curr Med Chem. 2022;29:4958-5009.

37. Rodrigues JR, Charris J, Camacho J, Barazarte A, Gamboa N, Antunes F. Cytotoxic effects of N'-formyl-2-(5-nitrothiophen-2-yl) benzothiazole-6-carbohydrazide in human breast tumor cells by induction of oxidative stress. Anticancer Res. 2012;32:2721-2726.

Turk J Pharm Sci 2025;22(3):217-225
DOI: 10.4274/tjps.galenos.2025.61569

ORIGINAL ARTICLE

Optimization of Rosella Extract-based Antioxidant Peel-off Mask Using Simple Lattice Design

Putriana RACHMAWATI[1]*, Albert KELVIN[1], Richard SIDHARTA[1], Gabriella LIONITA[1], Ikhwan Yuda KUSUMA[2]

[1]Atma Jaya Catholic University of Indonesia, School of Medicine and Health Sciences, Department of Pharmacy, Jakarta, Indonesia
[2]Harapan Bangsa University Faculty of Health, Pharmacy Study Program, Purwokerto, Indonesia

ABSTRACT

Objectives: The skin is highly vulnerable to damage caused by free radicals, which disrupt biological components and accelerate aging. While endogenous antioxidants provide some protection, external sources are often needed. Rosella (*Hibiscus sabdariffa L.*) is a rich source of flavonoids and astaxanthin, proven antioxidants that inhibit matrix metalloproteinase-1, prevent collagen degradation, and reduce ultraviolet-induced damage. The aim of the study was to optimize the formulation of a peel-off mask, incorporating Rosella extract as an antioxidant.

Materials and Methods: Rosella extract was analyzed using liquid chromatography-mass - mass spectrometry (LC-MS) to identify its antioxidant components. Freeze-dried Rosella powder was granulated and incorporated into a gel mask using polyvinyl alcohol (PVA) or gelatin as the base polymer. Formula optimization was conducted using simplex lattice design and evaluated for physical properties, antioxidant activity, and stability.

Results: LC-MS analysis detected astaxanthin, quercetin, rutin, and kaempferol in Rosella extract. Granulated Rosella exhibited good flowability and a particle size distribution of 250-425 µm. The optimized formula was PVA-based, containing 12.5% PVA and 7.5% propylene glycol. The product demonstrated desirable physical properties, including a drying time of 5.29 minutes, a pH of 5.32, a spreadability of 5.34 cm, an adhesivity of 6.86 seconds, and a viscosity of 30,658 cP. Stability tests confirmed the formula remained stable for 3 months, under room temperature, freeze-thaw cycles, and centrifugation. The final product, containing 15% Rosella, exhibited 45.33% antioxidant activity.

Conclusion: The PVA-based Rosella peel-off mask demonstrated optimal physical properties, stability, and antioxidant properties, offering a promising approach to incorporating antioxidants into cosmetic formulations.

Keywords: Peel-off mask, Rosella (*Hibiscus sabdariffa L.*), antioxidant, scrub, multifunction cosmetics

INTRODUCTION

Free radicals have garnered significant attention in the field of biology due to their crucial role in various physiological processes and their association with a wide range of disorders. They can be generated from both endogenous sources, such as mitochondria, peroxisomes, the endoplasmic reticulum, and phagocytic cells, as well as exogenous sources, including pollution, alcohol, and tobacco smoke. The skin is one of the body's most susceptible organs to damage caused by free radicals. Free radicals can negatively impact key biological components, including proteins, lipids, and nucleic acids, disrupting normal redox balance and leading to increased oxidative stress.[1]

The body produces some of the antioxidants required to neutralize free radicals, which are known as endogenous antioxidants. However, for the remaining antioxidant needs, the body relies on external (exogenous) sources. These exogenous antioxidants are commonly referred to as dietary antioxidants and can be found abundantly in vegetables, fruits, and grains.[2] Antioxidants also play a crucial role as active agents in cosmetics, helping to prevent the harmful effects of free radicals on the epidermis.

In today's fast-paced metropolitan lifestyle, individuals increasingly seek efficiency in various aspects, including maintaining their appearance. Hybrid cosmetics, which

***Correspondence:** putriana.rachmawati@atmajaya.ac.id, **ORCID-ID:** orcid.org/0000-0001-9389-1444
Received: 17.05.2024, **Accepted:** 02.06.2025 **Publication Date:** 01.08.2025

Cite this article as: Putriana RACHMAWATI P, KELVIN A, SIDHARTA R, LIONITA G, KUSUMA IY. Optimization of rosella extract-based antioxidant peel-off mask using simple lattice design. Turk J Pharm Sci. 2025;22(3):217-225

combine multiple functions in a single product, address this need effectively. According to a 2022 report, sales of hybrid beauty products increased by 24%. These products save time during application, reduce costs, and require less storage space. Data also show that 34% of French consumers reduced their cosmetic purchases following the COVID-19 pandemic, further emphasizing the demand for "multi-tasking" products. One such innovative hybrid product is a peel-off mask that incorporates micro-grains that function as a scrub, offering a practical and appealing solution.[3,4] Sustainability is another important factor driving the development of multifunctional products. Reducing the number of cosmetic products used directly contributes to minimizing cosmetic waste.[5]

Rosella (*Hibiscus sabdariffa* L.), a medicinal plant, is cultivated in tropical and subtropical regions, including Saudi Arabia, India, Thailand, Malaysia, and Indonesia. It contains various phytochemical components, including natural pigments, alkaloids, terpenoids, and phenolics.[6-8] Flavonoids, including flavonols and anthocyanin pigments, are present in Rosella petals. These compounds possess double-bond architectures that play a key role in protecting cells from ultraviolet (UV) radiation damage. A phytochemical analysis of Rosella petal extract conducted by the Faculty of Agricultural Technology at Udayana University revealed the following composition: flavonoids (42,938.72 mg/100 g), phenols [(1,758.68 mg/100 g gallic acid equivalent (GAE)], tannins (2,865.25 mg/100 g tannic acid equivalent), vitamin C (1,294.12 mg/100 g), antioxidant capacity (2,249.43 mg/L gallic acid equivalent antioxidant capacity), and positive saponins. These findings indicate that Rosella can be effectively utilized in cosmetics to enhance skin appearance by mitigating the harmful effects of oxidants. The chromophore groups (conjugated single and double bonds) present in flavonoids absorb UVA and UVB rays, thereby reducing UV-induced damage.[9]

This study aims to develop a multifunctional cosmetic formulation in the form of a peel-off mask with micro-grains that also function as a scrub, incorporating *Hibiscus sabdariffa* L. (Rosella) petal extract as the active ingredient, and to evaluate its antioxidant components.

MATERIALS AND METHODS

Materials

Rosella powder was supplied by Herbilogy® (Indonesia), while PVP (Polyvinylpyrrolidone) was donated by PT. Pharos Indonesia. Polyvinyl alcohol (PVA), gelatin, and other materials used were of pharmaceutical grade. DPPH (2,2-Diphenyl-1-picrylhydrazyl) was purchased from PT. Pasifik Kimia Indonesia (Indonesia). All other chemicals were of analytical grade and used as received without further purification.

Detection of antioxidant components in Rosella powder using LC-MS

Rosella powder was prepared in dichloromethane to solubilize astaxanthin and in methanol to solubilize flavonoids. The prepared samples were collected into tubes and immediately centrifuged at 3500 × g for 10 minutes. The supernatant was transferred into amber vials and filtered through a 0.45 µm nylon syringe filter. The analysis was performed using a liquid chromatography - mass spectrometry (LC-MS) /MS Sciex 4500 QTrap instrument. Separation was conducted using a C-18 column (2.1 mm × 150 mm × 2.5 µm). The column temperature was maintained at 25 °C, while the autosampler was set to 4 °C. The mobile phases consisted of 0.1% formic acid in water (phase A) and 0.1% formic acid in acetonitrile (phase B), with a flow rate of 0.5 mL/min. Separation and detection were optimized for astaxanthin and flavonoids, with retention times and mass-to-charge ratios (m/z) used to identify the compounds.

Granulation of Rosella powder

Rosella powder (11%) was mixed with a 5% PVP solution. The wet granules were sieved using a 425 µm mesh and dried via freeze-drying (Welch®). The dried granules were sieved again with a 425 µm mesh and characterized for the following properties: organoleptic properties: color, shape, and odor, measuring of particle size distribution (PSD) using Retsch AS 200, evaluating loss on drying (LOD) using a Mettler Toledo HE73, and assessment of flowability using an Erweka GTL instrument. These evaluations ensured the granules met the desired specifications for use in the peel-off mask formulation.

Optimization formula of peel-off mask that contains Rosella

The formulations were designed as multifunctional peel-off masks, with the additional capability of functioning as physical scrubs. This dual-purpose design combined the antioxidant benefits of Rosella powder with gentle exfoliation. The optimisation was done using a simple lattice design (SLD) with Design Expert version 13 from StatEase®. The studied parameters were the type of polymer, quantity of polymer, and plasticiser. The design formula was shown in Table 1.

First, PVA or gelatin, used as the base polymer, was dissolved in hot water at 70 °C and then allowed to cool to room temperature. Methylparaben, serving as a preservative, was dissolved in propylene glycol and subsequently added to the polymer premix. Rosella powder was pre-wetted with propylene glycol and, along with Rosella granules, incorporated into the premix. The mixture was homogenized using a DLAB® propeller mixer at a speed of 1,000 rpm until uniform consistency was achieved.

Evaluation of a peel-off mask that contains Rosella

Organoleptic evaluation

The finished product was assessed for appearance, odor, texture, and visual homogeneity. For homogeneity, 1 gram of the preparation was placed between two glass slides and visually inspected.

Viscosity

Viscosity was measured using a HAAKE® viscometer with an R7 spindle.

Drying time

One gram of the preparation was applied to the skin of the upper arm and spread over an area of 7 square cm. The drying

Table 1. Design formula of peel-off mask containing rosella

Materials	F1	F2	F3	F4	F5	F6	F7	F8	F9	F10
Rosella powder	4%	4%	4%	4%	4%	4%	4%	4%	4%	4%
Rosella granules	11%	11%	11%	11%	11%	11%	11%	11%	11%	11%
Propylene glycol	0%	2.5%	5%	7.5%	10%	1%	2%	3%	4%	5%
Methylparaben	0.1%	0.1%	0.1%	0.1%	0.1%	0.1%	0.1%	0.1%	0.1%	0.1%
PVA	20%	17.5%	15%	12.5%	10%	-	-	-	-	-
Gelatin	-	-	-	-	-	10%	9%	8%	7%	6%
Distilled water	Ad to 100%	Ad to 100%	Ad to 100%	Ad to 100%	Ad to 100%	Ad to 100%	Ad to 100%	Ad to 100%	Ad to 100%	Ad to 100%

Notes: Ad to 100% indicates the formula was adjusted to a total of 100% using distilled water, PVA: Polyvinyl alcohol

time was defined as the time required for the preparation to be continuously peeled off from the skin.

Spreadability

A sample of 0.25 grams of the preparation was placed between two glass slides. A 50-gram weight was applied to the top slide and left for 1 minute. The diameter of the spread preparation was then measured.

Adhesive strength

A sample of 0.25 grams of the preparation was placed between two glass slides. A 1 kg weight was applied to the top slide and left for 5 minutes. An 80-gram weight was then attached to a string connected to the upper glass slide, and the time required for the upper slide to separate was recorded.

Stability study

A stability analysis of the finished product, packaged in amber glass Type II containers, was conducted under ambient conditions (30 ˚C ±2 ˚C/65% RH ±5% RH). This temperature and humidity range was selected to represent the typical environmental conditions of tropical climates, where the product is expected to be marketed. The selection aligns with the International Council for Harmonisation guidelines for stability testing in Zone IV (hot and humid regions). The evaluation included organoleptic properties, viscosity, drying time, spreadability, and adhesive strength. Furthermore, a freeze-thaw stability test was performed using three cycles at -5 ˚C and 40 ˚C. In addition, the product underwent centrifugation at 3700 rpm for 5 hours, followed by visual inspection for changes.

The antioxidant property of the finished product using DPPH

The antioxidant activity was evaluated using the DPPH assay. A 1 mL sample of the peel-off mask containing 15% Rosella (11% granules and 4% powder) was dissolved in water. DPPH was prepared in methanol and mixed with the product in test tubes, which were kept in the dark for 30 minutes. Absorbance was measured at 517 nm, and antioxidant activity was calculated using the formula:

% of antioxidant activity=[(Ac-As)/Ac] x 100	[1]

Where absorbance of control: Absorbance of control, As: Absorbance of sample is the control reaction absorbance, and absorbance of sample is the testing specimen absorbance.

RESULTS

Antioxidant component detection in Rosella powder using LC-MS

The LC-MS analysis confirmed the presence of key antioxidant compounds in Rosella powder, including astaxanthin and flavonoids such as quercetin, rutin, and kaempferol. Astaxanthin was identified in dichloromethane extracts as shown in the extracted ion chromatogram (Figure 1), with a retention time of 5.3-5.4 minutes and a mass-to-charge ratio (m/z) of 597/147.1. Flavonoids were detected in methanol extracts. Quercetin (Figure 2) was observed at a retention time of 9.9 minutes and m/z 301.0/150.9, while rutin (Figure 3) appeared at 29 minutes, with m/z 609.2/300.0. Kaempferol (Figure 4) was identified at 15 minutes with m/z 284.9/93.0. Identification was based on retention times and mass spectra that were matched against an LC-MS library.

Granulation of Rosella powder

Granulation was performed to optimize the particle size and flowability of Rosella powder for use in the peel-off mask. The PSD (Figure 5) revealed that over 70% of granules ranged between 250 and 425 µm, aligning with the ideal size for physical scrubs. Table 2 details the physical properties of the granules, which were spherical, red, and odorless, with a LOD of 4.92±0.11%, a flowability of 5.60±0.93 g/s, and an angle of repose of 31.5±1.2˚C.

Optimization and evaluation of Rosella peel-off mask formula

The peel-off mask formulations were optimized for physical and functional properties using PVA and gelatin as base polymers. On day 0, the physical properties of the masks, including homogeneity and organoleptic characteristics, were evaluated (Figure 6). Viscosity analysis (Figure 7) showed that PVA-based formulations had higher viscosity than gelatin-based formulations. The higher viscosity in PVA-based formulations can be attributed to its superior gel-forming properties and

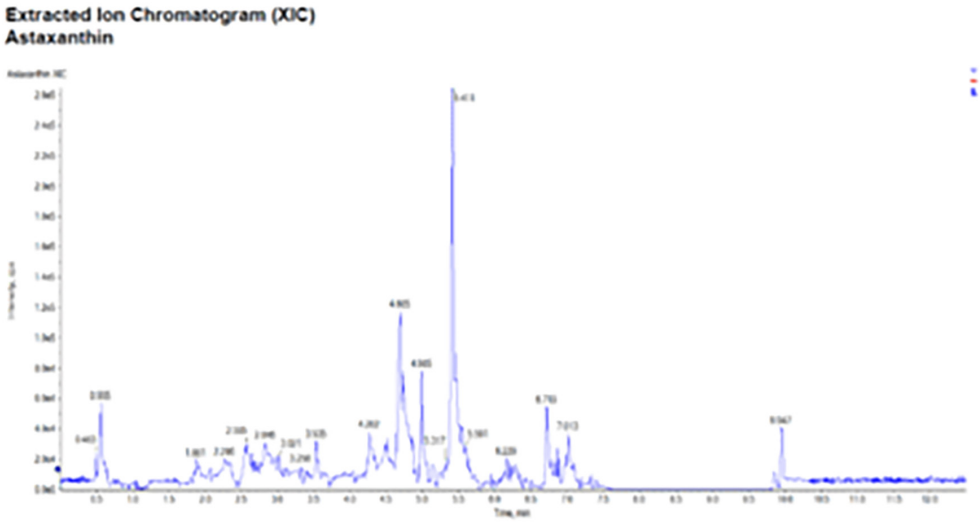

Figure 1. Extracted ion chromatogram from Rosella powder in dichloromethane for astaxanthin detection (Astaxanthin peak was 5.3-5.4 minutes and *m/z* 597/147.1)

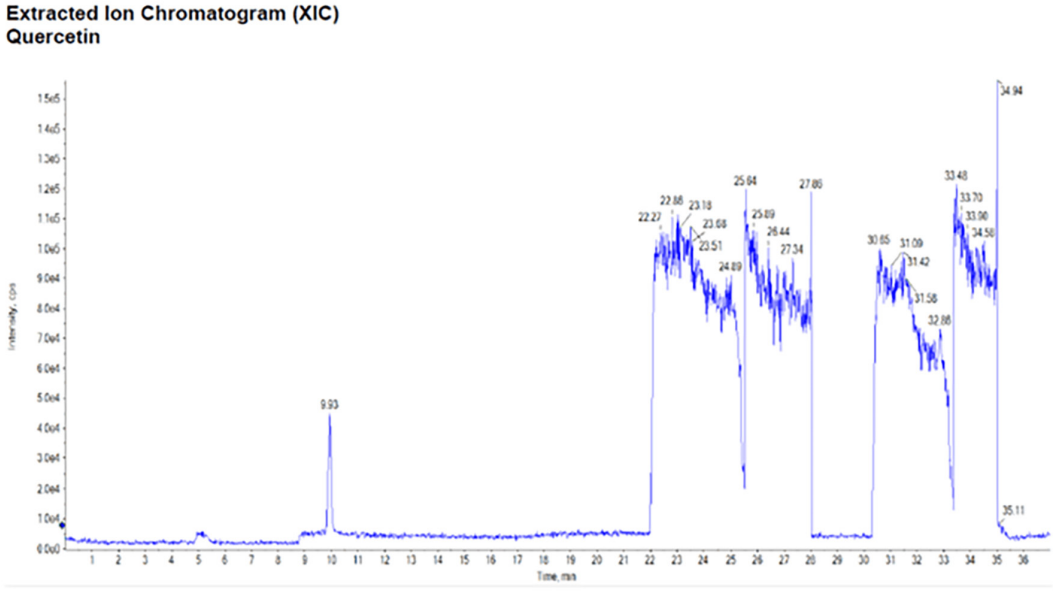

Figure 2. Total ion chromatogram from rosella powder in methanol for flavonoid detection (Quercetin peak was 9.9 minutes and *m/z* 301.0/150.9)

cohesive network structure. Gelatin-based formulations exhibited lower viscosity due to their higher hydrophilic content, which increased water absorption.

Stability study

The stability of the peel-off mask formulations was assessed under both ambient and stress conditions. Figure 8 presents the results of stability testing for the PVA-based formulation (F4) over three months, showing no significant changes in viscosity, drying time, pH, spreadability, or adhesivity. The freeze-thaw stability study (Figure 9) further demonstrated the robustness of the PVA-based formula, with no phase separation or degradation observed across three cycles. Comparative centrifugation tests (Figure 10) highlighted the superior stability of the PVA-based formulation (F4), which remained homogeneous, whereas the gelatin-based formulation (F6) showed phase separation.

DISCUSSION

Figure 1 shows that astaxanthin was detected in the Rosella powder and three types of flavonoids were identified in the samples was rutin, quercetin, and kaempferol (Figures 2-4). The intensity of astaxanthin in the sample was approximately 200,000, while the flavonoid intensity was relatively low. Retention times were matched with a database; validated reference standards were not used. These results provide preliminary qualitative data, and we acknowledge that semi-

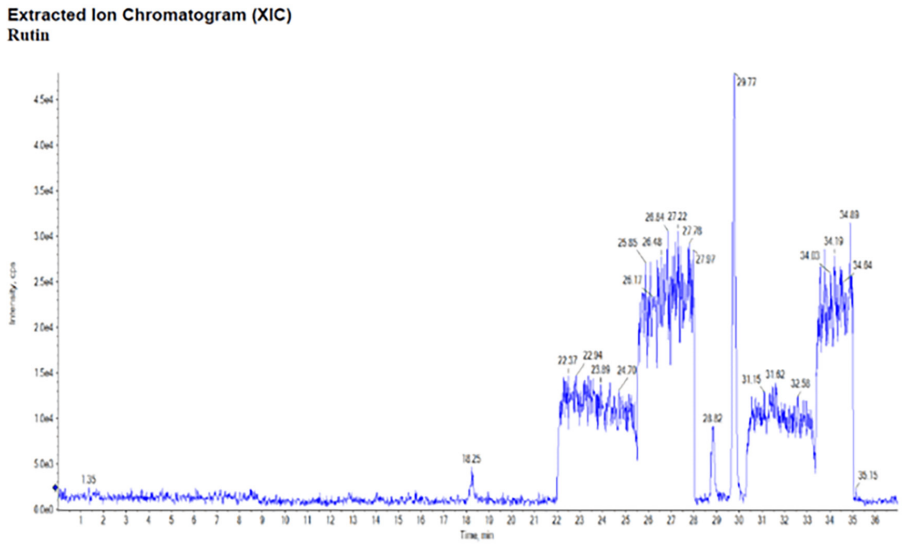

Figure 3. total ion chromatogram from Rosella powder in methanol for flavonoid detection (Rutin peak was 29 minutes and *m/z* 609.2/300.0)

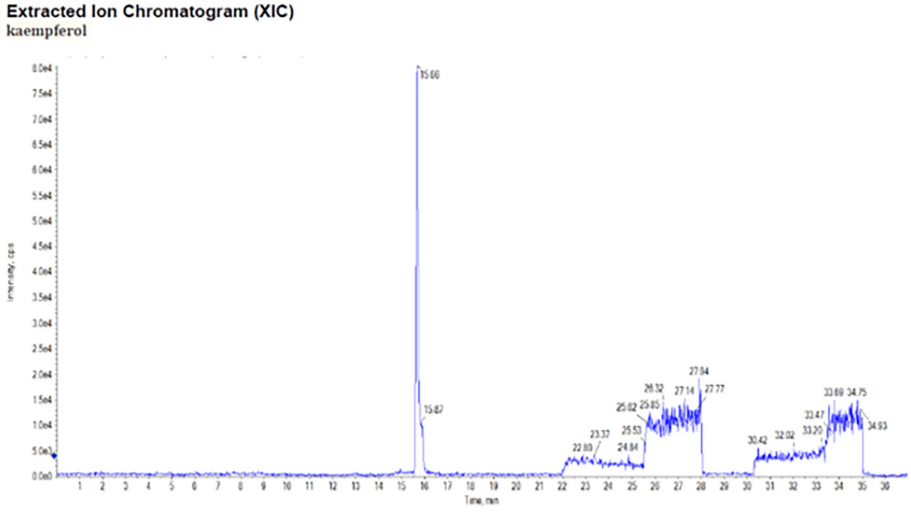

Figure 4. Total ion chromatogram from Rosella powder in methanol for flavonoid detection (Kaempferol peak was 15 minutes and *m/z* 284.9/93.0)

quantitative or quantitative LC-MS/MS analysis would offer stronger scientific support for the antioxidant capacity findings. Future studies will focus on purification and quantification steps using validated analytical standards to enable accurate comparison and potency determination.

Rosella powder, Herbilogy®, was processed through a 100-mesh sieve (150 µm). However, this particle size is too fine to be suitable for use as a skin scrub. Ideally, the particle size for a scrub should range from 150 to 600 µm, with an average size of approximately 250 µm.[10,11] Therefore, the granulation process should be performed to increase the particle size. Freeze-drying was selected as the granulation method because studies have shown that increasing temperature and pH leads to an increase in k values. (Note: The rationale for selecting freeze-drying based on the effects of temperature and pH on

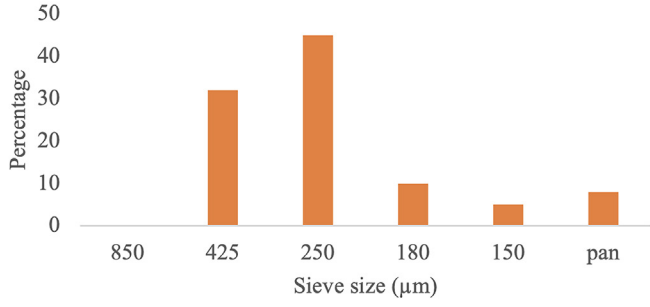

Figure 5. Particle size distribution of Rosella granules

k values should be clearly explained in the context.) Higher k values correspond to a faster reaction rate, which accelerates the degradation of antioxidants.[12]

Table 2. Physical properties of Rosella granules

Parameters	Description
Organoleptic	Red light spherical granules, un-odorized
Loss on drying	4.92±0.11%
Flowability	5.60±0.93 g/s
Angle of repose	31.5±1.2 ˚C

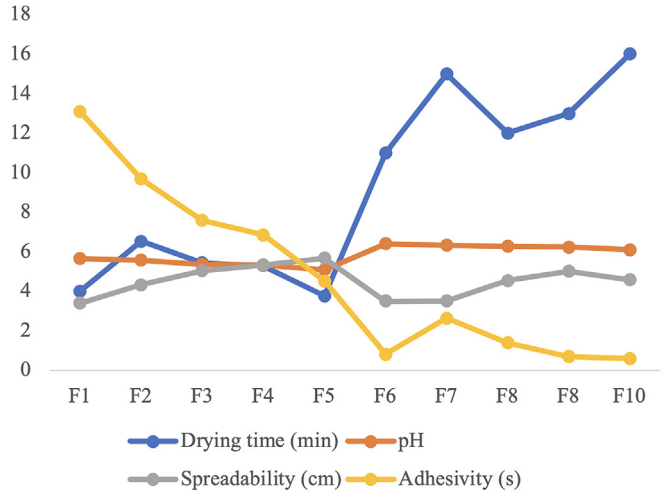

Figure 6. Physical Properties of Rosella peel-off mask at day 0

The granulation process was carried out using a PVP solution. The wet granules were solidified at -20 ˚C and dried for 24 hours. Wet granulation was selected as it ensures a more effective binding process through uniform wetting and produces spherical granules with improved flowability.[13] The evaluation results are presented in Figure 5 and Table 2. The granules exhibited good flowability, as indicated by the flow rate and angle of repose, placing them in the "good" category. This suggests that scaling up the batches using commercial equipment is highly feasible. The particle size was primarily distributed within the range of 250-425 µm, meeting the requirements for effective scrub particles. From the granulation process, more than 70% of the particles were found to have a size of ≥250 micrometers, which aligns with the objective of the granulation as a scrub process. Fines of <20% are commonly observed in granulation processes and do not affect the intended function.[14] Particle size plays a crucial role in skin friction; excessively large particles are only suitable for areas of the body with a thick stratum corneum or significant dead skin cells.[15]

The Rosella peel-off mask was formulated using two types of polymers: PVA and gelatin. Gelatin, with the appropriate bloom strength, provides good gel strength while remaining flexible enough to conform to the contours of the user's face. PVA is non-irritating to both skin and eyes. Both polymers are included on the generally recognized as safe list of materials.[16] The formula was designed using SLD, as shown in Table 1. The final dosage form was evaluated for physical parameters, presented in Figures 6 and 7.

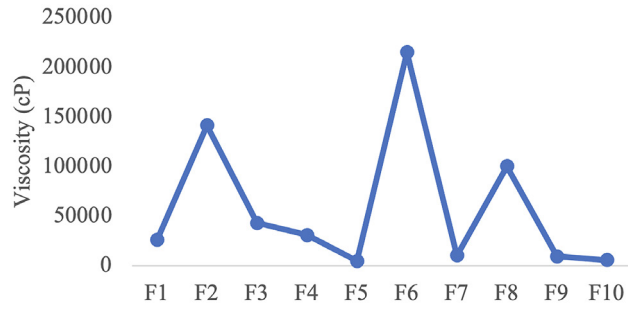

Figure 7. Viscosity parameters of Rosella peel-off mask at day 0

Based on the one-way ANOVA quadratic model, the concentrations of propylene glycol and PVA had no significant effect on the drying time parameter (*p* value=0.2247). Similarly, for the gelatin-based formula, the one-way ANOVA linear model indicated no significant effect on the drying time parameter (*p* value =0.4656). The PVA-based formula exhibited a shorter drying time compared to the gelatin-based formula. This difference is attributed to the lower water content in the PVA-based formula. In contrast, gelatin swells in an aqueous solution due to its abundance of hydrophilic groups. These hydrophilic groups, such as hydroxyl and amino groups, increase the equilibrium swelling ratio, enhancing the material's capacity to absorb water.[17] The increase in absorption capability is observed within the concentration range of 5 to 30, whereas this formula exhibits a narrow.

Er range of absorption capability. A higher absorption capability prevents the water present in the formula from being easily removed.

As shown in the day-0 evaluation (Figure 6), there is no significant difference in pH values across formulas with varying concentrations of PVA or gelatin. However, the pH of the gelatin-based formula is slightly higher than that of the PVA-based formula. This difference is attributed to the intrinsic pH values of the materials, with PVA having a pH range of 4.5-6.5 and gelatin (type B) a range of 5-7.5.[16]

The ability of a mask's material to spread makes it easier to cover the entire surface of the face, forming a thin and perfect layer.[18] The test is carried out by measuring the diameter of a number of preparations after being given a load of a certain weight (Deuschle et al.[19]). Spreadability is inversely correlated with viscosity.[20] In the PVA-based formula, spreadability increased as the concentration of PVA decreased. This trend aligns with the viscosity profile, which decreased from F2 to F3, as shown in Figure 7. According to the one-way ANOVA quadratic model, the concentrations of propylene glycol and PVA significantly affected viscosity (*p* value=0.0114). The coefficient values were 10.241 for propylene glycol and 2.5×10^5 for PVA, indicating that PVA had a more substantial impact on the viscosity profile.

For the gelatin-based formula, the spreadability did not show significant variation due to the narrow range of concentrations, a lack that was also reflected in the viscosity parameter. Based on the one-way ANOVA linear model, neither propylene glycol

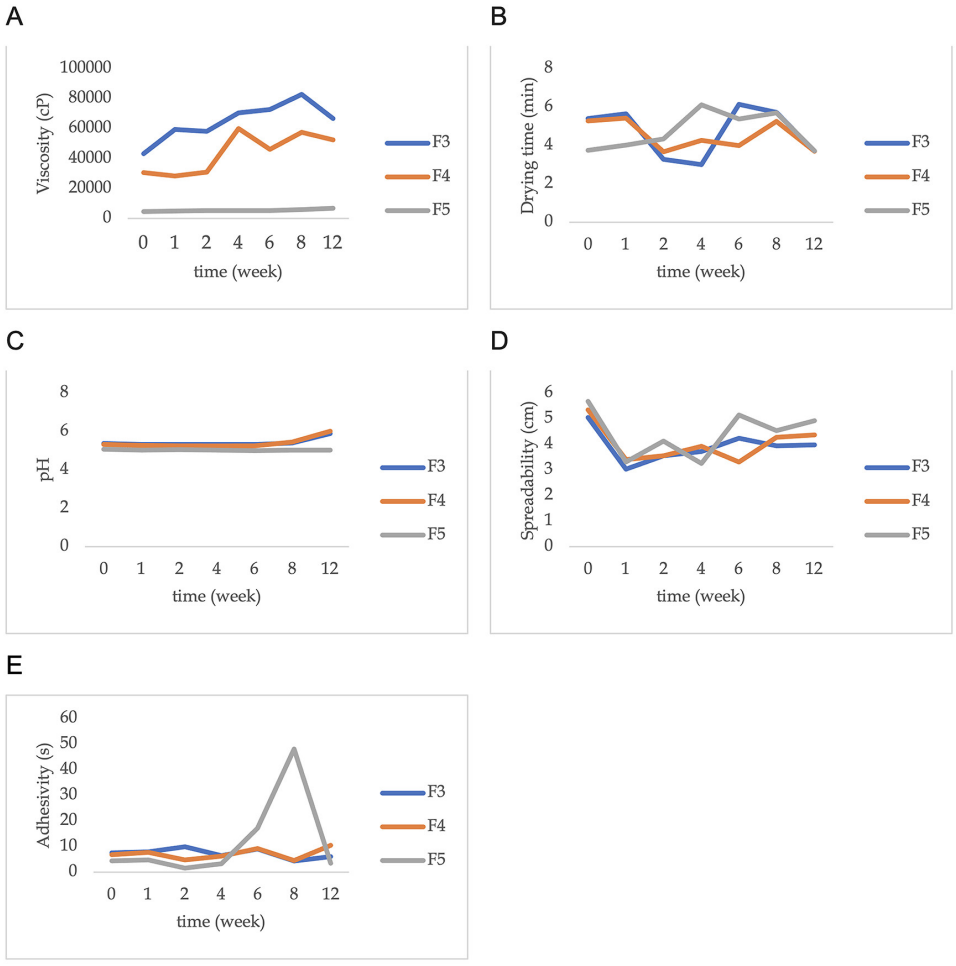

Figure 8. Stability study of Rosella peel-off mask PVA-based for (A) viscosity parameters, (B) drying time parameters, (C) pH parameters, (D) spreadability parameters, (E) adhesivity parameters

PVA: Polyvinyl alcohol

nor gelatin concentration had a significant effect on viscosity (p value=0.1642). In contrast, according to the one-way ANOVA linear model, the concentrations of propylene glycol and PVA significantly influenced adhesivity (p value=0.0041). The coefficient values were 4.36 for propylene glycol and 12.41 for PVA, demonstrating that PVA had a more pronounced impact on the adhesivity profile. Lower PVA concentrations resulted in reduced adhesiveness. The high adhesiveness of the hydrogel is attributed to the presence of carboxyl and hydroxyl groups in the PVA-COOH chain, which contribute significantly to the adhesion properties.[21]

The selected formula for the PVA-based formulation was F4, while F6 was chosen for the gelatin-based formulation based on the results of SLD numerical optimization. All formulations were stored at room temperature in amber glass containers and subsequently evaluated for viscosity, drying time, pH, spreadability, and adhesiveness. All gelatin-based formulations were found to be unstable in less than a month and therefore, were not considered optimal formulations. Similarly, the PVA-based formulations F1 and F2 were unstable after one month. In contrast, formulations F3, F4, and F5 remained stable for 7

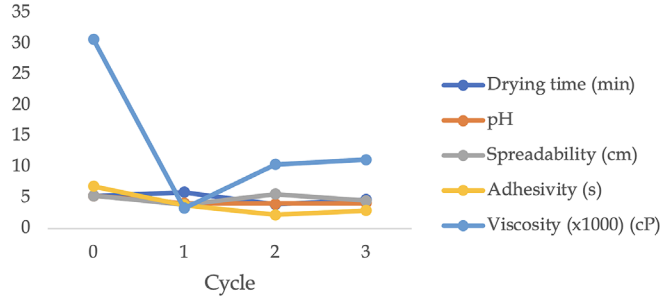

Figure 9. Freeze thaw stability study of Rosella peel-off mask PVA-based polymer (F4)

PVA: Polyvinyl alcohol

weeks at room temperature, and they maintained all parameters without phase separation for up to 3 months, as shown in Figure 8. Centrifugation results depicted in Figure 10 indicated phase separation in F6, whereas no phase separation was observed in F4.

The F4 formula was subsequently subjected to a freeze-thaw stability study and remained stable in terms of drying time,

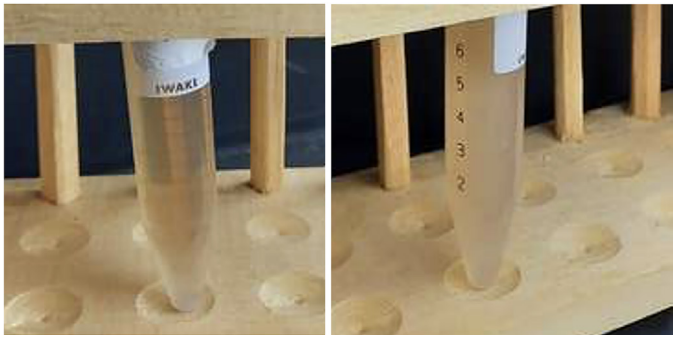

Figure 10. (a) Organoleptic of rosella peel-off mask PVA-based Polymer (F4) after centrifugation, (b) organoleptic of Rosella peel-off mask gelatin-based Polymers (F6) after centrifugation (Notes: Rosella granules were taken out from the formula to ensure that the separation phase of the base can be seen clearly)

PVA: Polyvinyl alcohol

pH, and spreadability parameters (Figure 9). However, the adhesiveness parameter showed a slight decrease, likely due to the freeze-thaw process triggering cross-linking, which reduces the availability of free functional groups responsible for the adhesion process.[22] Viscosity decreased significantly after the first freeze-thaw cycle, likely due to syneresis or solvent extraction caused by increased crystallinity levels during temperature fluctuations. With an increasing number of cycles, the percentage of crystalline regions within the hydrogel also increased, leading to a stiffer structure.[23,24]

According to Wu et al.,[12] the primary antioxidants in Rosella are polyphenols, with dehydrated Rosella calyces found to contain a total polyphenol concentration of approximately 683.13 mg GAE per 100 g. The DPPH radical scavenging activity ranged from 20% to 60% at sample concentrations of 1-5 mg/mL and exceeded 80% when the sample concentration reached 7.5 mg/mL. The findings of this study are consistent with these results, showing an antioxidant activity of 45.332% at a concentration of 2 mg/mL when compared to ascorbic acid as the standard.

Furthermore, this research can be extended to in vivo studies to evaluate its effectiveness in reducing the impact of free radicals. Additionally, user perspective testing can be conducted to assess its pharmaceutical aspects. The Rosella powder can also be purified to enhance its effectiveness in the formulation, and the active components responsible for its effects can be quantified. This study was conducted in a non-GMP laboratory environment, and as a result, microbiological testing was not performed; future studies will address this limitation by preparing the formulations in a GMP-compliant facility to ensure appropriate microbial control and testing.

CONCLUSION

This study successfully developed a multifunctional peel-off mask with scrub properties by incorporating a natural source of flavonoids and astaxanthin with antioxidant potential, *Hibiscus sabdariffa* L. (Rosella) extract. The formulation was optimized through a PVA-based system using a simplex lattice design to ensure optimal physical properties and stability. LC-MS analysis verified the presence of key antioxidant compounds in the extract, such as astaxanthin, quercetin, rutin, and kaempferol. Granulated Rosella powder, sized between 250-425 µm, exhibited good flowability and functioned effectively as a scrub agent. The optimized formula, containing 15% Rosella (11% granules and 4% powder), displayed favorable peel-off characteristics, including quick drying time, appropriate pH, excellent spreadability, and strong adhesiveness, while maintaining stability under ambient conditions, freeze-thaw cycles, and centrifugation stress. The product achieved an antioxidant activity of 45.33% relative to ascorbic acid. These results indicate that Rosella-based peel-off masks represent a viable solution for incorporating natural antioxidants into multifunctional cosmetic products, supporting sustainable and practical skincare innovations.

Ethics

Ethics Committee Approval: Not required.

Informed Consent: Not required.

Acknowledgments

The author expresses gratitude to Atma Jaya Catholic University of Indonesia, the home-based institution, for its support and encouragement in pursuing this research. Appreciation is also extended to PT. Pharos Indonesia, for providing the materials that were used in this study and for PT. Mulia Sejahtera Scientific for assisting with the analysis of Rosella powder using LC/MS.

Footnotes

Authorship Contributions

Concept: P.R., Design: P.R., Data Collection or Processing: P.R., A.K., R.S., G.L., Analysis or Interpretation: P.R., A.K., R.S., G.L., Literature Search: P.R., I.Y.K., Writing: P.R., I.Y.K.

Conflict of Interest: The authors declare no conflicts of interest.

Financial Disclosure: Material has been donated by PT. Pharos Indonesia and analysis by PT Mulia Sejahtera Scientific.

REFERENCES

1. Phaniendra A, Jestadi DB, Periyasamy L. Free radicals: properties, sources, targets, and their implication in various diseases. Indian J Clin Biochem. 2015;30:11-26.
2. Bouayed J, Bohn T. Exogenous antioxidants-Double-edged swords in cellular redox state: Health beneficial effects at physiologic doses versus deleterious effects at high doses. Oxid Med Cell Longev. 2010;3:228-237.
3. Redding M. Skincare Market Expands to Meet Consumers' Needs [Internet]. Beauty Packaging. 2022 [cited 2023 Sep 13]. Available from: https://www.beautypackaging.com/issues/2022-10-01/view_features/skincare-market-expands-to-meet-consumers-needs/
4. Sierra PR. Why are simplicity and multifunctionality new trends in the beauty market? [Internet]. Biomeca. 2022 [cited 2023 Sep 13]. Available from: https://www.bio-meca.com/en/simplicity-and-multifunctionality-in-the-beauty-market/
5. Martins AM, Marto JM. A sustainable life cycle for cosmetics: From design and development to post-use phase. Sustain Chem Pharm. 2023;35:101178.

6. Juhari NH, Petersen MA. physicochemical properties and oxidative storage stability of milled roselle (*Hibiscus sabdariffa* L.) Seeds. Molecules. 2018;23:385.
7. Juhari NH, Bredie WLP, Toldam-Andersen TB, Petersen MA. Characterization of Roselle calyx from different geographical origins. Food Res Int. 2018;112:378-389.
8. Wang H. A Review of the effects of collagen treatment in clinical studies. Polymers (Basel). 2021;13:3868.
9. Ramadhani RR, Pangkahila W, Wiraguna AAGP. Rosella Flower 3% (*Hibiscus sabdariffa*) extract inhibited the expression of matrix metalloproteinase-1 dan collagen reduction on wistar rat exposed to ultraviolet-B. International Journal of Science and Research (IJSR) [Internet]. 2019 [cited 2023 Sep 13]; Available from: https://www.ijsr.net/archive/v10i1/SR21112182003.pdf
10. Carli B. Start fresh with exfoliating encapsulates. Prospector Knowledge Center. 2018.
11. Mukherjee D. Exfoliating cosmetic formulation comprising powdered sapphire [Internet]. WO2017/134426 A1, 2017 [cited 2023 Sep 14]. Available from: https://patentimages.storage.googleapis.com/af/4f/03/e463ea23e2891e/WO2017134426A1.pdf
12. Wu H-Y, Yang K-M, Chiang P-Y. Roselle anthocyanins: antioxidant properties and stability to heat and pH. *Molecules*. 2018;23:1357.
13. Shanmugam S. Granulation techniques and technologies: recent progresses. Bioimpacts. 2015;5:55-63.
14. Zhu DQ, Zhou XL, Pan J, Shi BJ. Granulation behaviour of specularite fines in ferrous sinter mixtures. Mineral Processing and Extractive Metallurgy. 2016;125:172-177.
15. Ervina A, Santoso J, Prasetyo BF, Setyaningsih I, Tarman K. Formulation and characterization of body scrub using marine alga Halimeda macroloba, chitosan and konjac flour. IOP Conf Ser Earth Environ Sci. 2020;414:012004.
16. Rowe RC, Sheskey PJ, Quinn ME. Handbook of pharmaceutical excipients (6th ed). Londra; Pharmaceutical Press, 2009:506-509.
17. Sun M, Wang Y, Yao L, Li Y, Weng Y, Qiu D. Fabrication and Characterization of Gelatin/Polyvinyl Alcohol Composite Scaffold. *Polymers*. 2022;14:1400.
18. Apriani EF, Miksusanti M, Fransiska N. Formulation And Optimization Peel-Off Gel Mask with polyvinyl alcohol and gelatin based using factorial design from banana peel flour (*Musa paradisiaca* L) as antioxidant. Indonesian Journal of Pharmacy. 2022;32:261–268.
19. Deuschle VCKN, Deuschle RAN, Bortoluzzi MR, Athayde ML. Physical chemistry evaluation of stability, spreadability, *in vitro* antioxidant, and photo-protective capacities of topical formulations containing *Calendula officinalis* L. leaf extract. Brazilian Journal of Pharmaceutical Sciences. 2015;51:63-75.
20. Szulc-Musioł B, Dolińska B, Kołodziejska J, Ryszka F. Influence of plasma on the physical properties of ointments with quercetin. Acta Pharm. 2017;67:569-578.
21. Yu Y, Zhao X, Ye L. A new mussel-inspired highly self-adhesive & conductive poly (vinyl alcohol)-based hydrogel for wearable sensors. Appl Surf Sci. 2021;562:150162.
22. Lotfipour F, Alami-Milani M, Salatin S, Hadavi A, Jelvehgari M. Freeze-thaw-induced cross-linked PVA/chitosan for oxytetracycline-loaded wound dressing: the experimental design and optimization. Res Pharm Sci. 2019;14:175-189.
23. Ricciardi R, D'Errico G, Auriemma F, Ducouret G, Tedeschi AM, De Rosa C, Reupretre F, Lafuma F. Short time dynamics of solvent molecules and supramolecular organization of poly (vinyl alcohol) hydrogels obtained by freeze/thaw techniques. Macromolecules. 2005;38:6629-6639.
24. Kathuria N, Tripathi A, Kar KK, Kumar A. Synthesis and characterization of elastic and macroporous chitosan-gelatin cryogels for tissue engineering. Acta Biomater. 2009;5:406-418.